Osteogenic Differentiation of Human Mesenchymal Stem Cells by the Design of a Natural Microenvironment

Von der Naturwissenschaftlichen Fakultät

der Gottfried Wilhelm Leibniz Universität Hannover

zur Erlangung des Grades

Doktorin der Naturwissenschaften

Dr. rer. nat.

genehmigte Dissertation

von M.Sc. Sonja Kreß

geboren am 1. November 1983

in Hannover

2013

Referent: Prof. Thomas Scheper

Korreferentin: Prof. Cornelia Kasper

Tag der Promotion: 23.11.2012

Erklärung

Hiermit versichere ich, dass ich die vorliegende Dissertation selbstständig verfasst habe und die benutzten Hilfsmittel sowie eventuell zu Hilfsleistungen herangezogene Institutionen vollständig angegeben habe. Ferner versichere ich, dass die Dissertation nicht bereits als Diplomarbeit oder andere Prüfungsleistung verwendet worden ist.

Hannover, Februar 2013

Acknowledgment

Hiermit möchte ich mich bei Herrn Prof. Dr. Thomas Scheper herzlich für die Möglichkeit bedanken, im Institut für Technische Chemie der Leibniz Universität Hannover meine Dissertation anfertigen zu können. Außerdem danke ich ihm für die Übernahme des Referats.

Frau Prof. Dr. Cornelia Kasper danke ich für die Übernahme des Koreferats und die Unterstützung auf dem Gebiet des Tissue Engineering. Des Weiteren bedanke ich mich für die Vermittlung von verschiedenen Firmenkontakten, welche sehr hilfreich bei der Erstellung dieser Arbeit waren. Ein großer Dank geht an Herrn Sieker von GE Healthcare in Wunstorf für die Aufnahme der μCT Scans und an Herrn Westenberger von VSG für die Auswertung der generierten Daten.

Für die Finanzierung meiner Forschungsarbeiten im Rahmen des Projektes "Niedersächsisches GMP-Musterlabor" danke ich dem Land Niedersachsen. Für die finanzielle Unterstützung bei meinem Auslandsaufenthalt in Zaragoza (Spanien) möchte ich mich beim Deutschen Akademischen Austauschdienst (DAAD) bedanken.

Muchas gracias a Iñaki Ochoa por la possibilidad a hacer unos de los experimentos en la Universidad de Zaragoza en Espana y por revisar esta tesis. Gracias a Víctor Acosta Santamaría por la ayuda con los datos confinados y nonconfinados y por responder a todas mis preguntas. Muchas gracias tambien a Pedro Moreo y Victor Alastrué de la compania EBERS Medical por la possibilidad a trabajar con vuestras bioreactores y por la ayuda con estos.

Gracias tambien a todos los estudiantes en el grupo Ingeniería Biomédica (especialmente a Olfa, Siamak, Andrés, Oracio, Pablo, Sergio y Sara). Lo pasamos muy bien. Muchas gracias a Claudia Miacchia, no me puedo olvidar el tiempo que pasamos juntas (el perro esta sentado encima de mi pantalla). Un abrazo muy fuerte!

Bei Sascha Beutel und Thomas Scheper möchte ich mich für die Unterstützung beim Kampf gegen die Papierberge der NBank/GMP-Labor bedanken.

Antonina Lavrentieva möchte ich herzlich dafür danken, dass ihr unglaubliches Wissen gerne mit mir geteilt hat und immer einen guten Rat für mich hatte.

Bei meinen zahlreichen Bürokollegen (Anne S., Iliyana, Janis, Tonya, Kai, Daniel L., Michi, Anne N.) bedanke ich mich für die schöne Zeit ab 17:01, das Feierabendbier, die

Feuerzangenbowle, die netten Abende auf der Terrasse, „36 Grad und es wird noch heißer“, und alle aufmunternden Worte.

Außerdem bedanke ich mich bei der Werkstatt des Instituts für Technische Chemie und Thorleif Hentrop für die umfangreiche Hilfe bei Weiterentwicklung und Steuerung der Reaktorsysteme. Martin Pähler danke ich für die Durchführung und Optimierung zahlreicher PCR Experimente. Danke Wolff für einen Schlauch hier und ein Verbindungsstück da. Danke Daniel S. für die Durchführung einiger µCT Scans und die Hilfe bei der Auswertung.

Katrin Schulz und Christian Lorek danke ich dafür, dass sie im Rahmen ihrer Bachelorarbeit einen Beitrag zum Thema Knochen Tissue Engineering geleistet haben.

Ich möchte nicht vergessen, mich bei allen Leuten zu bedanken, die nicht nur dazu beigetragen haben die Arbeitszeit sehr angenehm zu gestalten, sondern auch die Freizeit: Danke Miri für dein ausgeprägtes Organisationstalent, tolle Ausflüge und Wanderungen. Danke Christan E. für die vielen Extrakt-Burger (ich hoffe das Extrakt geht ohne uns nicht Pleite). Danke Daniel L. für die netten Abende in der Glocke. Danke Kai für die Hilfe mit meinen Rechnern und die Feierabendbiere. Danke Anne S. und Fabsi für die vielen Stunden auf der Tanzfläche. Danke Mike, dass du versuchst in jedem Jahrgang die Traditionen aufrecht zu erhalten. Danke Tonya für die vielen kleinen Geschenke zu Weihnachten und Ostern und für die Bürodekoration.

Lieber Jan! Ich danke dir für deine starken Nerven, deine aufmunternden Worte und das rundum Sorglos-Paket der letzten Monate. Ohne dich hätte ich gehungert! Danke!

Kurzfassung

Für die Herstellung von künstlichen Knochentransplantaten eignet sich eine Kombination aus mesenchymalen Stammzellen und Biomaterialien. Dreidimensionale Matrices imitieren die natürlichen Umgebungsbedingungen des Gewebes, bilden das Grundgerüst für die Zellen und verleihen dem Transplantat seine Stabilität. In der Literatur sind diverse Biomaterialien für das Knochen *Tissue Engineering* beschrieben. Allerdings sind die Auswirkungen charakteristischer Faktoren wie beispielsweise Porengröße, Porosität, Festigkeit und Geometrie auf das Zellwachstum und die Differenzierung nicht eingehend untersucht.

Auf dieser Grundlage werden in der vorliegenden Arbeit sowohl die mechanischen Eigenschaften, als auch die Biokompatibilität verschiedener keramischer und Kollagen-basierter Biomaterialien untersucht und ihr potentieller Einsatz im Knochen *Tissue Engineering* evaluiert. Zur Herstellung eines Knochentransplantats werden mesenchymale Stammzellen meist unter statischen Bedingungen auf 3D Matrices differenziert. Diese Methode weist allerdings diverse Nachteile auf, wie beispielsweise die limitierte Nährstoffversorgung der Zellen und ein hohes Kontaminationsrisiko. Des Weiteren imitieren statische Experimente die *in vivo* Umgebungsbedingungen nur eingeschränkt.

Zur Lösung dieser Problematik werden dynamische Kultivierungen von mesenchymalen Stammzellen auf dreidimensionalen Trägermaterialien in verschiedenen Bioreaktoren durchgeführt. Dabei liegt der Schwerpunkt auf Perfusionsbioreaktoren und einem Reaktorsystem, welches Perfusion und Kompression vereint. Diese Systeme sollen den extrazellulären Fluss im Knochengewebe simulieren, Nährstoffversorgung optimieren und somit die Differenzierung fördern. Darüber hinaus werden dynamische Kultivierungen in einem ausgewählten Reaktorsystem unter regulierten Prozessbedingungen durchgeführt. Dafür ist die Anbindung des Bioreaktors an eine speziell entwickelte Steuereinheit notwendig. Dieses Vorgehen ermöglicht die reproduzierbare Herstellung von Gewebetransplantaten unter den Auflagen der guten Herstellungspraxis.

Schlagwörter: Knochen *Tissue Engineering*, 3D Matrix, dynamische Kultivierung, Bioreaktor, Scherstress

Abstract

Mesenchymal stem cells and three-dimensional biomaterials seem to be a potent combination for the production of artificial bone tissue constructs. Nowadays, many different biomaterials have been characterized for bone Tissue Engineering applications. Diverse biomaterial characteristics such as pore size, porosity, stiffness and geometry not only affect cell attachment and proliferation, but also the differentiation behavior of mesenchymal stem cells.

This thesis presents a detailed characterisation of the mechanical properties of different ceramic and collagen-based biomaterials and evaluates their capacity for bone Tissue Engineering applications. Further, to estimate the quality of biomaterials in order to produce an artificial bone transplant, static long-term cultivations using mesenchymal stem cells are performed. Static differentiation of mesenchymal stem cells on three-dimensional matrices is the simplest method to create bone structures; however, this technique buries several disadvantages, such as a weak distribution of cells and nutrients, a high risk of contamination and a non-physiological microenvironment.

In vivo bone cells are exposed to mechanical forces due to intersitial fluid flow and loading. To overcome these limitations and create a natural three-dimensional microenvironment, dynamic cultivations of mesenchymal stem cells on biomaterials are performed, applying different bioreactor systems. Dynamic cultivation includes the application of direct perfusion and a combination of perfusion and cyclic compression, which are shown to enhance osteogenic differentiation. Furthermore, the reproducible production of artificial bone transplants under good manufacturing practice conditions is investigated by connecting a dynamic bioreactor system to a control unit. This allows the regulation and documentation of all essential cultivation parameters and consequently ensures a constant product quality.

Keywords: Bone Tissue Engineering, 3D matrix, dynamic cultivation, bioreactor, fluid flow

Table of contents

List of abbreviations

µCT	micro computed tomography
µg	micro gram
µm	micro meter
2D	two-dimensional
3D	three-dimensional
adMSC	adipose-derived mesenchymal stem cells
AP	alkaline phosphatase
ATMP	Advanced Therapy Medicinal Product
av.	average
BMP-2	bone morphogenic protein 2
BMP-4	bone morphogenic protein 4
BSP-2	bone sialoprotein 2
CC	confined compression
ccm	cubic meter
cDNA	copy deoxyribonucleic acid
CICP	C-terminal of type I collagen
CO_2	carbon dioxide
COL I	collagen type I
COL III	collagen type III
cp.	compare
d	diameter
DAPI	4',6-Diamidino-2-phenylindol
DNA	deoxyribonucleic acid
ELISA	enzyme-Linked Immunosorbent Assay
EMA	European Medicines Agency
ERK	extracellular signal-regulated kinase
EU	European Union
FAK	focal adhesion kinase
fig.	figure
g	gram
g	gravity

HA	Aggregate Modulus
HAP	hydroxylapatite
hMSC	human mesenchymal stem cells
HPRT	hypoxanthine-guanine phosphoribosyltransferase
ht	height
kV	kilovolts
l	liter
LSCM	Laser scanning confocal microscopy
min	minute
ml	milliliter
mm	millimeter
mmHg	millimeter of mercury
mmol	millimol
mRNA	messenger ribonucleic acid
MSC	mesenchymal stem cells
N	Newton
n	quantity
N_2	nitrogen
nanoCT	nano computed tomography
nm	nano meter
O_2	oxygen
OC	osteocalcin
ODM	osteogenic differentiation medium
ODM-M	commercially available osteogenic differentiation medium from Miltenyi Biotec
OP	osteopontin
Pa	pascal
PCL	polycaprolactone
PCR	polymerase chain reaction
PLGA	poly(lactic-co-glycolic acid)
pO_2	partial pressure
RNA	ribonucleic acid
rpm	rounds per min
RT-PCR	reverse transcription polymerase chain reaction

RUNX	runt-related transcription factor
SEM	scanning electron microscope
tab.	table
TCP	β-tricalcium phosphate
TE	Tissue Engineering
U	unit
UC	umbilicial cord
UC	unconfined compression
ucMSC	umbilical cord-derived mesenchymal stem cells
ZrO_2	Zirconium dioxide
αMEM	alpha minimum essential medium

Introduction

Tissue Engineering (TE) is a young and interdisciplinary field of biotechnology, which promises a huge impact to medical practice. The main objective of TE is to regenerate or replace defective tissues and organs instead of repairing them. Examples of tissues used in preclinical or clinical studies include skin, cartilage, bone, blood vessels, skeletal muscle and the bladder [1].

Especially bone TE gained the attraction of many research facilities, since about 4 million bone replacement procedures are annually carried out worldwide. Bone is representing the second place on the list of transplanted materials [2]. Generally, bone has the capacity for self-healing. However, large bone defects require a replacement, if possible with an autologous bone graft (mainly derived from the iliac crest). If the derived material is not sufficient, an allogenic graft or an artificial construct can be implanted. Heterografts carry the risk of infection (e.g. AIDS or hepatitis) and immunoreactions in contrary to autografts [3]. These drawbacks evoke the development of alternative methods.

TE offers the opportunity to combine the skills of engineering and life sciences. This interdisciplinary background is used to design alternative bone grafts: Three-dimensional (3D) biomaterials in combination with human cells. Within this approach the selection of the cell type and the composition of the culture medium is of importance. Moreover, the influence of soluble or immobilized growth factors on cell behavior has nowadays been studied in detail [4-6]. Furthermore, the application of human mesenchymal stem cells (MSC) gained increasing attraction for TE applications [7], as well as for cell therapies [8]. However, these issues have already intensively been discussed [9]. Today, the key parameter of a tissue engineered bone graft seems to be the selection of a proper biomaterial [10].

In despite of the knowledge that MSC and differentiated tissue cells growth *in vivo* in a defined 3D surrounding of macromolecules, most TE experiments are still carried out on flat bottom surfaces of culture vessels made of glass or plastic [11]. First experiments to culture adherent cells on appropriate biomaterials were carried out during the mid 1980s [12]. Since then, research activity in the area of biomaterials for TE continuously increased (Fig. 1.2). Today, it is known that an appropriate biomaterial represents the extracellular matrix (ECM) *in vivo* and a culture substrate *in vitro*. For TE applications 3D biomaterials should be porous analogues of the ECM of the tissue that

has to be regenerated. *In vitro* these artificial matrices support cell proliferation, migration, orientation, adhesion, differentiation and the synthesis of ECM material. After transplantation, the main function *in vivo* is to provide mechanical support until the newly formed tissue takes over this role [13]. Therefore, it is important to adjust the biomaterial properties (e.g. porosity, pore size and surface area) as precisely as possible [14]. At present, however, the physical characteristics of biomaterials, which might control stem cell fate, have rarely been explored.

Another core aspect of bone TE is the exposure of MSC to adequate mechanical stimuli [15]. In a healthy tissue, cell differentiation is controlled by various environmental factors of the cell surrounding, like body fluids, fibers, muscles and bone, which serve together as a natural matrix [16]. A static natural surrounding can be reconstructed by biomaterials; however, this static microenvironment cannot display dynamic processes in bone tissue. In order to create a natural dynamic cell surrounding, cultivations in bioreactors are performed. Different systems applying, for example, fluid flow or mechanical loading were shown to support osteogenic differentiation of MSC by mimicking *in vivo* conditions [17]. Besides imitating the natural microenvironment, dynamic bioreactor systems reveal several advantages in the area of TE. In addition to enhanced MSC differentiation, dynamic cultivations allow to overcome the limitation of nutrient supply, which occurs in static samples due to the slow diffusion process. Moreover, the use of bioreactors minimizes the risk of contamination, human errors and reduces labor input by automation. Consequently, bioreactor cultivation diminishes the costs of *in vitro* cell culture [17]. Furthermore, automation allows for the reproducible production of tissue structures with constant high quality. Although, the combination of biomaterials and bioreactors cannot exactly replicate the natural cell microenvironment, it can significantly improve *in vitro* culture conditions.

Objectives

Main goal of this work is the improvement of MSC differentiation into osteoblasts by artificially creating a natural cell microenvironment with constant cultivation parameters.

Based on the described background, the practical part of this work deals with the investigation of different ceramic and collagen-based biomaterials and their qualification for bone TE applications. A detailed examination of the biomechanical properties helps to reveal the advantages and disadvantages for the production of artificial bone constructs.

Moreover, long-term proliferation experiments on 3D matrices with human MSC allow the evaluation of biocompatibility and the determination of cell distribution. The differentiation potential of human MSC on the 3D biomaterials is first investigated under static conditions to verify, whether the mechanical properties or the chemical compositions influence osteogenic differentiation.

In order to further optimize the *in vitro* 3D microenvironment and produce artificial bone transplants, cultivation experiments in different dynamic bioreactor systems are carried out. Core objective is the cultivation of MSC on a 3D matrix under perfusion conditions. Finally, one bioreactor system is connected to a control unit, which allows the regulation and documentation of cultivation parameters. This process is required to satisfy good manufacturing practice (GMP) regulations and to produce transplantable bone tissue structures with a constant quality.

1 Theoretical background on biomaterials and bioreactor systems for bone TE

This theoretical chapter highlights important micro-environmental properties for stem cell differentiation and the interaction of MSC with their surroundings. In detail, the influence of biomaterial stiffness, geometry, topography, porosity and pore size on the differentiation of MSC is discussed. Moreover, a mechanism of cell-biomaterial interaction is slightly revealed (Fig. 1.1).

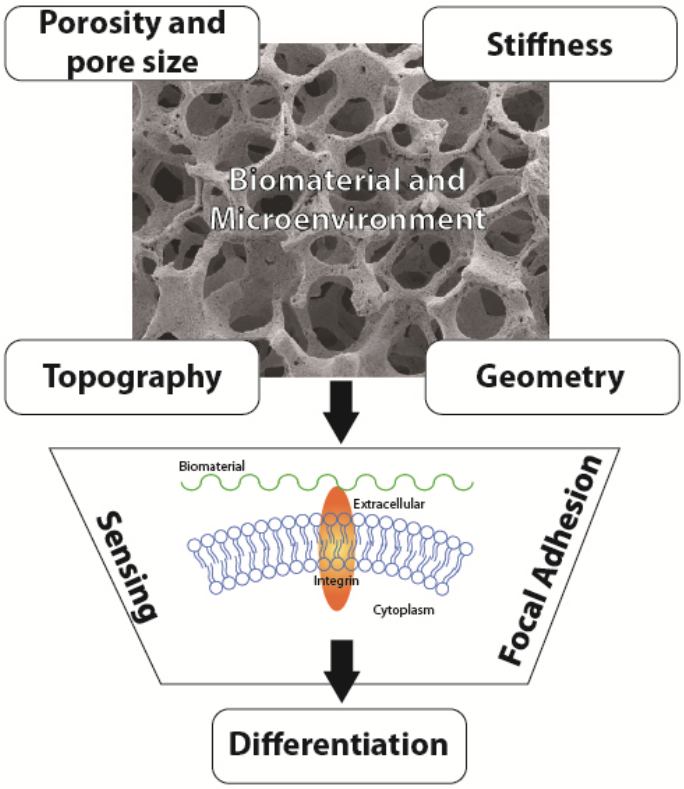

Fig. 1.1: Porosity, pore size, stiffness, topography and geometry of biomaterials have an impact on MSC differentiation transmitted by the focal adhesion complex.

Secondly, benefits of dynamic bioreactor systems for constructing artificial tissue structures are presented. The use of bioreactors, for example, not only minimizes the risk of contamination and labor input, but also allows for the application of different biomechanical stimuli, such as fluid flow or compression, which are known to enhanced MSC differentiation. Since the formulation of the Wolff's law (1892) [18] it is well known that bone tissue reacts and adapts to mechanical loads. Later, intensive research has been performed, especially in investigating the influence of fluid flow on MSC differentiation and tissue formation.

1.1 Biomaterials as an artificial extracellular matrix

Cells in 2D experiments lack the ability to form native tissue structures. Hence, investigations in the design of artificial 3D structures for TE applications increased tremendously over the last decade (Fig. 1.2). However, the selection of a biomaterial for *in vitro* cultivation and differentiation is often crucial. Generally, the ideal biomaterial should fulfill certain demands [14, 19, 20] in order to mimic the ECM. It should be:

1. Biocompatible.
2. Biodegradable or bioresorbable with a controllable degradation rate. Moreover, the degradation products should be non-toxic and shall not influence tissue regeneration.
3. Three-dimensional and highly porous with an interconnected architecture to allow for a uniform cell distribution and to facilitate the transportation of oxygen, nutrients and waste products.
4. Mechanically robust to withstand forces in the area of transplantation.
5. Equipped with a suitable surface for cell attachment, proliferation and differentiation.
6. Easily processible into various shapes and sizes to facilitate the incorporation into the damaged region.
7. Sterilizable to avoid bacterial, fungal and viral contaminations.

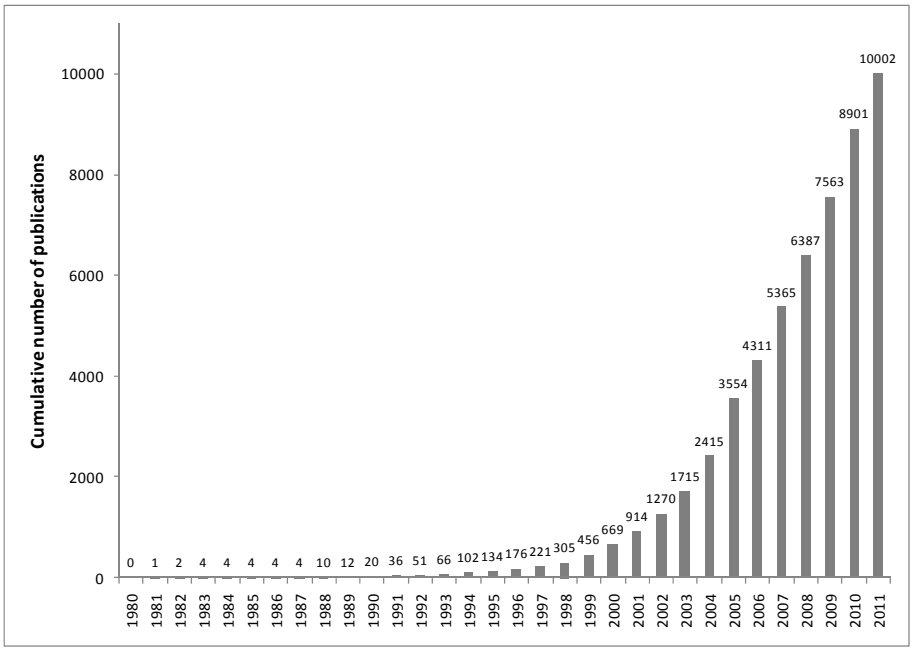

Fig. 1.2: Cumulative number of publications over the last three decades dealing with biomaterials in TE (entries in PubMed with the keywords "biomaterial" and "Tissue Engineering" until December 2011, searched at 01.06.2012).

For TE applications four groups of biomaterials have been studied intensively [19] (Tab. 1.1). Naturally derived organic biomaterials often lack the mechanical strength required by certain tissues, such as bone [10]. Other drawbacks are the rather low availability of these materials and their batch-to-batch variation [13]. Synthetic inorganic materials, such as β-tricalcium phosphate (TCP) or hydroxyapatite (HAP), are often used to engineer hard tissue matrices [21]. These materials are considered to be osteoinductive, as their surface supports osteoblastic adhesion, growth and differentiation [10]. But the rather brittle behavior of pure synthetic inorganic materials arouse the fabrication of composite materials [22], which combine synthetic inorganic materials with naturally derived components [20] (cp. section 1.1.1.5 Composite materials).

Tab. 1.1: Biomaterials for TE applications divided in four major categories.

Origin	Biomaterial	Reference
synthetic organic materials	aliphatic polyester	[23]
	polyethylene glycol	[24]
	poly-caprolactone (PCL)	[25-27]
	polylactic acid (PLA)	[28, 29]
	poly-(lactic-co-glycolic acid) (PLGA)	[30, 31]
synthetic inorganic materials	β-tricalcium phosphate (TCP)	[32]
	hydroxyapatite (HAP)	[32-36]
	glass ceramics	[37, 38]
organic materials of natural origin	Collagen	[39-43]
	gelatine	[44-46]
	fibrin	[47, 48]
	chitin/chitosan	[49-52]
	agarose	[45, 46]
	alginate	[53, 54]
inorganic materials of natural origin	corraline hydroxyapatite	[55, 56]
	magnesium (alloys)	[57-59]

1.1.1 The influence of biomaterial properties on stem cell differentiation

Controlling stem cell differentiation is nowadays one of the key issues in TE. It is well known that differentiation is influenced by a complex interplay of crucial parameters, for example, the combination of diverse growth and differentiation factors. But recent studies demonstrated that not only soluble biomolecules, but also the local microenvironment plays an important role in initiating and controlling MSC

differentiation [60]. The number of reports demonstrating that cellular behavior is modulated by biomaterial properties such as pore size, topography, geometry and stiffness increases steadily. These properties are described to control cell distribution, adhesion, migration, cell shape, proliferation and finally differentiation. The following chapters will mainly focus on the optimal biomaterial parameters for MSC differentiation into the osteogenic lineage.

1.1.1.1 Porosity and pore size

Porosity (percentage of void space in solid) and the pore size of biomaterials play a core role in tissue formation. A certain interconnected porous network is necessary to distribute oxygen as well as nutrients and to eliminate metabolic waste material. However, optimal pore sizes for the regeneration of different tissues have not yet been reported [61]. For bone TE applications pore sizes between 10 and 2250 μm have been implemented, resulting in varying degrees of tissue formation and in-growth [61-63]. Nevertheless, early studies of Hulbert *et al.* showed the minimum pore size required to generate mineralized bone to be 100 μm. Matrices with a smaller pore size resulted either in in-growth of unmineralized tissue or fibrous tissue [64]. Supposedly, too small pore sizes limit the transport of nutrients and the cell migration [61]. Additionally, increased porosity and pore sizes facilitate bone in-growth [65], even though depending on the biomaterials composition [66]. On the contrary, if pores are too large, the decrease in surface area limits cell adhesion [67] and increasing porosity affects the load-bearing capacity [68]. Therefore, porosity and pore size have to be within a specific range to maintain the balance between the optimal pore size for cell migration, mass transportation, vascularization and specific surface area for cell attachment, as well as mechanical stability.

A variety of optimal pore sizes for different tissues has been proposed (Tab. 1.2). These diverse numbers of optimal pore size and porosity might be caused by results obtained from various cell types or MSC derived from different origins. Another reason could be the difference in biomaterial fabrication, which results in varying pore architectures [69]. Many publications reported that for bone TE applications pores greater than 300 μm facilitate capillary formation and therefore direct osteogenesis [62, 66, 70]. To achieve osteoconduction pore sizes between 100 and 400 μm are generally preferred [71].

Designing matrix structures, which exactly imitate the *in vivo* bone formation is not a trivial process. Varying porosities and pore sizes are described for bone tissue *in vivo*. Human and mammalian bone is classified in two types:

1. Cortical bone, which is compact and usually located in the shaft of long bones (diaphysis) and in the outer bone shell.
2. Trabecular bone, also known as spongy bone, located in the end of long bones (epiphysis), in vertebrae and in flat bones like the pelvis.

Cortical bone is much denser, with a porosity of only 5 % to 10 % [72], whereas the porosity of trabecular bone ranges between 78 % and 92 % [73]. Because of the low porosity of cortical bone there exist no descriptions about pore sizes. However, various channels such as the Haversian channels cross the cortical bone. The Haversian channels contain blood vessels and nerve cells and are therefore responsible for nutrient supply and the conduction of nervous stimuli. These longitudinal channels have an average diameter of 50 μm [74]. The trabecular spacing has been measured by Hakulinen *et al.* via a quantitative ultrasound technique. A mean pore size 719 ± 110 μm has been calculated and compared to the data obtained by micro-computed tomography (μCT). Data of the μCT showed a much higher variation of trabecular spacing, with pore sizes ranging from 482 – 947 μm [75]. The difference in bone architecture indicates that the selection of a biomaterial with a certain pore size depends on the desired transplantation area.

Pore size and porosity do not only have an impact on stem cell fate, but also on the formation of shear stress in dynamic cell culture systems (cp. section 1.2 Bioreactors for Tissue Engineering applications). Small pore sizes, but especially tight intersections between the pores and a non-uniform pore distribution cause high shear stresses within the matrix. Briefly, shear stress can improve MSC differentiation, but a too high shear stress results in cell deformation or detachment. Irregular matrix geometries are mainly the consequence of the manufacturing process, such as freeze-drying [76] or salt-leaching [77], resulting in uneven pore distribution, which generates non-uniform shear stress profiles [78]. A solution could be the fabrication of matrices via rapid prototyping [79, 80]. Rapid prototyping is a method to construct complex matrix geometries layer-by-layer and at the same time control the pore size and pore distribution. On the one hand this procedure allows for the production of well defined model biomaterials, which suit GMP requirements. On the other hand these uniform geometries do not display *in vivo* physiological conditions. Another advantage of this fabrication procedure is the production of complex transplants by reading in data from computer-aided design drawings, allowing to exactly adjust the biomaterial to the damaged region.

Tab. 1.2: Proposed optimal porosities and pore sizes for the regeneration of different artificial tissues.

Differentiation	Cells	Biomaterial	Optimal Pore Size (µm)	Optimal Porosity (%)	References
Osteogenic	primary fetal bovine osteoblasts	PCL–HAP	450-750	60-70	[63]
Osteogenic	bm-hMSC	TCP	200-600	65	[65]
Osteogenic	rabbit BM-derived osteoblasts	natural coral	200	36	[81]
Osteogenic	bm-hMSC	coralline-HA	200	75	[82]
Osteogenic	rat bm-MSC	sintered titanium fiber mesh	250	86	[83]
Osteogenic	ad-hMSC	ZrO_2 ceramic	600	80-89	[84, 85]
Osteogenic	Dog bm-MSC	TCP	400-500	70	[86]
Chondrogenic	ad-hMSC	PCL	370-400	80-97	[69]
Chondrogenic	bm-hMSC	PCL	100-150		[87]
Chondrogenic	rabbit chondrocytes	chitosan-based hyaluronic acid hybrid polymer fibers	400	-	[88]
Chondrogenic	Human chondrocytes	Polycarbonate	8	-	[89]
Chondrogenic	Bovine chondrocytes	Polyurethane	<5-60	-	[90]
Myogenic	dog bm-MSC	50:50 PLGA	50-200	-	[91]
Hepatic	ad-hMSC	PLGA	120-200	50	[92]

1.1.1.2 Biomaterial stiffness

Even though most cells *in vivo* attach and proliferate on rather soft matrices, *in vitro* research today is mainly performed on stiff surfaces like glass or plastic. However, the influence of matrix stiffness on many cellular processes, for example migration [93, 94], adhesion [95, 96], cell shape [94, 96, 97], and proliferation [98] has already been verified. Furthermore, many recent publications confirm that matrix stiffness determines the fate of MSC and consequently their differentiation [99, 100]. Results of these experiments provide the evidence that MSC are able to sense the stiffness of their local microenvironment [101]. Discher *et al.* state that cells respond to the stiffness of their surrounding environment by adjusting their adhesion and their cytoskeleton. Their feedback to matrix stiffness is probably a change in the expression of integrins, cadherins and cytoskeletal proteins [97].

It has been found that elasticities similar to the *in vivo* tissue stiffness of brain (0.1 – 1 kPa), muscle (8 – 17 kPa) and nascent bone (> 34 kPa) evoked *in vitro* different hMSC responses. *In vitro* hMSC expressed neurogenic, myogenic and osteogenic key markers when cultivated in the same medium, but on biomaterials with the stated elasticities. Directed differentiation could be demonstrated without the addition of expensive differentiation factors [100]. Furthermore, Engler *et al.* stated that soluble differentiation factors tend to be less selective than matrix stiffness. MSC were cultured on soft matrices (0.1 to 1 kPa) in growth medium for either 1 or 3 weeks. Then, either myogenic or osteogenic differentiation medium was added. A decrease in gene expression of myogenic or osteogenic markers could only be observed during the initial week of cultivation in growth medium. After one week MSC committed to the lineage specified by the substrate stiffness. These results emphasize that the biomaterials surface stiffness has a significant influence on the determination of cell fate [100]. But by which mechanism do MSC sense the biomaterial stiffness and how do they transmit the information into differentiation signals? A possible answer to this question will be given in section 1.1.2: Sensing the Microenvironment.

1.1.1.3 Micro- and nanoscale topography

It is widely accepted that the topography of a biomaterial surface determines the biological cell reaction. The topography of matrices influences the cell adhesion [102], orientation and differentiation. However, these effects seem to be cell-dependent. Different cell types have been observed to show a preference for either a smooth or a rough topography [103]. According to their origin, osteoblasts prefer rougher surfaces, whereas fibroblasts favor smooth surfaces. In bone TE, it could be shown that an increased surface roughness enhances osteogenic differentiation [16, 104, 105]. These results, however, have been conflicting. Some publications report no change in response to rough surfaces [106] or even a reduction in cellular response [107]. One significant problem might be the low reproducibility of roughness. Even though two surfaces exhibit the same roughness, their topography can appear very different. Furthermore, intra-batch and inter-batch variations of biomaterials may cause difficulties. Other reports suggest the spacing between ligated integrins, which are essential for adhesion and signal transmission, to be less than 70 nm. Thus, larger nanoscale spacing fails to trigger differentiation signals [108-110].

It was demonstrated that cells may be influenced in their cell behavior and functionality by different topographic sizes, ranging from macro- to micro- and nanoscale features [111]. Until today the smallest feature size shown to affect cell behavior is 10 nm [112]. A sizable number of publications have described the positive

influence of nanoscale patterns on the differentiation of MSC. Osteogenic differentiation, for example, was observed on nano-pattern surfaces of 17-25 nm [113], 50 nm [114] and 100 nm [115, 116]. Even differentiation of hMSC into the neuronal lineage was monitored by using nanograftings of 350 nm as a culture substrate [117].

In several studies, cells grown on microscale rough surfaces demonstrated a lower proliferation rate compared to those grown on smooth surfaces. Furthermore, it was found that cells could not cross over large grooves, glens, holes and craters [16]. Cells within these irregular surface areas formed a confluent layer much faster than in regions of even surfaces due to limited space. Consequently, cells in grooves, glens, holes and craters showed the pile-up phenomenon, which results in bone nodule formation and finally in osteogenic differentiation. Moreover, cells grown on surfaces with strong roughness displayed a higher alkaline phosphatase activity and bone morphogenic protein production, which supports osteogenic differentiation. Graziano *et al.* also proved this effect by cultivating hMSC on convex and concave surfaces. Cells cultured on concave surfaces showed better cell-matrix interactions and after 30 days of cultivation the production of specific bone proteins, such as osteonectin and bone sialoprotein, was observed.

Summarizing the publications on the differentiation of MSC influenced by surface topography, it can be concluded that surface roughness may be used as an effective tool to enhance cell differentiation.

1.1.1.4 Geometry

Cells can not only sense the stiffness or roughness of their underlying substrate, but also the boarders and edges of their microenvironment. This so-called “pattern edge phenomenon” influences cell division, cell migration and the cytoskeleton dynamics [118, 119]. Nevertheless, the influence of two-dimensional substrate geometries (e.g. round or orthogonal edges) on stem cell differentiation has yet rarely been examined. Wan *et al.* hypothesizes that stem cell proliferation and differentiation is directed through positional defined mechanical stress and the resulting morphological cell changes [120]. In order to prove their hypothesis they cultivated human adMSC on different 2D patterns (rings of different diameters and rectangles of varying sizes). Osteogenic and adipogenic differentiation occurred in the same regions depending on the medium, containing cells with a small and elongated morphology. Within the ring patterns differentiation decreased with the radius from the inner to the outer ring, where mostly large spreading cells could be observed. Differentiation within the rectangles occurred mainly close to the short axis edge. Finally, it can be stated that the

geometry-derived forces affect cell morphology and cytoskeletal organization, which direct the stem cell proliferation and differentiation. Proliferation may be inhibited and differentiation may be induced by low levels of cytoskeletal tension due to increased cell-cell contacts. Similar results have been obtained by Wei Luo *et al*. They confirmed that the geometrical shape of the surface adhesion area affects the cell differentiation behavior. A pattern array of varying geometries, including octagon, pentagon, right triangle, square, trapezoid and triangle was designed to cultivate hMSC. Analysis of adipogenic differentiation was performed on day 3, 5, 10 and 14. Striking differences could be found in the rate of differentiation depending on the geometrical shape. To exclude the possibility that the surface area and therefore the population density influences the differentiation behavior, the area of each pattern was calculated for comparison. In summary, it was stated that only the pattern geometry has an influence on the adipogenic differentiation rate, but not the pattern area. However, a too low pattern area and therefore a decreased cell population does not result in cell differentiation. The differentiation process requires a minimum cell density [121]. The results of Wei Luo *et al.* presume that total differentiation within one pattern is elicit by the cells on the periphery of the pattern, which seem to be able to sense the edges of the pattern geometry [118, 119]. Introduction of high-throughput screening analysis tools will improve the knowledge of the correlation between pattern geometry and various differentiation directions.

1.1.1.5 Composite materials

Composite materials combine synthetic inorganic materials with naturally derived components [20] to construct a stable and bioactive matrix. The combination of these two components allows a precise adjustment of biomaterial properties. Four main different strategies to manufacture composite materials are well known (Fig. 1.3):

1. The physical mixture of a polymer and a ceramic component.
2. The embedding of bioactive molecules.
3. The integration of microspheres.
4. Surface functionalization.

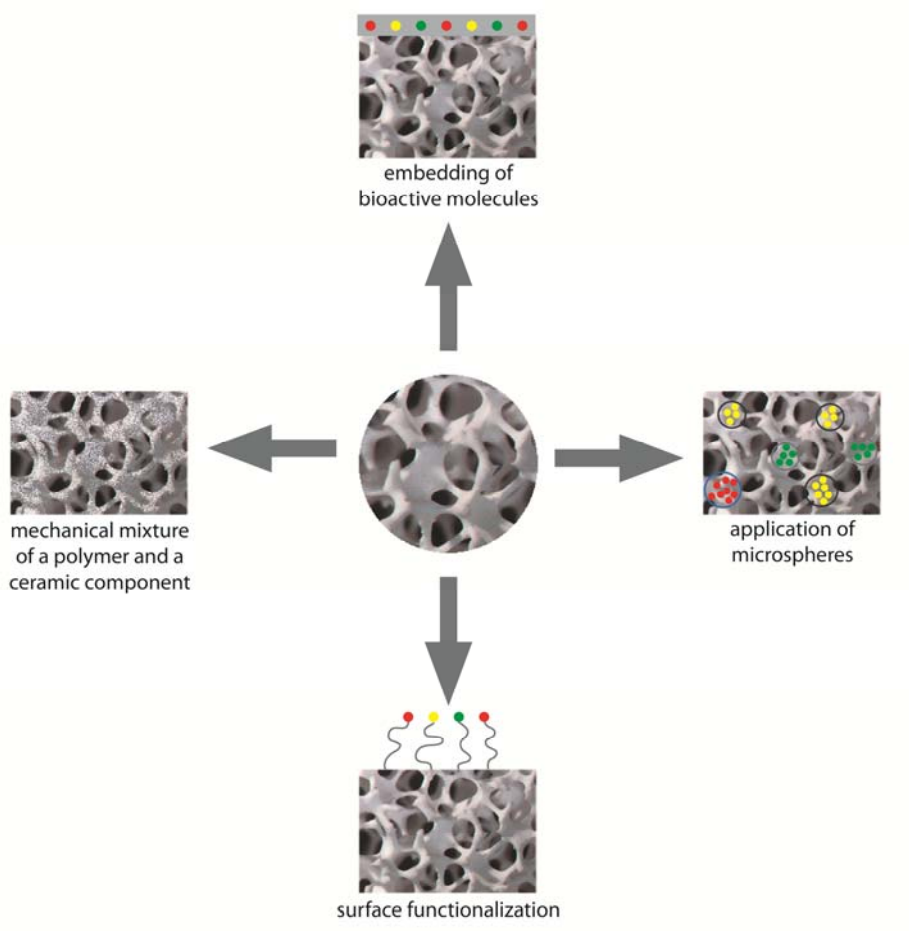

Fig. 1.3: Different fabrication methods of ceramic-based composite biomaterials (modified from [122]).

The most common method to fabricate composite materials is the physical mixture of a polymer and a ceramic component. The interaction of an organic and an inorganic component seems to be very attractive to regenerate hard matrix for bone TE application, because these composite matrices mimic natural bone properties. HAP and TCP are often used as inorganic components, since they are considered to be osteoinductive. Mostly they are mixed with the polymer as nano-particles or micro-particles.

The embedding of bioactive molecules into a suitable matrix is another effective approach for enhancement of stem cell differentiation. The objective is to control the release of signal molecules, for example, growth and differentiation factors. The release should be dose-dependent and exact in time and location. Different natural and synthetic polymers, such as PLGA [123, 124], gelatin [125], alginate [126] and fibrin [127] have been investigated for the embedding of bioactive molecules. These modified polymers can be combined with synthetic inorganic materials such as ceramics, resulting in a mechanically stable and bioactive matrix. The combination of these components can be realized by coating a porous ceramic with the modified polymer.

However, the polymer-coating can plug the pores of the ceramic and therefore negatively influence the transportation of nutrients and waste material. Thus, only biodegradable polymers such as poly-caprolactone [128] or poly-vinylpyrrolidone [129] in combination with highly porous ceramics should be applied. The release of the bioactive molecules is caused by the degradation of the polymer matrix. Degradation signifies the cleavage of polymers, due to an enzymatic or a hydrolytic process. Hence, dose and lifetime depend on the degradation rate; finally, resulting in a thin layer of bioactive molecules surrounding the matrix.

Another promising alternative to combine natural and synthetic components is the integration of microspheres. Microspheres are small spherical polymer particles with a porous inner matrix and a variable surface. Bioactive molecules can be captured within the inner matrix. Generally microspheres have a diameter of 1 to 500 µm. Smaller particles (10 to 1000 nm) are described as nanospheres. The biodegradable polymer microspheres are embedded in the pores of a ceramic matrix prior to cultivation. The major benefit of this method compared to the embedding of bioactive molecules into a polymer coating is the combination of different polymers with varying degradation profiles. Consequently, it is possible to create a time-controlled release of multiple growth and differentiation factors. Therefore, this method can be used to direct the differentiation behavior of MSC. The time-dependent release can be controlled by the variation of polymer properties. The most commonly used polymer for this application is PLGA [123, 124]. Moreover, alginates [130] and chitosans [131] are also frequently applied. An *in vivo* microenvironment can be simulated *in vitro* by applying different bioactive molecules and polymers with defined release profiles.

An alternative to create a bioactive surface on a ceramic matrix is its specific modification with biological compounds. Early studies showed a functionalization of the surface with extracellular matrix proteins, such as fibronectin or laminin [132]. These proteins support cell adhesion and proliferation. It is well known that only specific amino-acid sequences of these proteins interact with the integrins of the cells. Therefore, only short amino-acid sequences are used for surface modification. The sequence arginine-glycine-aspartic acid (RGD) [133-135] supports cell adhesion and has been studied in detail. Additionally, the AA sequences YIGSR (tyrosine-isoleucine-glycine-serine-arginine) [136], REDV (arginine-glutamine-aspartic acid-valine) [137] and IKVAV (isoleucine-lysine-valin-alanine-valine) [136] are used for TE surface modification. These sequences can be introduced into the 3D matrix network by physical, chemical, photochemical and ionic cross-linking.

1.1.2 Sensing the microenvironment

The modulating effect of matrix stiffness, topography and geometry upon cellular responses to biomaterials has been studied in detail over the past decades. It is obvious that cells have the ability to sense their microenvironment and react to the properties of their surrounding in a different manner. But what mechanism do the cells use to identify their substrate and how do they process the information obtained? Prior to sensing the surface elasticity, roughness or geometry the cells need to adhere on the substrate. The adhesion procedure is modulated by integrins, which are located in the cell membrane. Three mechano-chemical features are important during the adhesion process [138]: (1) The biomaterial-integrin binding forces have to pass a critical threshold, (2) the integrins must mechanically link the artificial matrix to the cytoskeleton in order to transmit extracellular forces to the cell interior and (3) the transmitted forces have to be translated to biochemical signals (mechanotransduction), resulting in a cellular response. But not only integrins are involved in the procedure of cell-matrix adhesion and signal transmission. Diverse protein networks dynamically link the artificial ECM to the intracellular actin cytoskeleton. These supramolecular structures are called focal adhesion. Proteins joining the focal adhesion complex have the ability to translate mechanical forces to biochemical signals and pass the information to the nucleus. However, the exact signaling pathways linking focal adhesion with the commitment of MSC are yet not completely understood. Nevertheless, several studies suggest that for osteogenic lineage commitment integrins activate the focal adhesion kinase (FAK), which influences cellular events through adhesion-dependent phosphorylation of downstreaming signaling molecules, especially the extracellular signal-regulated kinase (ERK) [139]. The ERK is a member of the mitogen-activated protein kinase (MAPK) family, which acts as a mediator of cellular differentiation. The final step of modulating differentiation is the translocation of ERK 1/2 to the nucleus, where it affects the expression of specific cellular transcription factors, such as Runx2, which regulates the expression of many osteoblast genes (Fig. 1.4) [100, 109, 138]. Even the time scale for this pathway has rudimentary been identified. The ERK is activated 30 min after the adhesion, which leads to the phophorylation of the osteogenic transcription factors within 8 days. After 16 days an increased level of osteogenic markers could be observed and after 21 days mineralized matrix was formed. These results confirm the observation in the study of Engler *et al.* (2006) that after one week a reprogramming of MSC by changing the differentiation medium is not possible.

Through focal adhesion and the FAK pathway cells can sense their surrounding stiffness, topography and geometry. However, the complete differentiation process is influenced by a variety of signals [138].

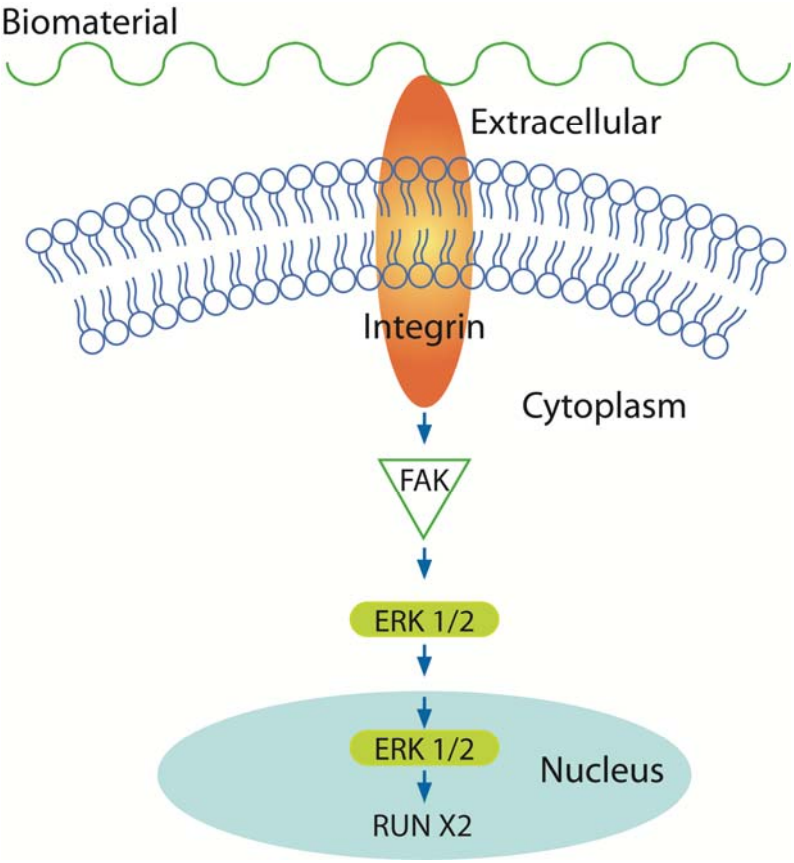

Fig. 1.4: The focal adhesion kinase (FAK) pathway. The first step in the transmission of extracellular forces presents the cell adhesion on the substrate modulated by integrins. The integrins activate the intracellular FAK and via multiple phosphorylation steps the ERK is translocated into the nucleus, where it affects the expression of specific transcription factors, such as Runx2.

1.1.3 Future perspectives on artificial extracellular environments

The effect of local microenvironment on cell behavior has important implications for regenerating tissues or healing disease-affected tissues. Therefore, further investigations in optimizing 3D structures of biomaterials which imitate a specific *in vivo* ECM in detail could be the key to future success in clinical TE. The results of Engler *et al.* demonstrated that the substrate features might even be more important than the medium composition [99]. Hence, a combination of, for example, different topologies or pore sizes within one biomaterial could be used to differentially functionalise implants without adding growth or differentiation factors. Thus, after transplantation different "zones" within one implant fulfill distinct functions [111]. These materials could, for example, be beneficial to create bone-cartilage constructs. Kon *et al.* achieved osteochondral regeneration in a sheep model by using a multilayered biomaterial [140]. The region mimicking the cartilage features contained

100% collagen type 1. In contrast, the area mimicking the bone ECM exhibited only 30% collagen type 1 and 70% HAP, which is considered to be osteoinductive. The transition between these two regions presents a layer of 60% collagen 1 and 40% HAP. However, the fabrication of matrices with varying features still remains a technical challenge [68].

An alternative future step in the optimization process could be a combination of TE and gene therapy. In 2002, Samuel *et al.* published the delivery of plasmid DNA to chondrocytes via a collagen–glycosaminoglycan matrix [141]. The idea is to genetically modify the cells which have direct contact to the biomaterial, in order to produce the required growth factors themselves and to modulate their own differentiation.

1.2 Bioreactors for Tissue Engineering applications

In order to engineer an artificial tissue not only the creation of a defined microenvironment plays a critical role, but also the exposure of the cells to adequate stimuli is shown to be beneficial [15]. For this purpose, numerous types of dynamic bioreactor systems have been designed for bone TE applications (Tab. 1.3).

Bioreactors are in many ways essential in the area of TE. Not only an enhanced differentiation of MSC (e.g. [142], [84]) could successfully be shown due to mechanical stimulation, but also an improved cell proliferation (e.g. [143], [144]) and distribution (e.g. [145], [146]) within the matrix. Moreover, the use of bioreactors minimizes the risk of contamination, reduces labor input due to automation and therefore diminishes the costs of *in vitro* cell culture. For example, the cell seeding process and the medium changes, could be automated by using a control unit [17]. Furthermore, the application of a bioreactor system often allows for monitoring various cultivation parameters, such as temperature, pH and oxygen concentration. This enables the engineering of tissues under controlled and reproducible production conditions [147] (Fig. 1.5). The production of an artificial transplant can be divided in two main parts: The controlled expansion of MSC [148] and the directed differentiation. Both steps shall be performed under controlled and regulated conditions in order to guarantee constant product quality and to satisfy GMP requirements. Therefore, research is intensively focusing on bioprocess monitoring. Several online measurement methods have, for example, been developed to monitor and determine the cell number during proliferation without detaching the cells from their substrate. These methods are often optical techniques based on light absorbance or real-time imaging [149]. However, not only monitoring of cell proliferation is important for product quality, but also the regulation and

documentation of cultivation parameters (pH, oxygen concentration and temperature) during proliferation and differentiation [150].

Tab. 1.3: Selection of dynamic bioreactor systems for bone TE applications (modified from [15]).

Bioreactor	Cells	Biomaterial	Reference
spinner flask	rat osteoblasts	PLGA foam discs	[145]
	rat MSC	PLGA foam discs	[143]
	human MSC	collagen films and biomaterials	[142]
rotating	rat osteoblasts	PLGA foam discs	[145]
	rat MSC	PLGA	[151]
	human MSC	Sponceram ceramic	[84]
Perfusion	rat osteoblasts	PLGA	[145]
	rat MSC	PCL/collagen	[152]
	human MSC	collagen membranes	[153]
direct mechanical strain	human osteoblasts	silicone dish	[154]
	human MSC	collagen type I	[144]
pulsed electromagnetic fields	rat osteoblasts	2D polystyrene	[155]
	human MSC	calcium phosphate	[156]

An additional process, which can be realized by using a bioreactor system, is the automated internal cell seeding. This step decreases the risk of contamination, because the operator does not have to reopen the bioreactor after sterilization, in order to place the biomaterial (Fig. 1.5). Automated dynamic internal cell seeding also results in an homogenous cell distribution [150], because the matrix is usually perfused by a cell suspension. A homogenous cell distribution cannot be accomplished by using conventional static cell seeding procedures, since the biomaterial is only perfused by the force of gravity. This static procedure usually results in an insufficient and superficial cell distribution, whereas cell proliferation and differentiation only occurs on the periphery of the matrix [157]. Lately, it has been investigated that the initial cell distribution is related to a uniform tissue generation. This could, for example, be proved by using a spinner flask containing biomaterials and a high density cell suspension. Cell seeding was generated by convection [150].

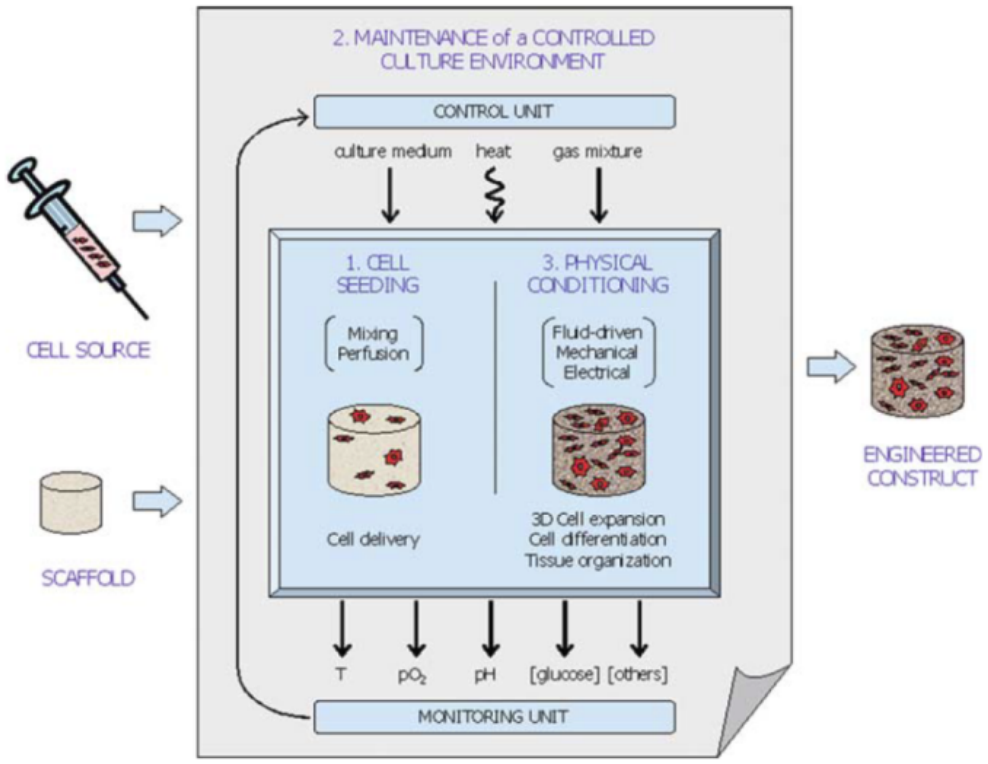

Fig. 1.5: Application of a control unit to direct cell seeding, culture environment and physical conditions in order to perform cell proliferation or differentiation. The monitoring unit documents and regulates the cultivation parameters (adapted from [147]).

Another important benefit of dynamic bioreactor cultivation is the enhanced nutrient transport compared to static cultures [17]. In a 3D static culture oxygen, glucose and other nutrients, as well as metabolic waste products are only exchanged by diffusion. The result is a gradient with a decrease of nutrient concentration toward the centre of the matrix [17]. Especially, in larger bone grafts, with a radius of more than 200-300 µm [158, 159], this effect results in reduced cell survival, with a necrotic core and an external shell of viable cells [159]. Further limitation of nutrient supply is generated by the production of mineralized ECM on the shell of the matrix. *In vivo* this limitation does not occur, since bone is a vascularized tissue with active nutrient transport. In addition to these advantages, dynamic cultivation exposes the cells to hydrodynamical or mechanical shear stress (Tab. 1.3), which act as a stimulus for MSC and often enhance differentiation, by triggering mechano-transduction signaling pathways (see chapter 1.2.1 and 1.2.2 for detailed examples).

1.2.1 Perfusion bioreactor system

The knowledge of limitation in mass transportation for static 3D cell culture approaches has led to the development of perfusion bioreactors using laminar flow. A further benefit of using these bioreactors is application of shear stress to the cells via

fluid flow. It is well known that applying load to bone generates interstitial fluid flow in the pores. Bone cells *in vivo* sense and react to the shear stress by increasing the intracellular calcium concentration and the release of signal molecules, such as nitric oxide and prostaglandin E_2 [160]. It is estimated in literature that bone cells experience *in vivo* shear stresses between 8 and 30 dyn/cm² [78]. In contrast, for dynamic 3D experiments the most common values are 0.1 to 0.5 dyn/cm². These values are even 10 to 50 times lower, then for experiments with 2D cell monolayers (about 5 dyn/cm²). This follows from the investigation of cell morphology in 3D microenvironments. Cells attach to a 3D surface in one of two morphologies: Flatly or bridged. Applying shear stress, bridged cells experience greater cytoskeletal deformation than flat cells. McMahon *et al.* explored cell morphology in a collagen-glycosaminoglycan matrix (pore size 95 µm, porosity > 98 %) with a confocal microscope and suggested 75 % of bridged and 25 % of flatly cell [2]. This phenomenon explains the low values implemented in 3D dynamic cultivations. Higher shear stress values might cause cell disruption.

Kim *et al.* explored the variation of medium flow within a special perfusion bioreactor system. The difference of parallel and transverse medium flow was investigated in detail, because diverse flow profiles create different biomechanical microenvironments within a 3D matrix [161]. In parallel flow conditions only the cells on the exterior of the matrix are exposed to fluid shear stress, where as in transverse flow conditions cells throughout the construct are exposed (Fig. 1.6). Since one major purpose of bioreactor systems is the generation of a suitable environment for the design of an artificial tissue construct, it is important to understand the influence of fluid flow patterns on the development of hMSC phenotype.

To determine the effect of parallel and transverse flow the following perfusion bioreactor was investigated (Fig. 1.6): A culture chamber with grooves for three biomaterials (in this case polyethyleneterephthalate) in a row connected to a medium container. To create parallel medium flow conditions, the two inlets of the bioreactor were connected with tubes to a multichannel peristaltic pump. Through the two outlets of the bioreactor the medium was pumped back to the reservoir. A flow rate of 0.1 ml/min was used for each medium channel. In order to create transverse flow conditions the bottom inlet and the top outlet of the culture chamber were locked forcing the medium to transversely pass the matrices with a flow rate of 0.2 ml/min. Dynamic cultivations were carried out for a period of 14 days for parallel and transverse conditions, respectively.

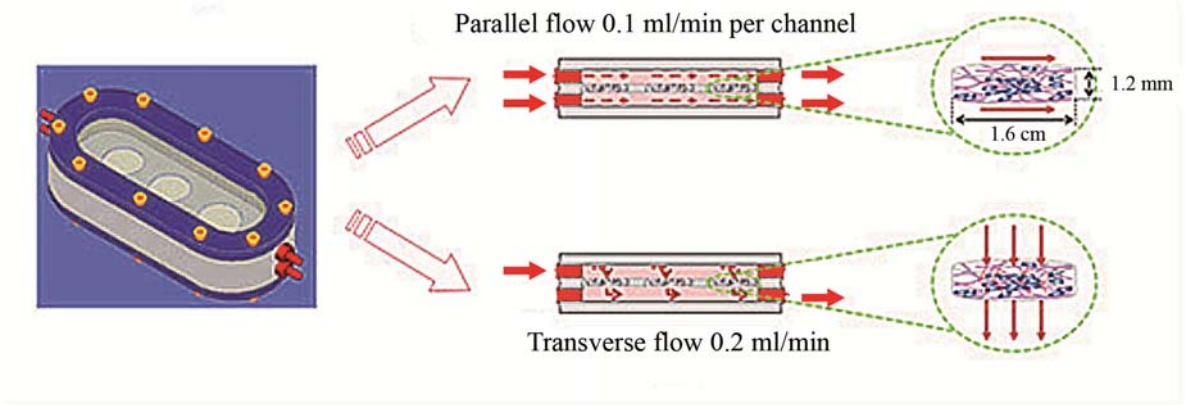

Fig. 1.6: Perfusion chamber to cultivate MSC under parallel or transverse flow conditions (modified from [161]).

Parallel flow conditions resulted in a constant ECM protein and mitogenic growth factor production. Moreover, the hMCS proliferation potential could be preserved. On the other hand transverse flow conditions induced osteogenic differentiation, proved by a higher alkaline phosphatase activity, calcium deposition and mRNA up-regulation of osteogenic bone markers, such as bone morphogenic protein 2, alkaline phosphatase, runt-related transcription factor 2 and osteocalcin. The results demonstrate the importance of regulating macroscopic flow to create the desired cell microenvironment. A potential future approach might be the successive application of parallel and transverse flow, in order to proliferate MSC prior to differentiation.

1.2.2 Biaxial rotating bioreactor system

Most bioreactors described in literature work with a uni-axial homogenous medium flow, such as the perfusion bioreactor system described in section 1.2.1 or rotating wall vessel bioreactors. Rotating wall vessel bioreactor systems were basically designed to simulate microgravity. Beneficial is the low level of shear stress caused by the laminar flow along the horizontal axis, the enhanced nutrient supply and removal of waste products due to rotation. Nowadays, different designs of rotating bioreactor systems are available for 3D bone TE (Fig. 1.7). One major disadvantage of the originally rotating wall vessel bioreactor is that matrices do collide with the wall of the chamber, which can damage the material or disrupt attached cells. This problem has been solved by using rotating bed bioreactors, in which matrices are fixed on the vessels wall. However, this solution could also not overcome the major disadvantage: Mineralization effects and culture benefits only occur on the outside of the matrices. The fluid flow through the biomaterials within this culture system is too small to optimally supply cells with nutrients and oxygen [15]. Consequently, various direct

perfusion bioreactors have been developed and tested for their application in TE (section 1.2.1 and Tab. 1.3).

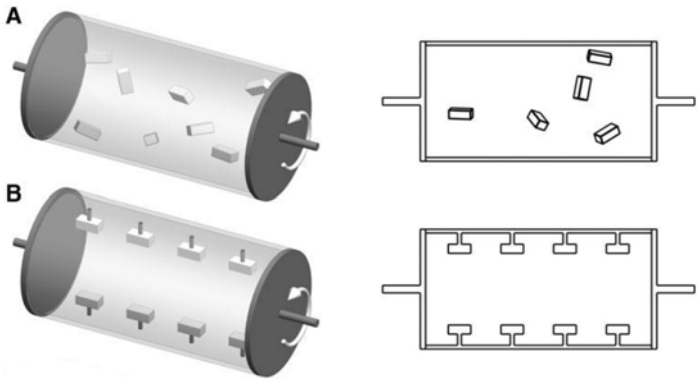

Fig. 1.7: Rotating wall vessel bioreactor (A) and rotating bed bioreactor (B) (modified from [15]).

Zhang *et al.* tried to overcome this uni-axial approach by designing a biaxial rotating wall vessel bioreactor with improved flow dynamics. Moreover, the bioreactor shall improve mechanical stimulus in order to activate mechano-transduction and promote osteogenic differentiation. This biaxial rotating wall vessel bioreactor consists of a spherical culture chamber with bioactive PCL-TCP composite matrices fixed to a stiff pin, which itself is located on the cap of the chamber. A medium reservoir and a pump allow the exchange of medium in the spherical compartment. The spherical culture chamber is developed to rotate around two axes (x and y) simultaneously (Fig. 1.8). In a first approach, matrices cultured with human fetal MSC under static or dynamic conditions were analyzed for cell viability, proliferation and osteogenic differentiation [162]. The culture of human fetal MSC on PCL-TCP in the dynamic biaxial bioreactor reached earlier cell confluence, higher cellular viability in the core of the matrix (2000 µm from the surface), greater alkaline phosphatase expression, calcium deposition and bone nodule formation. In a further approach, the artificially manufactured bone constructs were implanted to mice. The result was a higher *in vivo* ectopic bone formation compared to statically cultured matrices [162].

Furthermore, the biaxial rotating wall vessel bioreactor was systematically compared with the three most commonly used bioreactor systems for bone TE applications: Spinner flask, perfusion bioreactor and uni-axial rotating wall vessel bioreactor [158]. Samples of the biaxial rotating wall vessel bioreactor showed earlier cellular confluence and a more homogenous cell distribution. Additionally, they presented a higher level of osteogenic differentiation, verified by von Kossa staining, alkaline phosphatase expression and calcium deposition. Samples of the other three bioreactor systems showed significantly less osteogenic differentiation. These results suggest the clinical application of this bioreactor setup to treat critical size bone defects.

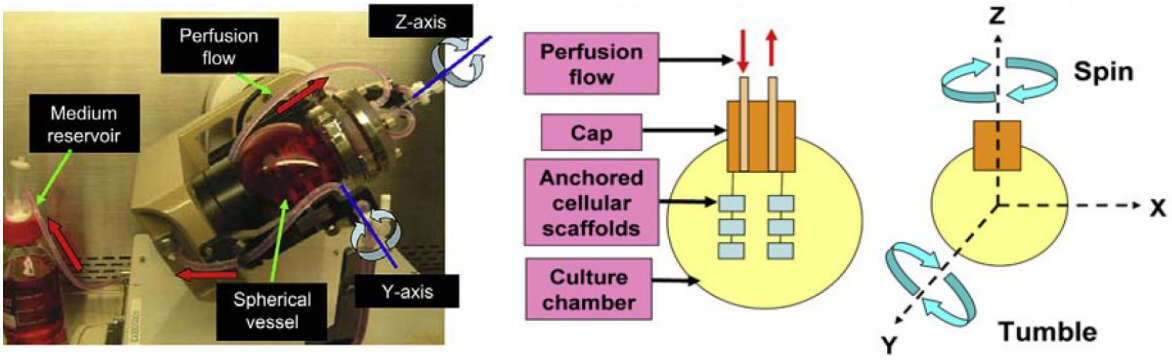

Fig. 1.8: Biaxial rotating wall vessel bioreactor consisting of a spherical vessel and a medium reservoir. Biomaterials are fixed on a stiff pin, which itself is located on the cap of the vessel. In addition, the vessel rotates around the x- and the y-axis (adopted from [162] and [158]).

Summing up the theoretical background of this work, it can be stated that shaping the biomaterials mechanical properties in means of porosity, pore size, stiffness and topology can significantly influence MSC behavior and differentiation. Investigations in this area will have a great impact on future 3D cell culture experiments. Furthermore, bioreactors for dynamic cultivation procedures gained of importance over the last two decades. Intensive investigations showed the benefit of mechanical stimulation to osteogenic differentiation of MSC. In addition, dynamic bioreactor systems can be setup to fulfill the requirements for a GMP-conform production of tissue structures, such as an automated regulation of process parameters and a continuous documentation.

2 Practical work

Goal of the experimental part is to enhance osteogenic differentiation of adipose and umbilical cord derived MSC (adMSC and ucMSC) by artificially creating a natural surrounding. MSC isolation procedures are described in detail in section 5.5.1 and 5.5.2. Therefore, 2D cultures of MSC are first stimulated with fluid flow using a dynamic culture system, in order to imitate the natural fluid flow within bone tissue. In a second approach, MSC are statically proliferated and differentiated on various soft and hard 3D biomaterials, trying to imitate the natural bone structure. Previously, the mechanical properties of these biomaterials are characterized in detail. The identification of, for example, pore size and pore distribution is essential to describe the cell microenvironment. The following step attempts to combine these two approaches by using 3D biomaterials and applying fluid flow stimulation. To reach this aim, different dynamic bioreactor systems are developed and optimized. In a last step one specialized bioreactor system is set up for the connection to a control unit, which has been developed in cooperation with Sartorius Stedim Biotech (Goettingen, Germany). This approach is essential to create stable and reproducible production conditions for artificial bone tissues. These so called GMP conditions are required to ensure a constant transplant quality. The developed system allows the control, regulation and documentation of the following cultivation conditions: pH, pO_2, temperature, gas flow, weight, pump rate, fresh medium supply and waste removal.

2.1 Fluid flow stimulation MCS cultures in a 2D microenvironment

Previous works have shown an enhanced osteogenic differentiation of MSC by mechanical fluid flow stimulation. However, most of the experiments were carried out with osteoblast cell lines or non-human MSC [78]. It was shown that non-human MSC react to a fluid shear stress of 0.1 to 20 dyn/cm² in a 2D microenvironment applying different flow types (steady, pulsatile or oscillatory) with osteogenic differentiation. Most commonly, the application of 5 dyn/cm² is described in literature. In this context, a 2D culture chamber (µ-Slide $I^{0.8}$ Luer, Collagen IV coated) for the cultivation of adherent cells from the company IBIDI GmbH (Fig. 2.1) was used to stimulate adMSC and ucMSC by fluid flow. Cell seeding and medium exchange was performed according to the instruction in section 5.7.1. Briefly, $2.8*10^4$ cells in 200 µl culture medium were seeded per µ-Slide and cultivated until 100 % confluence prior to applying fluid flow.

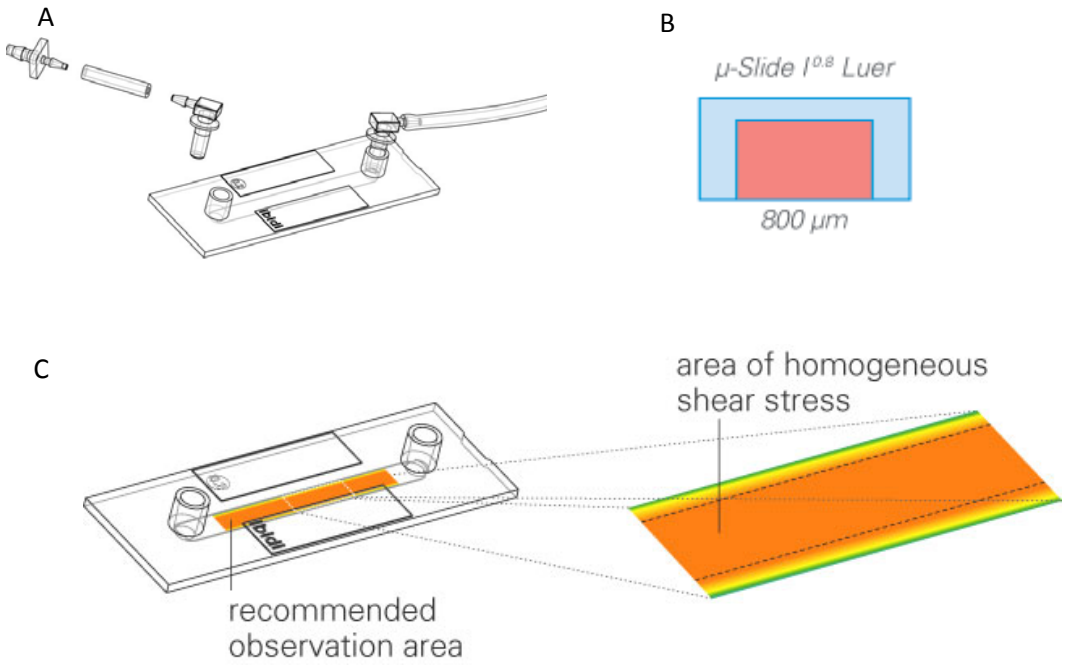

Fig. 2.1: (A) IBIDI μ-Slide $I^{0.8}$ Luer, with luer lock connection, for the 2D cultivation of adherent cells applying fluid flow, (B) height of the μ-Slide $I^{0.8}$ channel is 800 μm and containing a volume of 200 μl, (C) area of homogeneous shear stress is only given in the labeled area of the μ-Slide (pictures adopted from the manufactures website).

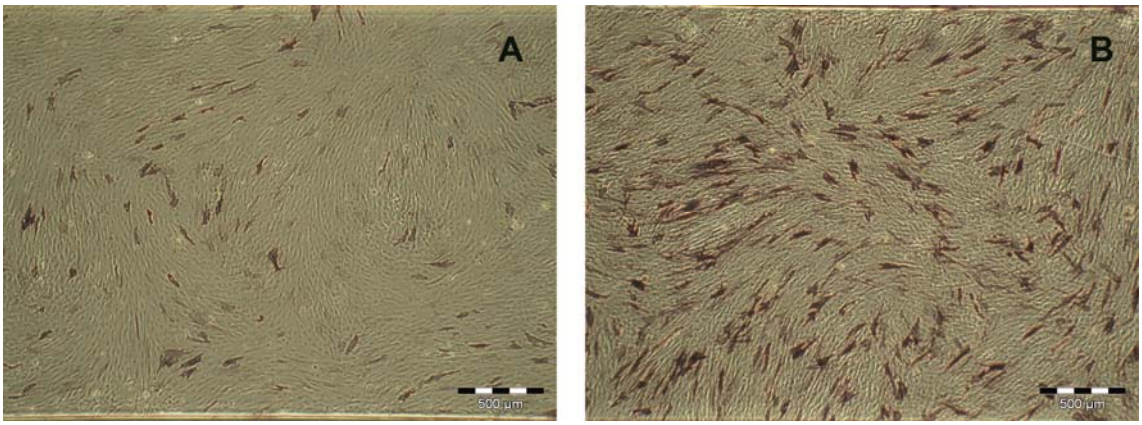

Fig. 2.2: (A) Membrane-bound AP staining of ucMSC after static cultivation and (B) after dynamic cultivation applying two times 4 hours fluid flow of 0.1 dyn/cm² with a 4 hour break in-between.

In a first experiment, a confluent ucMSC culture was only stimulated two times for 4 hours with 0.1 dyn/cm² and a 4 hour break in-between. Applying this stimulation pattern a significantly higher production of membrane-bound alkaline phosphatase (AP) can be observed compared to static cultivation (Fig. 2.2). AP is well known as a specific marker of bone synthesis and an early indicator for osteogenic differentiation [163, 164].

In a next approach, stimulation of 2D cultures in IBIDI μ-Slides $I^{0.8}$ Luer were carried out for seven days with a daily increasing fluid flow rate from 0.1 to 1.2 dyn/cm², according to the pattern shown in section 5.7.1 (Fig. 5.8). First, the experiments were carried out with culture medium using ucMSC. This experiment already reveals a beginning osteogenic differentiation of ucMSC, compared to the static control (Fig. 2.3, A, B). Mineralization of the ECM can be observed by von Kossa staining. However, the osteogenic differentiation can once more be enhanced by replacing culture medium for osteogenic differentiation medium from Miltenyi Biotec (ODM-M) (Fig. 2.3, C, D). Besides mineralization of the ECM by using ODM-M, also calcium accumulations can be detected with the help of Calcein staining (Fig. 2.4). These accumulations were not observed in experiments using culture medium.

Identical experiments, carried out with adMSC, show similar results; an enhanced membrane-bound AP production (Fig. 2.5, A, D) and a beginning mineralization of the ECM (Fig. 2.5, B, E). However, after the stimulation with fluid flow for seven days using culture medium already calcium accumulations can be observed (Fig. 2.5, C, F). An advanced osteogenic differentiation of adMSC can be achieved without using osteogenic differentiation medium, which contains differentiation factors, such as α-ascorbate and β-glycerolphosphate. The isolated amount of RNA was not sufficient to perform PCR experiments.

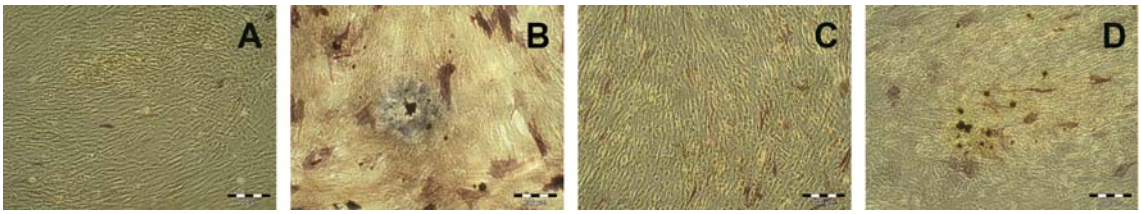

Fig. 2.3: Von Kossa staining of ucMSC after seven days of (A) static cultivation and (B) dynamic cultivation in culture medium, (C) static cultivation and (D) dynamic cultivation in ODM-M.

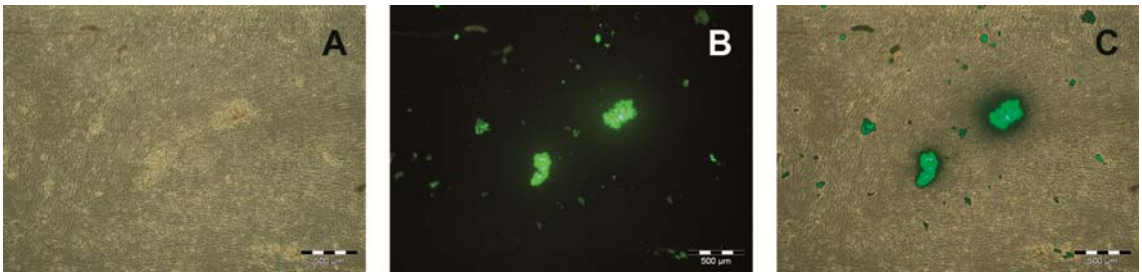

Fig. 2.4: Calcein staining of ucMSC after 7 days of dynamic cultivation in ODM-M: (A) Phase contrast image of the selected area, (B) fluorescence microscope image and (C) overlay.

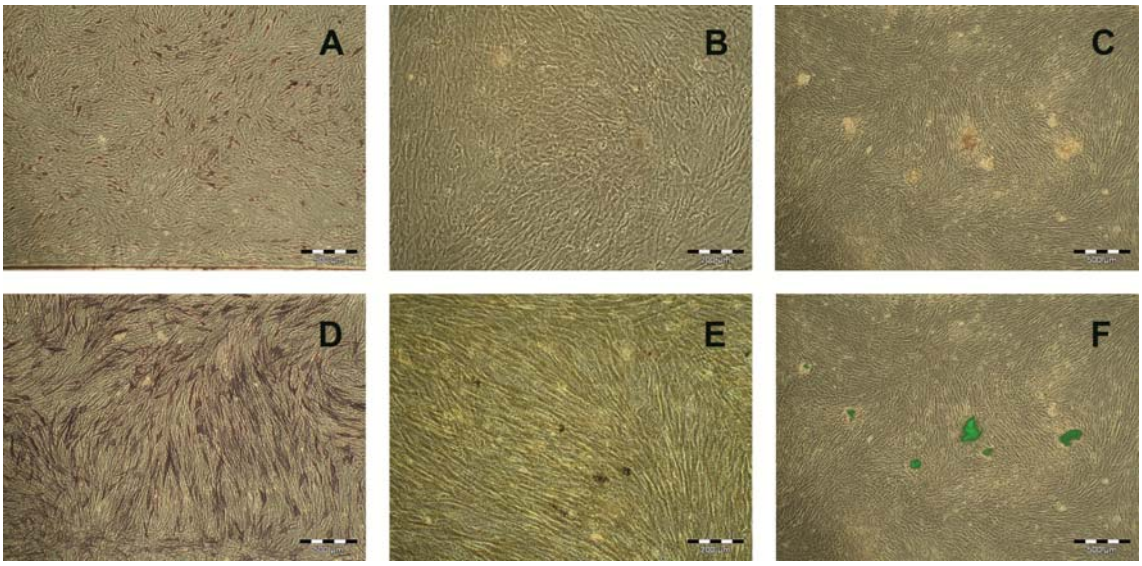

Fig. 2.5: Membrane-bound AP staining of adMSC after 7 days of (A) static and (D) dynamic cultivation in culture medium; von Kossa staining: (B) static and (E) dynamic cultivation; Calcein staining of the dynamic cultre: (C) phase contrast image and (F) fluorescence image overlay.

In addition to the osteogenic differentiation a change of morphology can be observed by applying fluid flow. Cells are not aligning to the direction of fluid flow, but especially adMSC possess a elongated cell shape compared to the static control (Fig. 2.5, A, D). Moreover, a non-uniform cell distribution in the μ-Slide channel can be noticed (Fig. 2.6). Less cells can be observed at the entrance of the fluid flow than in the middle of the chamber or at the exit. Most cells are found at the exit of the chamber. This indicates a migration of the cells with the fluid flow or they also might detach from the μ-Slide surface at the entrance and reattach at the exit. Detachment generally occurs during cell division, as cells reduce their contact to the surface.

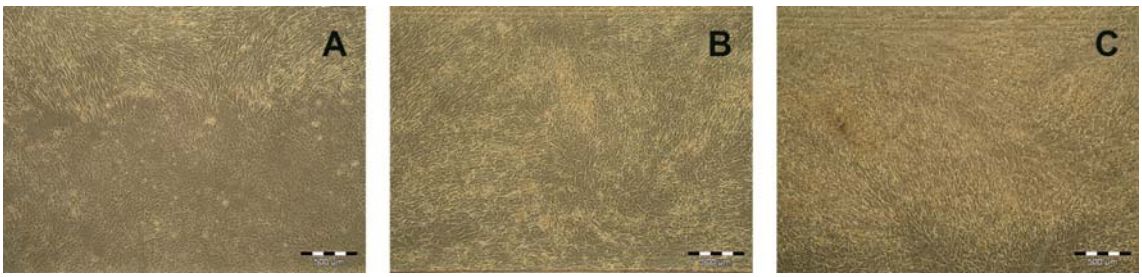

Fig. 2.6: Phase contrast microscope images of ucMSC after 7 days of dynamic cultivation in ODM-M at the entrance of fluid flow into the μ-Slide chamber (A), in the middle of the chamber (B) and at the exit (C).

In summary, applying fluid flow on 2D MSC cultures using a commercially available culture camber caused a change of cell morphology, but no alignment of the cells to the direction of fluid flow. Moreover, the application of fluid flow enhanced the production of membrane-bound AP and caused a beginning mineralization of the ECM, without using any differentiation factors. These processes are major indicators

for the osteogenic differentiation of MSC. It could also be shown that the combination of fluid flow and osteogenic differentiation medium containing differentiation factors is a potent combination to further enhance the differentiation process. Calcium accumulations in the ECM of ucMSC could only be identified by applying fluid flow and using ODM-M.

Long-term cultivation (> one week) of MSC within this system was not feasible, since this culture system does not display physiological cell conditions. After one week of dynamic cultivation cells started detaching from the surface, as the surface area was not sufficient for further cell proliferation. Therefore, a homogenous mineralization of the ECM could not be achieved. In order to create rather physiological cell surroundings 3D biomaterials are often used (described in detail within the next chapters). An interesting approach in TE is the combination of 3D matrices, fluid flow and osteogenic differentiation medium to achieve an advanced and homogenous MSC differentiation (cp section 2.6). Another future approach could possibly be the separation between the proliferation and differentiation process. Proliferation could e.g. be performed under static conditions, followed by a dynamic cultivation procedure to evoke differentiation. MSC proliferation decelerates over the cultivation period with the number of cell divisions and due to limited space. With this approach the risk of cell detachment could be minimized.

2.2 Characterization of 3D biomaterials to define the microenvironment for bone Tissue Engineering applications

3D biomaterials are known to be utilized in the production of alternative bone grafts. In the area of TE 3D matrices are frequently applied, because their often highly porous structure increases the available surface area for MSC or other cell types. Moreover, biomaterials have the advantage to imitate physiological environment. The combination of 3D materials with MSC is studied intensively to build up a functional tissue graft. In this approach the selection of a suitable matrix is a crucial factor. Biomaterials should not only obtain a highly porous and interconnected geometry to allow vascularization, but also withstand mechanical loads after transplantation. Moreover, the matrix should have a rough surface structure to improve cell attachment and enhance adhesion. Therefore, the detailed characterization of the biomaterials mechanical properties is of importance [165].

The following characteristics were investigated for the ceramic biomaterials mentioned in Tab. 2.1: Porosity, pore size, homogeneity of pore size, surface area, permeability,

surface texture and stability. These analyses are necessary to ensure stable matrix quality within one batch of biomaterial production. A constant matrix quality is indispensable to satisfy GMP requirements. For the collagen-based matrices mentioned in Tab. 2.2 only the materials 3D geometry and the stability were characterized.

Tab. 2.1: Intensively characterized ceramic biomaterials.

Biomaterial	Manufacturer	Dimension	Chemical composition	Fabrication
Sponceram-Al	Zellwerk GmbH	d = 10 mm ht = 3 mm	zirconium dioxide ceramic with aluminum oxide coating	Sintering
Osseolive	Curasan AG	d = 10 mm ht = 3 mm	calcium alkali orthophosphate glass ceramic	slip-cast technique
Cerasorb M	Curasan AG	d = 10 mm ht = 2 mm	ß-tricalciumphosphate ceramic (TCP)	slip-cast technique
45S5-Bioglass	University Erlangen-Nuremberg, Department of Materials Science and Engineering	d = 10 mm ht = 3 mm	silicate glass ceramic	sintering

Tab. 2.2: Characterized collagen biomaterials.

Biomaterial	Manufacturer	Chemical composition	Fabrication
Matriderm	Medskin solutions Dr. Suwelack	Bovine collagen with 1.3 - 1.7 % estastin hydrolysate	Freeze-drying
Collagen-BG	Medskin solutions Dr. Suwelack	Bovine collagen with 6% of bioglass	Freeze-drying
Collagen-Silk	Medskin solutions Dr. Suwelack	Bovine collagen with 10 % of silk protein	Freeze-drying

2.2.1 Characterization of the surface texture

The surface texture was observed by taking multiple images with a scanning electron microscope (SEM). Lower magnifications give a first impression of the biomaterials formation (Fig. 2.7, A-D), while, higher magnifications show the surface structure in detail (Fig. 2.7, E-H).

SEM images indicate a rather rough surface for all tested ceramic biomaterials, but with clear differences. Sponceram-Al, for example, shows the very small-sized, but rough aluminum oxide coating on the materials surface, however, the coating does not seem to be uniform. The surface of Osseolive is also uneven, but possessed a honeycomb structure. These two biomaterials possess a macro-porous structure (Fig. 2.7, A, B), but their surface is compact (Fig. 2.7, E, F). On the contrary, Cerasorb M and 45S5-Bioglasss possess open structured micro-porous surfaces (Fig. 2.7, G, H). This design increases the biomaterials' roughness and surface area, respectively

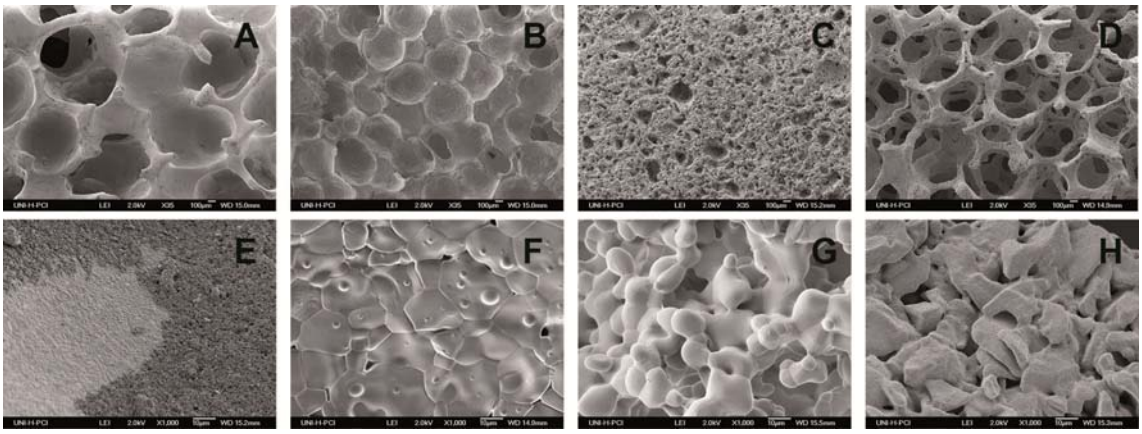

Fig. 2.7: SEM images of Sponceram-Al, Osseolive, Cerasorb M and 45S5-Bioglass with 35-times magnification (A-D) and 1000-times magnification (E-H).

2.2.2 Characterization of the 3D architecture

Given that the analysis of the biomaterials geometry is not feasible by taking 2D SEM images, the 3D morphology was investigated by using the high resolution nanofocus computed tomography (nanoCT) technique (cp. section 5.6.2). Experiments were carried out at GE Healthcare (Wunstorf, Germany). By means of the obtained data and different mathematical methods, the identification of various quantitative data was possible. Mathematical calculations were performed by VSG (Visual Sciences Group, Duesseldorf, Germany).

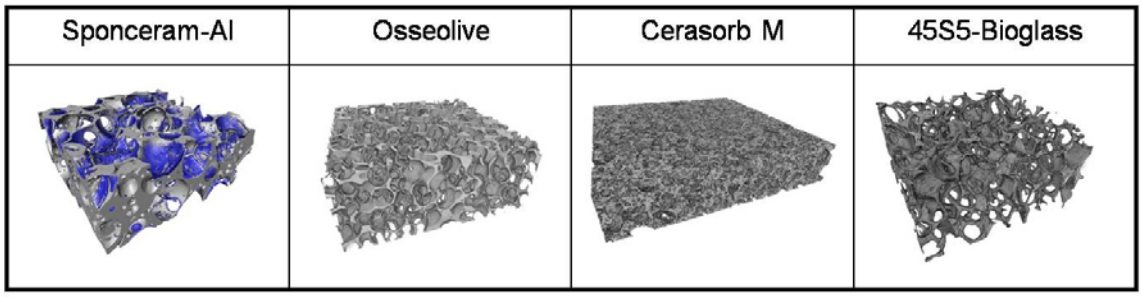

Fig. 2.8: 3D images of the geometry of different ceramic biomaterials created by nanoCT scans.

NanoCT images give an impression of the biomaterials 3D architecture. 45S5-Bioglass, for example, indicates a highly porous and interconnected structure, compared to Cerasorb M, which appears very dense. Moreover, the nanoCT image reflect that the aluminum oxide coating on Sponceram-Al does not cover the entire surface (Fig. 2.8, indicated in blue).

Cross-sections of collagen-based biomaterials created by nanoCT scans indicate that these matrices consist of a dense mesh of collagen fibers (Fig. 2.9). Significant differences can be detected between the three collagen-based biomaterials. Matriderm consists of a dense mesh of very short collagen fibers, whereas Collagen-BG and

Collagen-Silk additionally contain longer fibers. Collagen fibers in Matriderm and Collagen-Silk are not arranged in one specific direction. In contrast, the 3D image of Collagen-BG indicates an alignment of longer fibers. Moreover, the nanoCT image of Collagen-BG allows for the detection of the bioglass component within the collagen network. They are displayed as small, round, white dots in the matrix. Collagen has been mixed with a bioglass powder of 5 µm particle size.

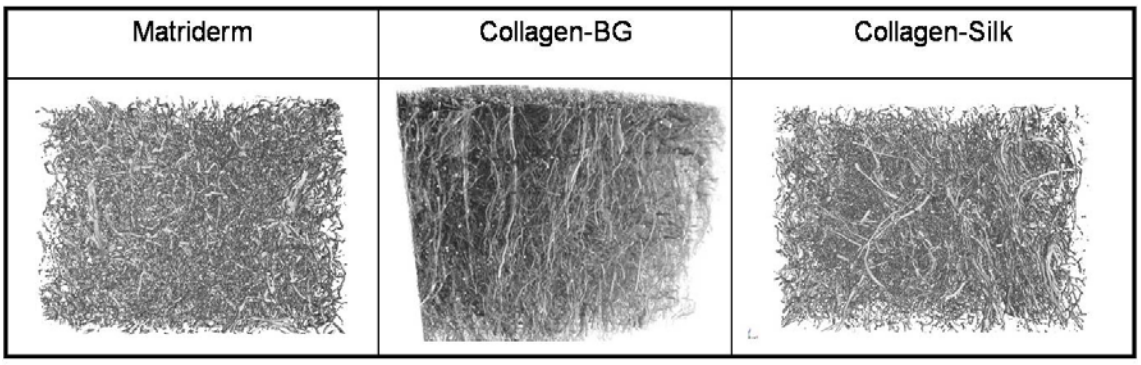

Fig. 2.9: 3D images of the geometry of different collagen-based biomaterials created by nanoCT scans.

2.2.3 Determination of porosity, pore size and surface area

In a next approach five samples of each ceramic biomaterial were scanned by nanoCT and the data mathematically analyzed (cp. section 5.6.2), in order to determine the intra-batch variability. In doing so, the porosity, pore size, homogeneity of pore size and surface area were in main focus.

The tested biomaterials show a huge difference in interconnected porosity. Cerasorb M possesses with 17.52 % (n = 5) the lowest porosity, whereas 45S5-Bioglass has an average porosity of 89.49 % (n = 5). Fig. 2.10 (A) indicates that Osseolive has a high variability of interconnected porosity (n = 5), whereas the other ceramic biomaterials show a rather low variability. A detailed look on the five Osseolive samples shows porosities from about 13 % to 56 % (Fig. 2.10, C). A vertical cross-section image of Osseolive indicates compact areas within the matrix without any void space (Fig. 2.11, A). Moreover, an average non-interconnected (closed) porosity of 1.36 % was calculated for Osseolive (not graphically shown). In comparison, no compact areas (Fig. 2.11, C) and only a closed porosity of 0.12 % is detected in 45S5-Bioglass. For Sponceram-Al not only a cross-section was generated, but also closed porosity (2.04 %) is presented in a 3D image (Fig. 2.12). Closed porosity within the matrix is indicated by spheres of different colors, signifying varying volumes.

Though, Cerasorb M obtains the lowest porosity, it has the highest surface area (n = 5) of all scanned biomaterials (7.22 mm^2/mm^3). This effect results from very small pores

(average pore diameter of 190 µm, Tab. 2.3), a micro-porous surface structure (Fig. 2.7, G) and a good balance between void space and biomaterial (Fig. 2.11, B), compared to the other matrices. The average surface area of Sponceram-Al and 45S5-Bioglass is about 5 mm^2/mm^3 and of Osseolive 3.56 mm^2/mm^3 (Fig. 2.10, B). This is the consequence of enormous compact areas and enclosed surface area within the Osseolive biomaterial (Fig. 2.11, A).

Furthermore, 2D cross-section images created from the nanoCT scans help to identify the wall thickness of the pores. It is obvious that, for example, pores of Osseolive obtain thicker walls than 45S5-Bioglass. Generally, thicker pore walls result in a higher stability (cp. section 2.2.5), which also is dependent on the biomaterials chemical composition.

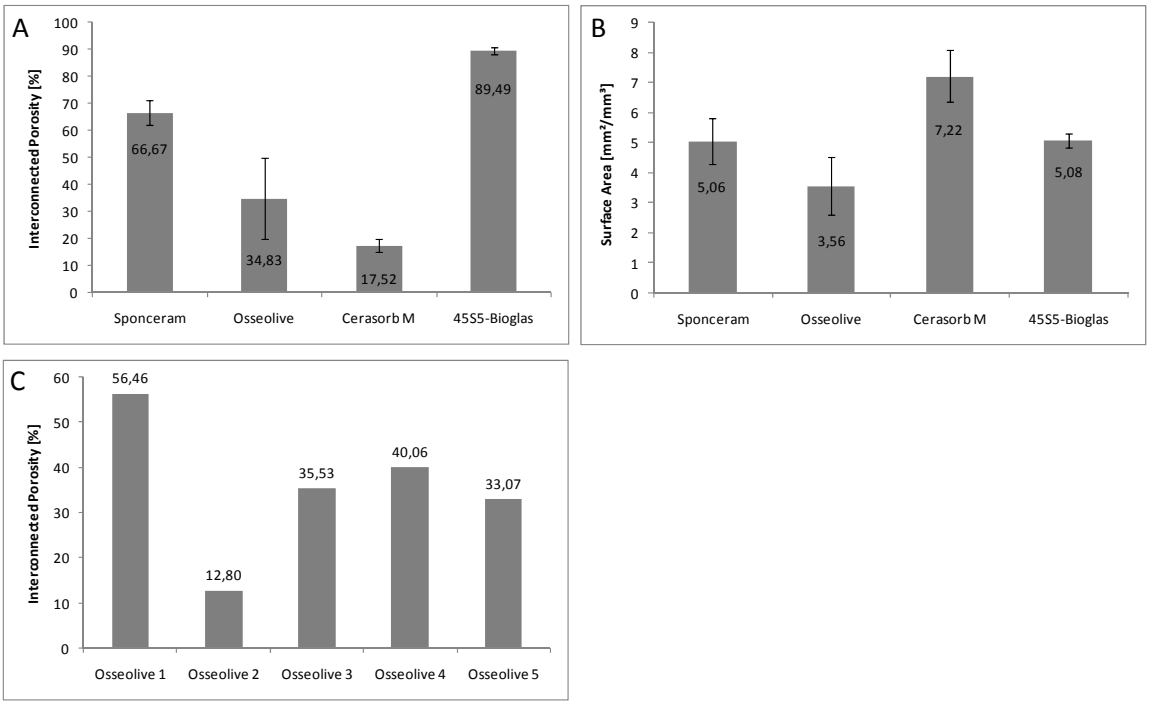

Fig. 2.10: (A) Interconnected porosity (n = 5) of the ceramic biomaterials, (B) surface area (n = 5) and (C) interconnected porosity of five different samples of Osseolive.

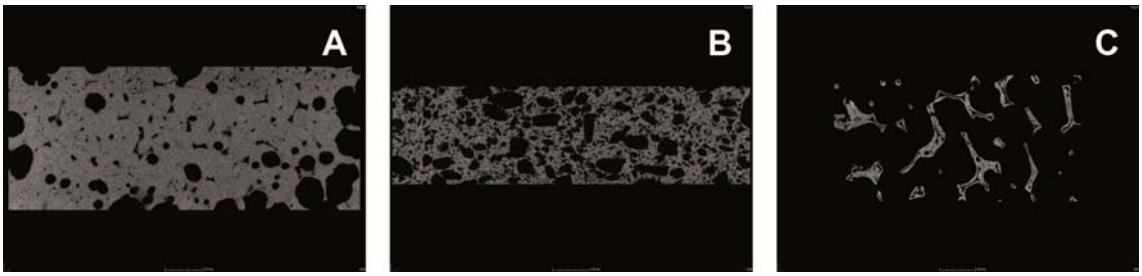

Fig. 2.11: Vertical cross-section of Osseolive, sample 2 with 12.8 % porosity (A), Cerasorb M (B) and 45S5-Bioglass (B), generated by a nanoCT scan.

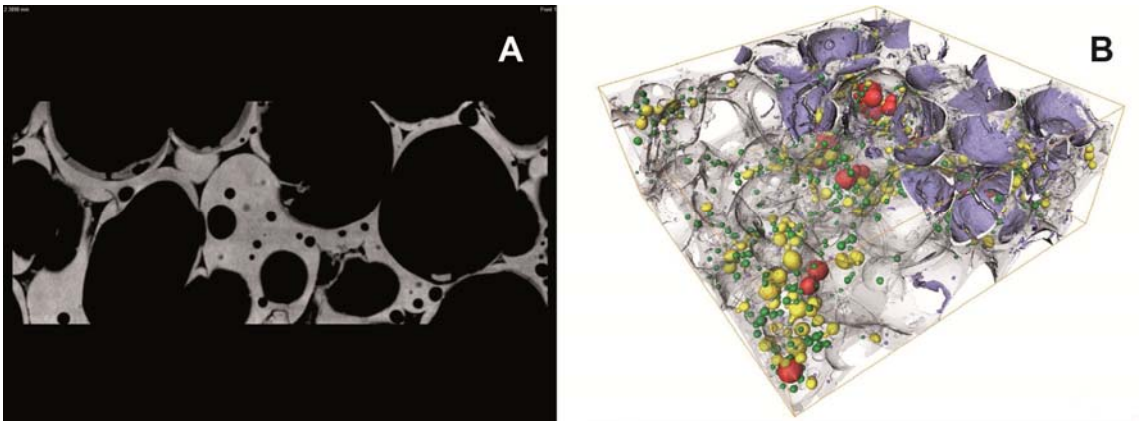

Fig. 2.12: Vertical cross-section of Sponceram-Al generated by a nanoCT scan (A) and 3D image of non-interconnected (closed) porosity generated by Avizo (B).

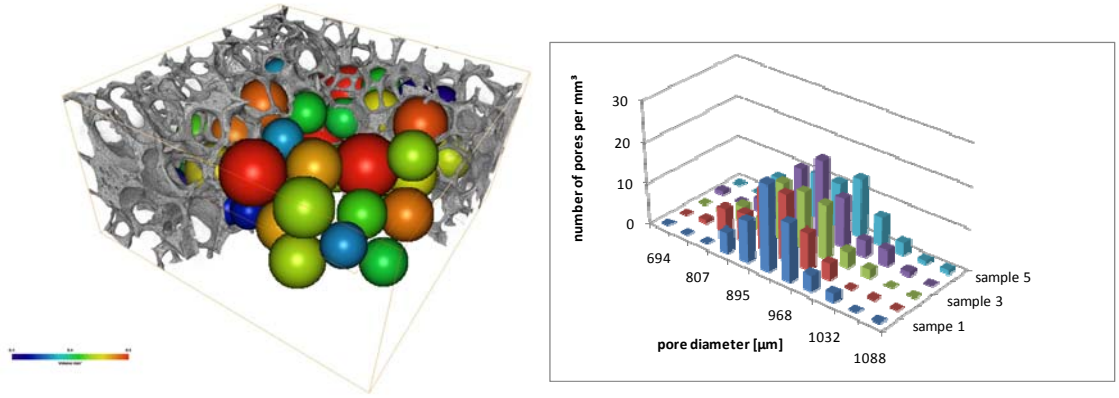

Fig. 2.13: 3D nanoCT image of 45S5-Bioglass containing spheres to calculate the average pore diameter (left) and distribution of pore diameters within five samples of 45S5-Bioglass (right).

Tab. 2.3: Calculated average pore size/diameter of the ceramic biomaterials.

	Sponceram	**Osseolive**	**Cerasorb M**	**45S5-Bioglass**
av. pore size [µm]	510	495	190	926

By fitting spheres of different sizes to the interconnected pores within the matrix, the average pore size/diameter of each biomaterial was calculated; exemplarily shown for 45S5-Bioglass (Fig. 2.13). The average pore size for the ceramic biomaterials ranges from 190 µm for Cerasorb M to 926 µm for 45S5-Bioglass (Tab. 2.3). Pore size and pore size distribution has an influence on the biomaterials permeability (cp. section 2.2.4), which is important for dynamic fluid flow experiments (cp. section 2.6).

Distribution of the pore diameters within five matrices is exemplarily shown for 45S5-Bioglass (Fig. 2.13, right). The pore diameters range between 690-1090 µm, with an average pore diameter of 926 µm. The average pore diameters for sample one to five

range from 907-936 µm. In summary, it can be stated that the pore variability within each sample is relatively high; pore diameters differ in about 400 µm. However, the variability within the five samples is very low.

2.2.4 Permeability and shear stress

The permeability of biomaterials is of great importance for 3D dynamic fluid flow experiments. A low permeability is the result of a low porosity, small pore sizes, a weak interconnectivity and compact areas within the matrix [166]. In general, a low permeability causes a higher wall shear stress at same flow rates, compared to biomaterials with a high permeability, because the fluid is forced through the interconnected areas of the matrix. However, wall shear stress is as well depending on pore intersections. The wall shear stress is important for dynamic fluid flow experiments, as the cells are directly exposed to it (cp. section 2.6). The calculation of shear stress within 3D constructs is not trivial [78], since most biomaterials have a non-uniform pore geometry. Therefore, the materials permeability is taken as an indicator for possible shear stress.

Wall shear stress within the matrix can, for example, be visualized by a simulation using the AVISO software, applying data from the nanoCT scan and carrying out the absolute permeability experiment. In this simulation fluid flow is applied onto the middle top of the biomaterial with an initial pressure of 130 kPa and a viscosity of 0.001 Pa*s. Speed of fluid flow within the matrix is indicated in different colors. Shear stress is defined as force over an area (Formula 1). Since the force implies the movement over time, the speed of fluid flow within the matrix can be correlated with shear stress.

$$\tau = \frac{F}{A}$$

Formula 1: Shear stress τ is indicated as force F over an area A. τ is given in N/m^2 = Pa.

The simulation is exemplarily shown for a Sponceram-Al matrix (Fig. 2.14). Usually shear stress values are given as averages over the entire matrix, but this simulation obviously shows that the distribution of shear stress within the matrix is non-uniform. A few areas show a very low shear stress (indicated in blue), whereas other areas obtain a higher shear stress (indicated in read). Varying shear stress results from different pore sizes and non-uniform pore intersections.

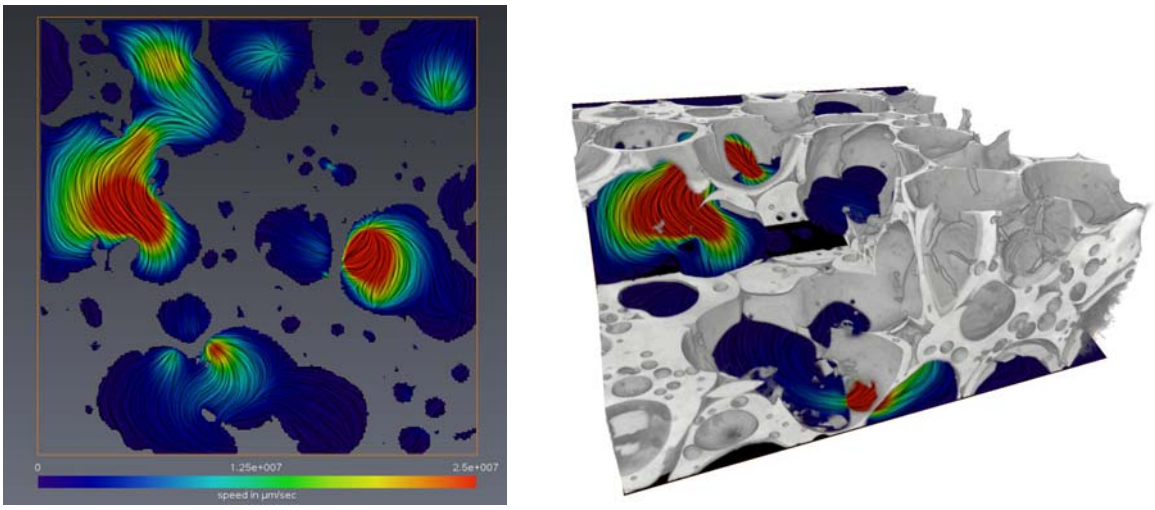

Fig. 2.14: NanoCT images of Sponceram-Al with modeled fluid flow through the matrix, 2D (left) and 3D (right).

The biomaterials permeability was calculated according to the protocol described in section 5.6.3. Briefly, the pressure difference across the biomaterial was measured at different fluid flow rates (50, 100, 150, 200, 300 and 400 ml/min). For Cerasorb M the pressure difference could only be measured up to 250 ml/min, because the upper limit of the differential pressure instrument was reached (Fig. 2.15, A, B). Although these fluid flow values greatly exceed those allied for *in vitro* fluid flow experiments, they were selected to determine a significant pressure difference between the different fluid flow rates. By applying Formula 2, the specific permeability k could be calculated (illustrated in Fig. 2.15, C, D), taken into account the determined pressure difference. Because of the low availability of 45S5-Bioglass and its very poor stability, the permeability for this material could not be determined. Even careful handling of 45S5-Bioglass resulted in destruction of the biomaterial.

$$k = \frac{\mu t}{A} \frac{Q}{\Delta P}$$

Formula 2: Formula to determine the specific permeability k. Thereby, k indicates the specific permeability, t the thickness of the biomaterial, A the area, Q the volumetric flow rate, ΔP the pressure difference across the biomaterial and μ the dynamic viscosity of the liquid (ddH$_2$O 0.001 m²/s or Pa*s).

As presumed from the biomaterials geometry, Cerasorb M shows the lowest and Sponceram-Al the highest permeability (Fig. 2.15, C, D). As mentioned before, this is a result of the porosity, pore size and interconnectivity. Especially the pore size is identified to affect the shear stress level [166]. Cerasorb M has an average pore size of 190 µm and a porosity of 17.8 %. These properties cause a low specific permeability; however, a low permeability causes high shear stress within the matrix.

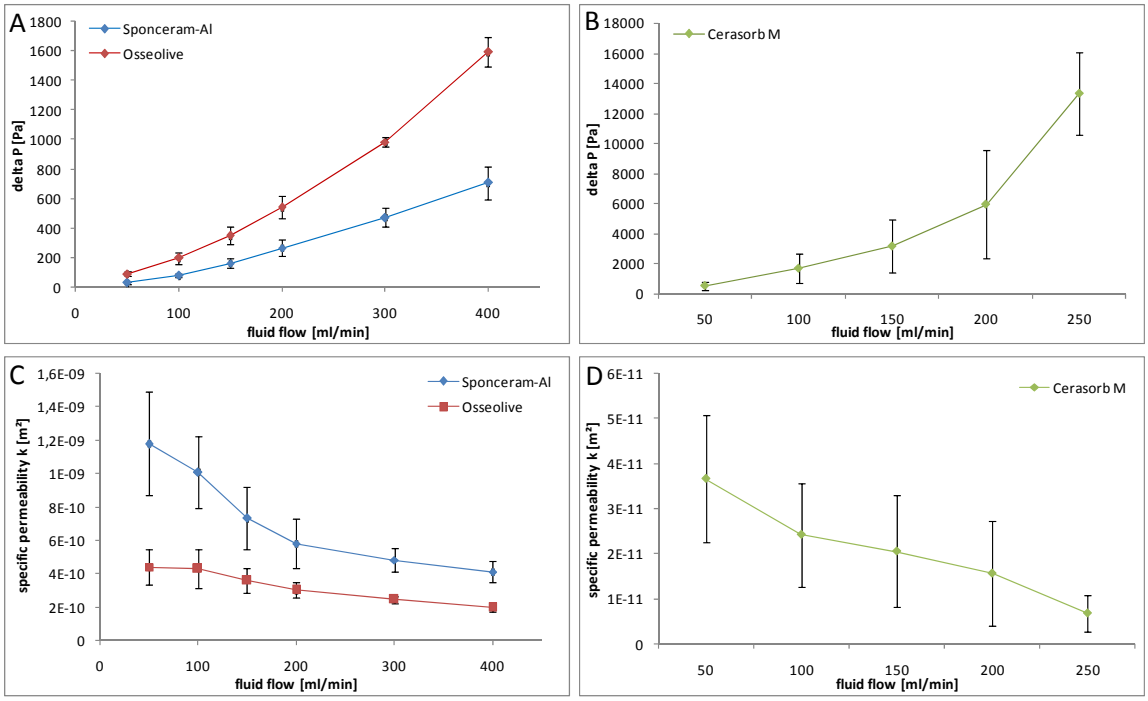

Fig. 2.15: Determined pressure difference across the ceramic biomaterials and calculated specific permeability k of Sponceram-Al and Osseolive (A, C) and of Cerasorb M (B, D). Standard deviation is given for n = 3.

2.2.5 Characterization of the stability

The stability of an artificial bone graft is important, as it has to withstand the forces in the transplanted area until the newly formed bone tissue takes over this function. Stability is created by small pores, small pore intersections and a low porosity. Unfortunately, these demands are in conflict with the requirements for a uniform cell and nutrient distribution, as well as vascularization. Estimation of the biomaterials' stability was carried out according to the instructions in section 5.6.4. Briefly, uniaxial static unconfined (UC) and confined (CC) compression tests were performed with a force of 50 N. The stability was calculated with the Young Modulus (Es) applying the UC data and the Aggregate Modulus (HA) applying the CC data (n = 5). During the UC test, the biomaterial can be laterally deformed as load is applied to the material. On the contrary, during the CC test the lateral deformation is avoided by a fixed volume (Fig. 2.16). Due to the low availability of 45S5-Bioglass, its stability could not be determined, since even careful handling of 45S5-Bioglass indicated a very weak performance.

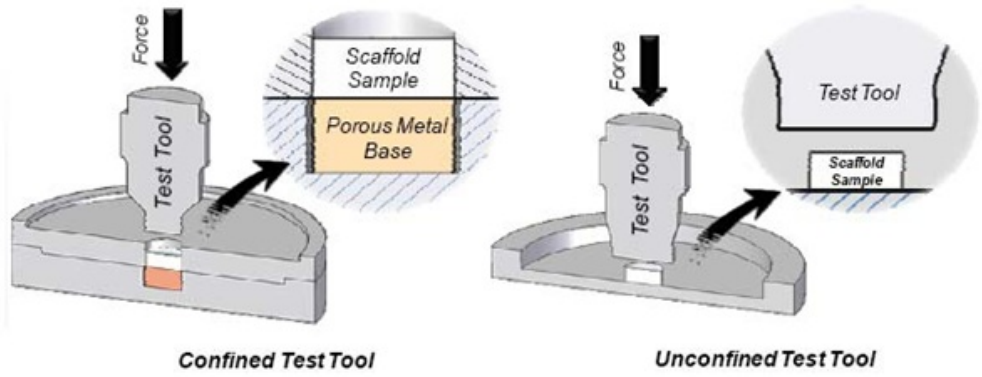

Fig. 2.16: Setup to characterize the mechanical stability under confined compression (left) and unconfined compression (right) (modified from dissertation Victor Acosta Santamaría [167], University Zaragoza, Spain).

Tab. 2.4: Stability of ceramic biomaterials determined by unconfined and confined compression (n = 5).

Modulus	Sponceram-Al	Osseolive	Cerasorb M
HA (CC) [MPa]	30.1 +/- 10.6	14.9 +/- 0.8	1193.6 +/- 156.7
Es (UC) [MPa]	13.3 +/- 5.6	10.1 +/- 3.9	1405.6 +/- 50.3

Tab. 2.5: Stability of collagen-based biomaterials determined by unconfined and confined compression (n = 5).

Modulus	Matriderm	Collagen-BG	Collagen-Silk
HA (CC) [MPa]	0.45 +/- 0.03	0.60 +/- 0.07	0.40 +/- 0.09
Es (UC) [MPa]	0.15 +/- 0.01	0.32 +/- 0.06	0.19 +/- 0.06

Obtained results revealed that Cerasorb M possesses a very high stability. The material is about 40-140 times stronger than Sponceram-Al and Osseolive. The high stability of Cerasorb M is generated by its compact matrix structure with a low porosity and very thick pore walls. However, it has to be taken into account that due to the manufacturing process Cerasorb M exhibits a plane surface, which facilitates positioning the matrix in the measuring device. Consequently, the applied load is distributed evenly over the complete matrix. On the contrary, Sponceram-Al and Osseolive possess a uneven surface. Hence, load may only be applied to a restricted area. Since the load is not distributed evenly over the matrix, the force on this restricted area is higher, which causes faster destruction of the biomaterial. As a result, significantly lower stability might be measured for Sponceram-Al and Osseolive than for Cerasorb M.

However, it can be noted that Sponceram-Al obtains under CC as well as under UC conditions higher stability than Osseolive. Though, both materials exhibit improved

stability under CC conditions. Avoiding lateral displacement stabilizes these biomaterials. Cerasorb M on the contrary obtains lower stability under CC conditions. This is a phenomenon resulting from the very dense 3D architecture of Cerasorb M. A greater pore wall thickness allows for a larger lateral displacement under UC conditions without destruction of the biomaterial, whereas deformation under CC conditions is restricted. A pore of a biomaterial with small pore wall thickness has the potential for great deformation under CC conditions. On the contrary, a pore with large pore wall thickness does not undergo great deformation, if lateral displacement is avoided (CC conditions), which results in the collapse of the pore (Tab. 2.4).

The stability of collagen-based biomaterials is significantly lower compared to ceramic matrices. However, materials obtain a higher stability in the CC test by avoiding lateral displacement. Stability under CC conditions is approximately twice as high than under UC conditions. Furthermore, the bioglass component of Collagen-BG imparts a certain strength to the material. The stability of Collagen-BG is under CC and UC conditions significantly higher compared to other collagen biomaterials (Tab. 2.5).

2.2.6 Summary on characterization of 3D biomaterials for bone Tissue Engineering applications

To date, the influence of porosity and pore size on cell proliferation and differentiation has not clearly been identified. In literature pore sizes between 10 and 2250 μm [61-63] with varying porosities are reported for bone TE applications (cp. Tab. 1.2, section 1.1.1.1). However, a minimum pore size of 100 μm is reported to generate mineralized bone [64]. Smaller pore sizes limit cell migration and nutrient supply. To achieve vascularization a minimum pore size of 300 μm is reported [66]. Additionally, larger pore sizes and higher porosities are known to facilitate bone in-growth [65]. These requirements are in conflict with the demands to obtain a sufficient stability. The biomaterials stability is generated by a low porosity, small pore sizes and the chemical composition. Furthermore, too large pores or compact areas within the matrix decrease the surface area and consequently limit cell adhesion. The main biomechanical parameters of all tested ceramic biomaterials are summarized in Tab. 2.6.

For dynamic fluid flow experiments shear stress within the matrix plays a significant role. Shear stress is created by the materials porosity, pore size and pore intersections. Shear stress was exemplarily simulated in a Sponceram-Al matrix. It is obvious that shear stress within the matrix is highly unequal. Consequently, cells on the biomaterial experience different values of mechanical stimulation when applying fluid flow. This may result in cell disruption due to too high shear stresses. On the other hand, shear

stress in some areas might be too low to have a positive influence on the MSC osteogenic differentiation behavior. Researchers are trying to overcome this limitation by the fabrication of matrices via rapid prototyping [79, 80]. This method allows the production of complex matrix geometries with identical pore sizes and intersections.

Tab. 2.6: Summary of the main biomechanical characteristics of the tested ceramic biomaterials. Given is the average value of five samples (n = 5).

	Sponceram-Al	**Osseolive**	**Cerasorb M**	**45S5-Bioglass**
porosity [%]	66.7	34.8	17.5	89.5
pore size [μm]	510	495	190	926
surface area [mm^2/mm^3]	5.1	3.6	7.2	5.1
stability (CC)	30.1	14.9	1193.6	N/A
stability (UC)	13.3	10.1	1405.6	N/A

From the biomaterials characterization it can be concluded that Osseolive is not feasible for the production of artificial bone tissue structures under GMP-conform conditions. Within the same batch huge differences in the materials porosity and pore size could be detected, which results in a varying tissue quality. Moreover, Osseolive exhibits compact areas, which decrease the degree of interconnected porosity, as well as surface area. 45S5-Bioglass is neither feasible for the construction of bone tissue transplants. It is indeed highly porous, but extremely brittle. Hence, this biomaterial is not able to even withstand very small loads in the transplanted area. Furthermore, due to its fragility 45S5-Bioglass is not applicable for fluid flow experiments. For the application of fluid flow the 3D biomaterial has to be fixed in a bioreactor system (cp. section 2.6). This fixation would already change or disrupt the biomaterials structure. Cerasorb M obtains a very high stability and might withstand high forces within the transplanted area, but it has a very low porosity (17.5 %) which could negatively affect cell distribution (cp. section 2.3) and the integration of the biomaterial into the existent bone [65]. Besides, the pore size of 190 μm does not allow for vascularization [66]. The core objective of biomaterial production is to maintain the balance between optimal pore size and porosity. This requirement may be fulfilled by Sponceram-Al. It obtains a porosity of about 67 % and an average pore size of 510 μm. These parameters allow for optimal cell migration, mass transportation and vascularization. In addition, the aluminum oxide coating generates a highly rough surface to improve cell attachment and adhesion. Sponceram-Al was identified to obtain the highest permeability. If the permeability is taken as an indicator for shear stress, lower shear stresses are generated

within the Sponceram-Al matrix, than in Osseolive and Cerasorb M matrices. Since the distribution of shear stress within these matrices is highly unequal, it might be better to use a matrix with lower shear stresses. Too high shear stress may disrupt the cells from their substrate.

NanoCT images revealed that the collagen-based biomaterials consist of a dense mesh of collagen fibers, which might support cell adhesion. Differences between the tested collagen-based matrices can only be found in length and arrangement of the fibers. Collagen-based biomaterials possess, compared to the ceramic matrices, a very weak stability, which denies their application in transplantation sides exposed to load. Highest stability showed Collagen-BG, which obtains, compared to the other collagen-based matrices, a content of 6 % bioglass.

2.3 Biocompatibility and 3D static long-term cultivation

In order to validate the biocompatibility of all biomaterials, long-term cultivations using MSC were performed. The proliferation capacity of MSC on each matrix was recorded to estimate the biomaterials potential for bone TE applications. But not only the proliferation of MSC is important to create a bone tissue construct, also cell distribution within the biomaterial plays a crucial role. Desired homogenous mineralization of an artificial bone construct can only be achieved, if the cells are evenly distributed on the matrix. To determine the biocompatibility and observe the proliferation and distribution of MSC on the different biomaterials, static cultivations according to the instructions in section 5.7.2 were performed. Briefly, $6*10^4$ cells were seeded on the top of each biomaterial (collagen-based samples d = 16 mm) and cultivated in culture medium for 5 weeks. The medium was changed (1 ml) every first, third and fifth day of the week. In order to investigate cell distribution on ceramic biomaterials, SEM images were taken and 4',6-Diamidino-2-phenylindol (DAPI) or Calcein-AM stainings performed. In addition to visual observation of MSC proliferation and distribution indirect proliferation assays, based on cell metabolic activity, were carried out. To determine the viability of MSC on ceramic biomaterials the MTT assay was used, on collagen biomaterials the CellTiter-Blue assay. Tests were performed according to the protocols in section 5.8.2 and 5.8.3 on day 1, 7, 14, 21, 28 and 35 (n = 3) of cultivation. Viability assay for MSC on 45S5-Bioglass could not be carried out due to the low availability of the material. Furthermore, medium samples were collected during each change of the medium and the glucose and lactate concentration was determined (not shown).

The cell distribution on the top of each ceramic biomaterial (location where the cell suspension was applied) is exemplarily demonstrated for adMSC by SEM images. It can clearly be noticed that after 5 weeks of cultivation MSC are spread over the entire biomaterials' surface. On Cerasorb M and 45S5-Bioglass a compact layer of cells and ECM can be observed, whereas on Sponceram-Al and Osseolive the tips of the biomaterials break through the cell layer (Fig. 2.17).

To determine whether MSC proliferate and migrate through the material during the cultivation period, DAPI or Calcein-AM images of the top and bottom of the matrix were taken after 5 weeks of static cultivation. Images are exemplarily shown for adMSC. Obviously, more cells can be detected on the top of the matrix, where the cell suspension was applied, than on the bottom. However, on all biomaterials adMSC can be identified on the bottom of the matrix after the cultivation period (Fig. 2.18).

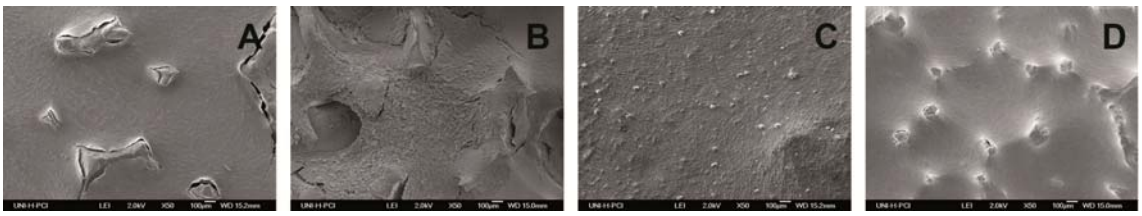

Fig. 2.17: SEM images of adMSC cultivated for 5 weeks on (A) Sponceram-Al, (B) Osseolive, (C) Cerasorb M and (D) 45S5-Bioglass in culture medium.

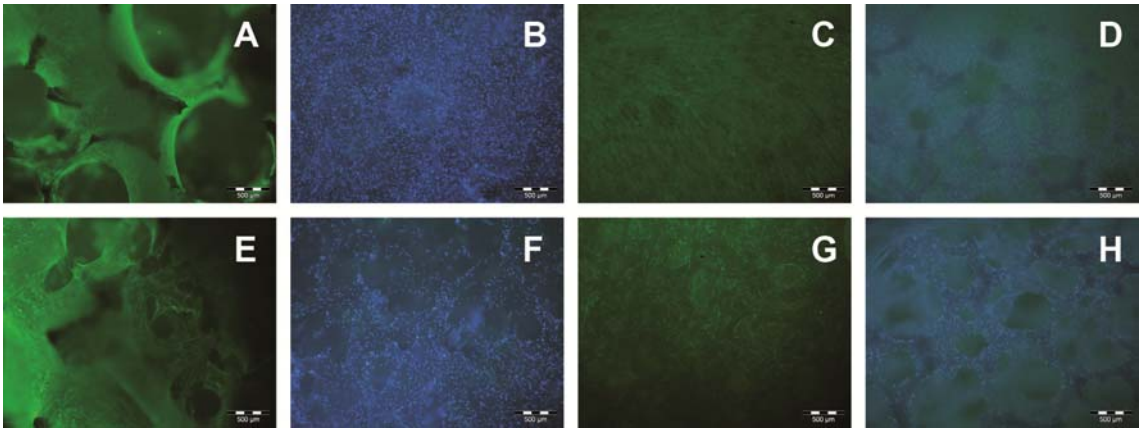

Fig. 2.18: Calcein-AM images (green) or DAPI images (blue) of adMSC cultivated for 5 weeks on Sponceram-Al (A, E), Osseolive (B, F), Cerasorb M (C, G) and 45S5-Bioglass (D, H) in culture medium; (A-D) top of the biomaterial, (E-H) bottom.

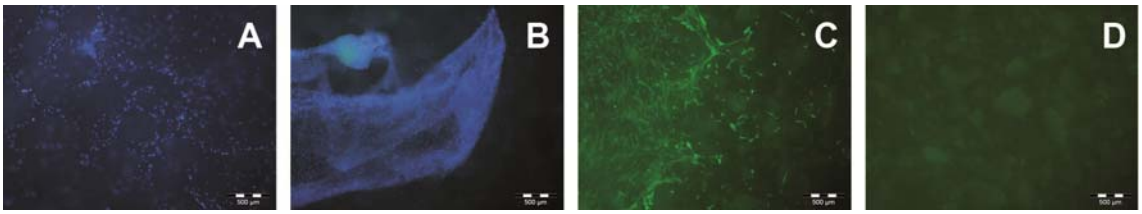

Fig. 2.19: (A) DAPI image of adMSC on Osseolive (bottom) after 3 weeks of static cultivation, (B) DAPI image of adMSC cell layer detaching from the surface of Osseolive after 5 weeks of cultivation, (C) Calcein-AM image of ucMSC on Cerasorb M (bottom/edge) after 5 weeks of static cultivation and (D) Calcein-AM image of ucMSC on Cerasorb M (bottom) after 5 weeks of static cultivation.

DAPI or Calcein-AM images only allow observing the cell distribution on the top and bottom of the biomaterials' surface. An examination of the cell distribution inside the matrix is only possible by preparing small slices of the biomaterial, which is due to their brittle behavior a difficult procedure. However, Calcein-AM images of Cerasorb M give the impression that the cells are growing on the top of the material and around the edges (Fig. 2.19, C), but not into the biomaterial. After the cultivation of ucMSC for 5 weeks, no cells can be detected on the bottom of the biomaterials (Fig. 2.19, D). Cell migration through Sponceram-Al and Osseolive is, because of the incomplete interconnectivity of the matrices, a rather slow process. Fig. 2.19 (A) indicates only few MSC on the bottom side of Osseolive after 3 weeks of static cultivation. This effect was not observed for 45S5-Bioglasss after 3 weeks of static cultivation (not shown), since it obtains a fully interconnected geometry with rather large pore sizes (av. 926 µm).

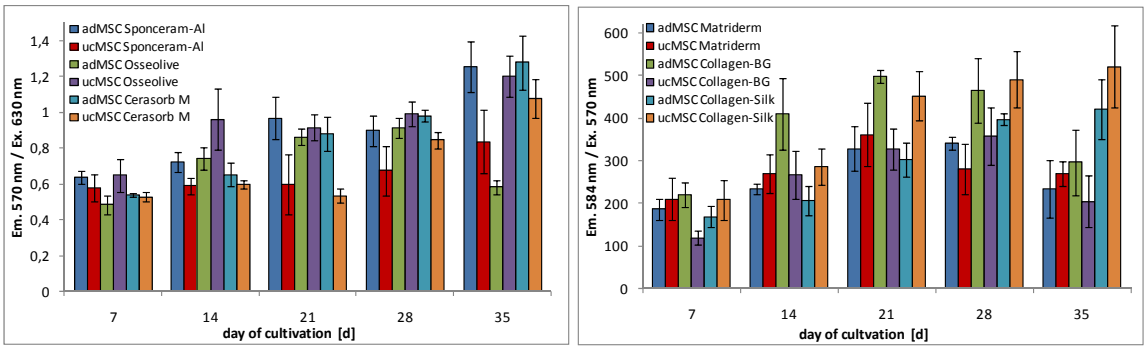

Fig. 2.20: MTT viability assay for adMSC and ucMSC on ceramic biomaterials (left) and CellTiter-Blue viability assay for adMSC and ucMSC on collagen-based biomaterials (right). Standard deviation is given for n = 3.

All biomaterials can be identified as biocompatible. Enzymatic assays for metabolic activity do not show a reduction of viability within 3 weeks of static cultivation.

Constant cell proliferation on ceramic biomaterials can be identified for adMSC and ucMSC on Cerasorb M, as well as for adMSC on Sponceram-Al and for ucMSC on Osseolive. These combinations of cells and biomaterials show increasing cell

proliferation over the cultivation period of 5 weeks. UcMSC on Sponceram-Al rather indicate a cell survival, no reduction or increase of signal intensity can be observed. AdMSC on Osseolive proliferate until week 4. After the last week of cultivaiton a significant reduction of cell viability can be noticed. This effect is caused by detachment of the cell layer. After 5 weeks of cultivation the complete suface of Osseolive is covered by adMSC and cells start detaching from the materials surface due to the lack of space. This statement can also be proven by DAPI staining (Fig. 2.19, B). The image reveals that a dense cell layer detaches from the surface. Cell detachement might also be enhanced by the rather smooth surface of Osseolive compared to the surfaces of the other ceramic biomaterials (cp. Fig. 2.7, E-H). UcMSC on Osseolive do not detach from the materials surface after 5 weeks of cultivation, because they possess a smaller cell morphology and therefore occupy less surface area.

Constant cell proliferation can be observed for MSC on all tested collagen-based biomaterials until week 3 and on Collagen-Silk until week 5. However, ucMSC on Matriderm show already after week 4 a decreased viability and ucMSC as well as adMSC on Collagen-BG after week 5. Differences in viabiliy on the collagen-based biomaterials are caused by the biomaterials composition. Silk fibroin, emitted by the silk worm, is not only biocompatible and biodegradable, but also known to enhace MSC proliferation and attachment [168].

In summary, it can be stated that MSC on Cerasorb M presented good proliferation capacity, which is a result of the high available surface area, compared to other ceramic biomaterials. However, cell distribution on this matrix was very weak. Only few cells could be detected on the bottom of the matrix after 5 weeks of cultivation. This effect is a result of the low porosity and small pore size of Cerasorb M (cp. section 2.2.3). Consequently, Cerasorb M is not applicable as a matrix for an artificial bone tissue construct. UcMSC showed constant proliferation over 5 weeks on Osseolive and adMSC on Sponceram-Al. Moreover, the cells were homogenously distributed on the matrix. Cell proliferation before differentiation into osteocytes should not exceed a 5 week cultivation period, since adMSC, for example, started detaching from the surface of Osseolive after 5 weeks of cultivation. Constant cell proliferation over 5 weeks on collagen-based biomaterials could only be achieved using Collagen-Silk. Other collagen-based biomaterials showed a decrease in proliferation before reaching week 5.

2.4 3D static differentiation of MSC

As previously described in the theoretical part of this work the biomaterials surface roughness, porosity, pore size and stiffness can direct stem cell differentiation. These biomaterial characteristics have been determined in section 2.2. Now osteogenic differentiation of adMSC and ucMSC on the 3D ceramic and collagen-based biomaterials was performed and the influence of varying matrix structures on the differentiation behavior was investigated. Differentiation experiments were carried out according to instructions in section 5.7.2. Briefly, $6*10^4$ cells were seeded on the top of each biomaterial (d = 16 mm for collagen matrices) and cultivated for 1 week in culture medium. Then, medium was switched to ODM-M for the following 4 weeks. The medium was changed (1 ml) every first, third and fifth day of the week. Medium samples were collected during each change of the medium. In order to reduce the number of samples, the medium of three wells of each biomaterial were pooled. The glucose consumption and the lactate production were measured as an indirect factor for cell survival and proliferation during cultivation. Proliferation assays for 3D static cultivation in ODM-M were not carried out. Furthermore, medium samples were used to analyze CICP production via ELISA. CICP signifies the C-terminal of type I collagen, which is the main component of the ECM of MSC differentiated into the osteogenic lineage. After the cultivation and differentiation period osteospecific histological stainings (AP, Sirius Red, von Kossa and Calcein) were performed. A detailed description of the staining procedures is given in section 5.8.8. Besides histological stainings, differentiation on ceramic biomaterials could as well be identified by SEM images. Cells undergoing osteogenic differentiation change their morphology. They do not appear flat and elongated as during proliferation, but they form so-called bone nodules, which can be identified via SEM. The combination of MSC and ECM appears rough. Moreover, expression of osteogenic genes was verified by PCR analysis.

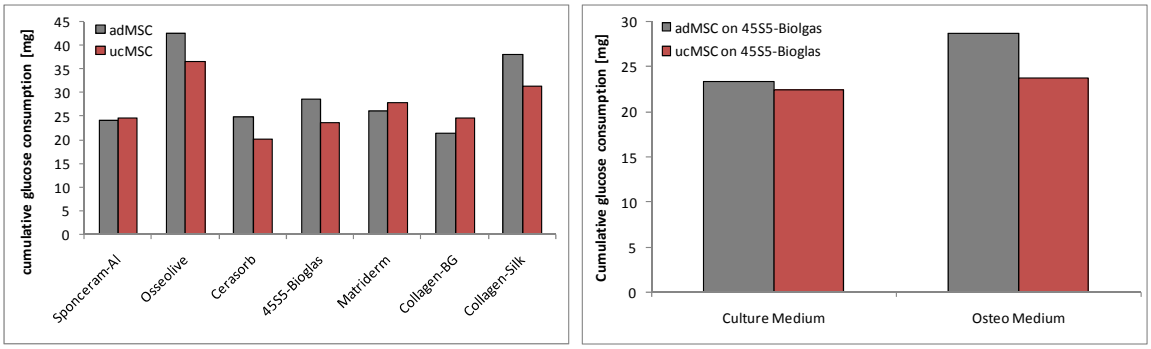

Fig. 2.21: (Left) cumulative glucose consumption of adMSC and ucMSC on different ceramic and collagen-based biomaterials after a cultivation period of 5 weeks (1 week culture medium and 4 weeks ODM-M) and (right) cumulative glucose consumption of adMSC and ucMSC on 45S5-Bioglass after 5 weeks in culture medium, in comparison to 1 week culture medium and 4 weeks ODM-M.

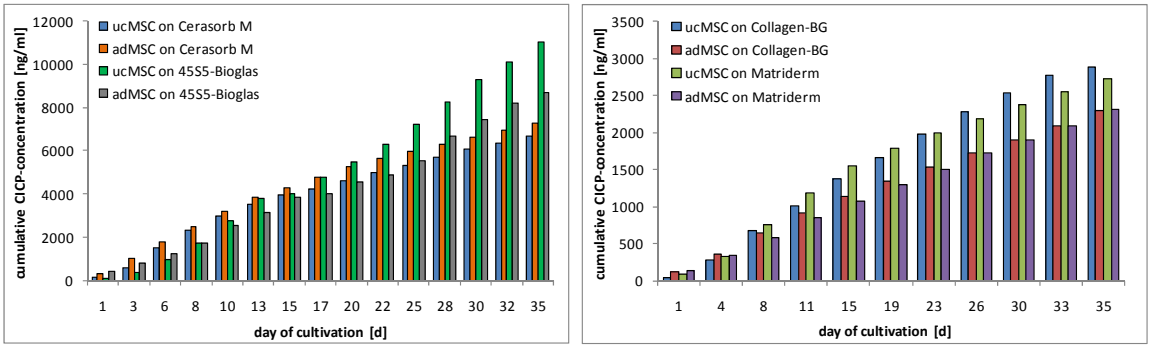

Fig. 2.22: Cumulative CICP-concentration produced by ucMSC and adMSC over the cultivation of 1 week in culture medium and 4 weeks in ODM-M on Cerasorb M and 45S5-Bioglass (left) and on Collagen-BG and Matriderm (right).

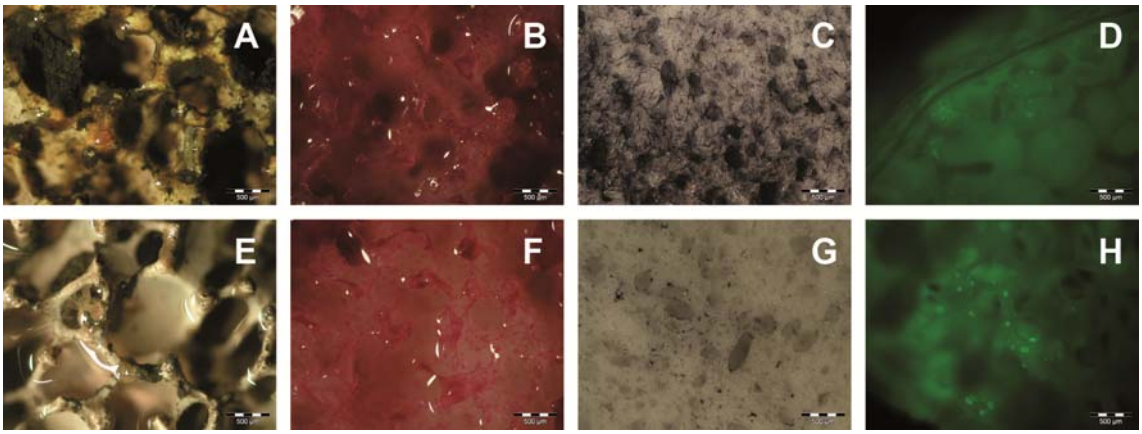

Fig. 2.23: Osteospecific histological stainings of adMSC (A-D) and ucMSC (E-H) on Sponceram (A, E) von Kossa staining, on Osseolive (E, F) Sirius Red staining, on Cerasorb M (C, G) membrane-bound AP staining and on 45S5-Bioglass (D, H) Calcein staining, after cultivation of 4 weeks in ODM-M.

The glucose consumption of adMSC on Osseolive, Cerasorb M, 45S5-Bioglass and Collagen-Silk is higher than for ucMSC. Since the same number of cells has been seeded onto each biomaterial, this effect implies that adMSC on these biomaterials need higher amounts of glucose to maintain their metabolic activity or to perform osteogenic differentiation. Another possible explanation is that a higher glucose consumption results from enhanced proliferation capacity of MSC on the different biomaterials. The glucose consumption of MSC on collagen-based biomaterials matches, for example, the proliferation assay. MSC on Collagen-Silk show the highest glucose consumption in ODM-M and highest viability in culture medium (cp. Fig. 2.20, right). The highest glucose consumption of MSC on ceramic biomaterials is shown for Osseolive. This result, however, cannot be related to the proliferation assay (cp. Fig. 2.20, left). Consequently, high glucose consumptions can not only be related to cell survival and proliferation, but also to other cell activities, such as differentiation.

No tendency can be noticed, if adMSC or ucMSC produce higher levels of CICP. UcMSC produce, for example, on collagen-based biomaterials and on 45S5-Bioglass

significantly higher amounts of CICP, compared to adMSC (Collagen-Silk not shown). On the contrary the production of CICP on Sponceram, Osseolive and Cerasorb M was higher for adMSC (only shown for Cerasorb M, Fig. 2.22, left). However, the CICP production on collagen-based biomaterials is about two to three times lower, than on Cerasorb M or 45S5-Bioglass (Fig. 2.22).

Osteogenic differentiation of ucMSC and adMSC after 4 weeks of static cultivation in ODM-M can be observed in different degrees on all ceramic biomaterials. Different staining procedures were used, because some staining methods cannot be combined with certain biomaterials. Cerasorb M, for example, contains calcium and is therefore not compatible with the Calcein staining. Osteogenic differentiation of adMSC was enhanced on all biomaterials, compared to ucMSC. This can especially be seen for Sponceram-Al (Fig. 2.23, A, E) and Cerasorb M (Fig. 2.23, C, G). In detail, this result is revealed for differentiation on 45S5-Bioglass in Fig. 2.24. LSCM (laser scanning confocal microscopy) images after Calcein staining present a stronger calcification of the adMSC ECM. Moreover, adMSC on 45S5-Bioglass present a significant stronger staining of membrane-bound AP. Furthermore, adMSC on Sponceram-Al, Osseolive and Cerasorb M only partially produce membrane-bound AP (shown for Cerasorb M in (Fig. 2.23, C), whereas this protein is expressed by adMSC on the entire matrix of 45S5-Bioglass (Fig. 2.24, C). These results indicate an advanced osteogenic differentiation of adMSC on 45S5-Bioglass compared to adMSC on other ceramic biomaterials.

The change of cell morphology after 4 weeks of cultivation in ODM-M is exemplarily shown for ucMSC (Fig. 2.25). A significant morphological change can be identified for ucMSC on all ceramic biomaterials. After 5 weeks of cultivation in culture medium cells present a flat and elongated morphology (Fig. 2.25, E-H). However, after 4 weeks of cultivation in ODM-M the ECM containing MSC appears very rough. The morphological change is especially significant on Sponceram-Al (Fig. 2.25, A, E) and Osseolive (Fig. 2.25, B, F). In the pores of Osseolive a strong formation of bone-nodules can be observed.

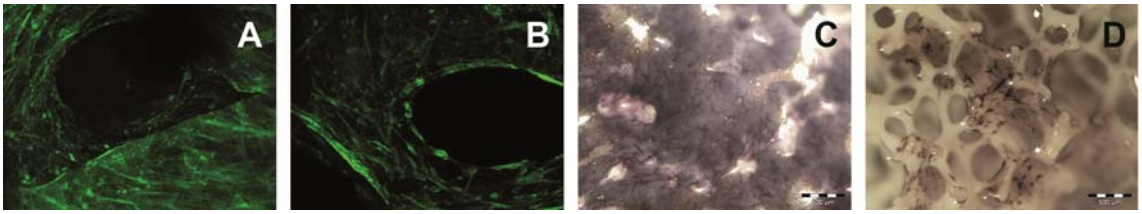

Fig. 2.24: LSCM images after Calcein staining for the detection of calcium accumulations in the ECM of adMSC (A) and ucMSC (B) and bright field microscopy images of membrane-bound AP staining on 45S5-Bioglass containing (C) adMSC and (D) ucMSC after cultivation of 4 weeks in ODM-M.

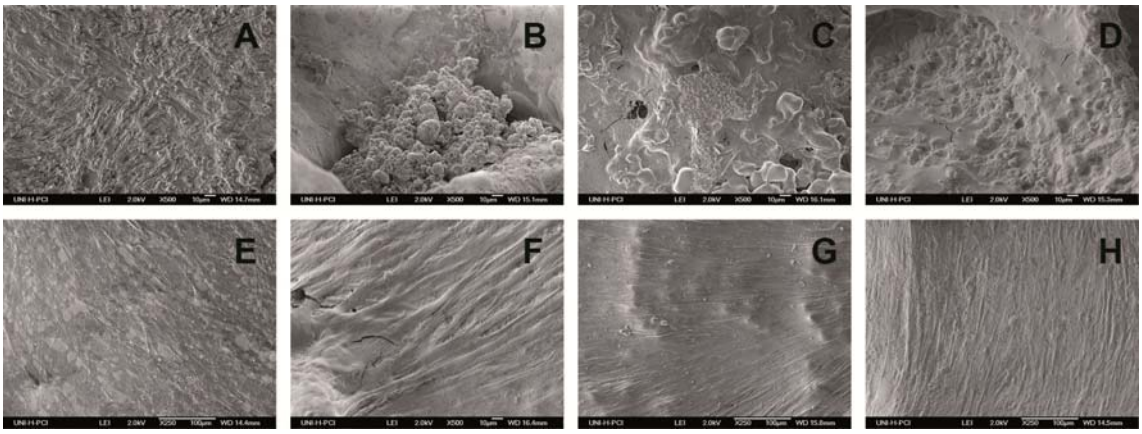

Fig. 2.25: SEM images of ucMSC after a cultivation period of 1 week in culture medium and 4 weeks in ODM-M (A-D) compared to a cultivation of 5 weeks in culture medium (E-H) on Sponceram-Al (A, E), Osseolive (B, F), Cerasorb M (C, G) and 45S5-Bioglass (D, H).

Tab. 2.7: Differentiation of adMSC and ucMSC on different collagen-based biomaterials after the cultivation of 4 weeks in ODM-M investigated by AlizarinRed and von Kossa staining of cryosections (25 µm). The visual differentiation level is evaluated from one + (low) to five +++++ (high).

Cells	Biomaterial	AlizarinRed	von Kossa	Evaluation
adMSC	Matriderm	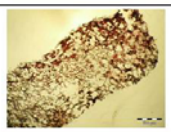	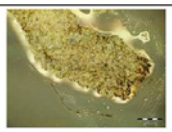	+ (5)
adMSC	Collagen-BG	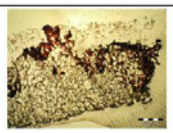	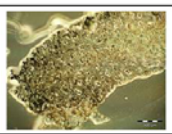	++ (5)
adMSC	Collagen-Silk	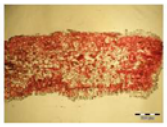	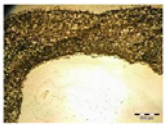	+++++ (5)
ucMSC	Matriderm	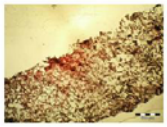	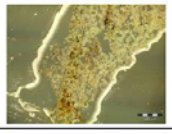	+ (5)
ucMSC	Collagen-BG	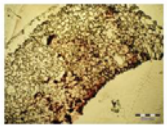	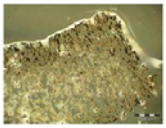	++ (5)
ucMSC	Collagen-Silk	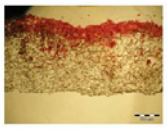	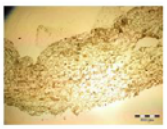	++ (5)

Mineralization of the ECM of adMSC and ucMSC on collagen-based biomaterials is revealed by AlizarinRed and von Kossa staining. The visual differentiation level is evaluated from one (low) to five (high). Osteogenic differentiation on Matriderm is

very weak for adMSC and ucMSC, respectively. Mineralization on Collagen-BG is enhanced compared to Matriderm. However, differentiation only occurs partially. Especially, cells on the edges of the biomaterial differentiate. Strongest mineralization can be observed on Collagen-Silk using adMSC. Cells differentiated throughout the entire biomaterial (Tab. 2.7).

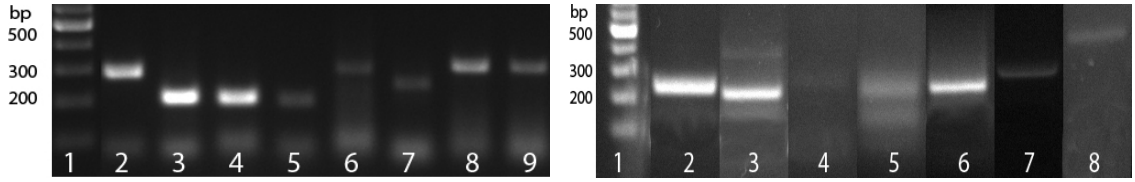

Fig. 2.26: RT-PCR after the static cultivation of ucMSC on Sponceram-Al for 5 weeks (left) Lane 1: ladder, lane 2: *HPRT*, lane 3: *COL I*, lane 4: *COL III*, lane 5: *RUNX*, lane 6: *BSP-2*, lane 7: *OP*, lane 8: *BMP-2*, lane 9: *AP*. RT-PCR after the static cultivation of adMSC on Cerasorb M for 5 weeks (right): Lane 1: ladder, lane 2: *HPRT*, lane 3: *COL I*, lane 4: *BMP-4*, lane 5: *RUNX*, lane 6: *BMP-2*, lane 7: *OP*, lane 8: *AP*.

PCR analyses are exemplarily shown for ucMSC on Sponceram-Al and adMSC on Cerasorb M. UcMSC on Sponceram-Al show mRNA expression of all tested osteospecific primers: *COL I (Collagen I), COL III (Collagen III), RUNX (Runt-related Transcription Factor), BSP-2 (Bone-Sialoprotein 2), OP (Osteopontin), BMP-2 (Bone Morphogenic Protein 2)* und *AP (Alkaline Phosphatase)*. *HPRT (Hypoxanthine-guanine Phosphoribosyltransferase)* is a housekeeping gene and served as a control. mRNA expression levels for adMSC on Cerasorb M can be identified for *COL I, RUNX*, *BMP-2*, *OP* and *AP*. No mRNA expression can be revealed for *BMP-4* (Fig. 2.26).

Evaluation of the MSC differentiation level on ceramic biomaterials is not trivial. Images of the histological stainings can only be taken of the biomaterials top and bottom. A look inside the matrix is a difficult procedure. Moreover, some staining methods are not compatible with certain biomaterials and the matrices have to be washed intensively after the staining procedure to remove the unbound dye. However, it can be recorded that adMSC generally differentiated better on the tested ceramic biomaterials than ucMSC. They revealed a higher production of membrane-bound AP and showed except for the cultivation on 45S5-Bioglass higher levels of CICP-concentration. However, a morphological change of ucMSC in the ECM could also be detected via SEM, which implies a beginning osteogenic differentiation. Only 45S5-Bioglass with adMSC and ucMSC presented a positive Calcein staining, which is a very sensitive method to determine calcium in the ECM. This result indicates an advanced osteogenic differentiation of MSC on 45S5-Bioglass, compared to the other ceramic biomaterials. The enhanced differentiation of MSC on 45S5-Bioglass might be caused by the biomaterials structure. 45S5-Bioglass obtains a high porosity (av. 89.5 %) and huge pores (av. 926 μm), which allows for an improved nutrient supply under static

conditions. Moreover, the micro-porous surface structure increases the biomaterials roughness, which is known to enhance osteogenic differentiation [16, 104, 105].

Evaluation of the MSC differentiation level on collagen-based biomaterials is slightly easier. Stainings of vertical cryosections (25 µm) also give an impression of mineralization in the core of the matrix. Moreover, it is easier to remove the unbound dye after staining, and therefore achieve a very precise staining result. It is obvious that strongest differentiation could be achieved by cultivating adMSC on Collagen-Silk. Mineralization occurred throughout the entire biomaterial. In contrast, differentiation of MSC on Matriderm and Collagen-BG mainly aroused on the edges of the biomaterial. This effect can be induced either by weak cell migration or poor nutrient distribution. Finally, the differentiation level can also be an effect of the biomaterials composition. MSC, for example, cultured on matrices or thin films containing silk fibroin achieved strong osteogenesis *in vitro* and bone formation *in vivo* [169]. Also the application of bioactive glass components for the construction of artificial bone substitutes is intensively discussed in literature. Bioglass is described to be osteoinductive [170] and known to promote bone growth *in vivo* after transplantation [171]. However, the component elastin, which is part of Matriderm, is not known to positively influence osteogenic differentiation. On the other hand, the quantity of elastin determines the materials stiffness, which can have an impact on MSC differentiation [172]. The lower CICP-concentration for collagen-based samples compared to ceramic samples might result from a smaller material volume. Therefore, cell proliferation is limited and less cells are present to produce CICP. Another possible explanation could be a negative feedback loop. Cells might be able to sense the collagen of their microenvironment and therefore reduce the production of internal natural collagen. Many positive and negative feedback loops for osteogenic differentiation are well described in literature [173].

Generally, osteogenic differentiation level was increased for adMSC on different ceramic and collagen-based biomaterials compared to ucMSC. This might explain the higher glucose consumption of adMSC on some tested biomaterials. Glucose consumption may not only used as an indicator for cell survival and proliferation, but also for differentiation activity. This hypothesis can be supported by taking into account the results of Fig. 2.21 (right) and the osteogenic differentiation of MSC on 45S5-Bioglass. The glucose consumption of adMSC and ucMSC on 45S5-Bioglass is equal in culture medium. However, the cumulative glucose consumption of adMSC in osteogenic differentiation medium is about 5 mg higher compared to ucMSC. Moreover, adMSC on 45S5-Bioglass show a significantly stronger osteogenic

differentiation. These results indicate that higher glucose consumption can be correlated with differentiation activity. However, conflicting observations have been described by Pattappa *et al*. They found a lower glucose consumption in osteogenic samples, compared to the static control [174]. To verify the hypothesis that glucose consumption can be correlated with differentiation activity, further investigations on different biomaterials have to be performed.

2.5 Biomaterials' potential for bone Tissue Engineering applications

Concluding the results of mechanical properties, 3D cell proliferation and differentiation the following statements can be made:

MSC on Osseolive show a good proliferation and differentiation capacity. However, this biomaterial cannot be used for the production of artificial bone constructs under GMP-conform conditions. Due to the current fabrication process, Osseolive cannot be produced with a constant matrix quality. Samples within one batch show, for example, a high variability of porosity. Moreover, compact areas within the matrix reduce the available surface area. By optimizing the fabrication procedure, the production of more homogeneous structures might be possible.

Due to its large available surface area MSC on Cerasorb M present proliferation capacity over 5 weeks. Moreover, the low porosity and small average pore size creates a high matrix stability. Matrices are able to withstand forces up to 1400 MPa. On the contrary, these characteristics of Cerasorb M cause a very weak cell distribution and nutrient supply. Consequently, MSC differentiation does only occur on the top of the biomaterial (location where the cells have been seeded). Even though Cerasorb M is accredited as an osteo dental implant, it is, according to the obtained results, not feasible for the production of artificial bone tissue structures under static conditions.

Though, MSC presented an advanced differentiation on 45S5-Bioglass compared to other ceramic matrices, this biomaterial can neither be used for bone TE applications nor for further experiments of this dissertation. The mechanical properties of 45S5-Bioglass are too weak to withstand even very low forces in the area of transplantation or to use it in bioreactor experiments. Positioning the matrix in a dynamic bioreactor and applying fluid flow, would already cause partial damage of the material. If the mechanical properties of 45S5-Bioglass could be improved, the cultivation of MSC on this matrix in a dynamic bioreactor system is an interesting approach.

The mechanical properties of Sponceram-Al allow for a good cell distribution and the formation of vascularized tissue. The matrices can also withstand forces up to 30 MPa.

Moreover, Sponceram-Al presents low matrix variability and therefore a constant matrix quality is assured. Especially adMSC on Sponceram-Al present good proliferation and differentiation capacity. Consequently, Sponceram-Al matrices are used in the following dynamic cultivation experiments. The only disadvantage is the uneven distribution of shear stress in the matrix when applying fluid flow. However, the shear stress is lower in Sponceram-Al, as in Osseolive and Cerasorb M.

Due to the already very strong mineralization of ECM on Collagen-Silk under static conditions, this biomaterials presents a good potential for the application in bone TE. However, generally all collagen-based biomaterials cannot be implanted into areas, which are exposed to high mechanical load. Collagen-based matrices are not able to withstand small permanent loads. A future challenge could be the design of a composite biomaterial using silk (cp. section 1.1.1.5). The silk component shows the capacity to enhance osteogenic differentiation, but needs a framework to gain stability. For this approach inorganic components such as HA and TCP could be used.

Nevertheless, for further dynamic experiments of this dissertation Collagen-Silk is not applied. The core objective of dynamic cultivation experiments is to show an improved osteogenic differentiation by mechanical stimulation of MSC compared to a static control. If mineralization occurs through the entire matrix already under static conditions, an enhanced osteogenic differentiation is difficult to determine. Therefore, Matriderm and Collagen-BG are used in the following dynamic cultivation experiments.

2.6 3D dynamic microenvironment for the cultivation and osteogenic differentiation of MSC

Dynamic perfusion conditions create *in vitro* a natural environment for MSC and therefore improve bone TE. Perfusion bioreactors are designed to overcome the limitation of nutrient supply within a biomaterial by convectively transporting medium through the 3D matrix. This process also creates fluid shear stress within the material, which is known to positively influence bone differentiation and enhance mineralization [175]. Depending on the design of the perfusion bioreactor and the biomaterial, a shear stress between 0.001 and 0.005 dyn/cm² is usually applied in 3D dynamic experiments [78]. However, the definition of shear stress rates in a 3D matrix is difficult to determine; due to the fabrication processes the distribution of fluid flow and shear stress within the biomaterials is not homogenous (cp. section 2.2.4). In this chapter different dynamic perfusion bioreactors are introduced, which were designed

to suit the requirements for bone TE, applying either ceramic or collagen biomaterials. MSC are stimulated by constant fluid flow using a conventional direct perfusion bioreactor, either disposable (P3D-6/10, EBERS Medical) or non-disposable (EBERS Medical). Another bioreactor system combines the mechanical forces of perfusion and compression to enhance MSC stimulation (Greiner Bio-One). It is has already been discovered in 1892 that mechanical loading is correlated with bone growth *in vivo* (Wolff's Law) [176]. To date, the correlation between mechanical loading and new bone formation is not fully explored [177], but it is well-known that the mechanism of mechanical loading enhances fluid flow *in vivo* and *in vitro*, respectively. A further approach will be made by the design of a drip-perfusion bioreactor (Leibniz University of Hanover), which allows perfusion only by the force of gravity. An overview on the different combinations of used bioreactors, biomaterials and MSC is given in Tab. 2.8. The design of the bioreactors will be explained in detail in the following chapters.

Tab. 2.8: Overview on the performed dynamic cultivation experiments.

Bioreactors	Sponceram-Al	Cerasorb M	Collagen-BG	Matriderm
 disposable perfusion chamber P3D-6/10 (EBERS Medical)	-	ucMSC	ucMSC	-
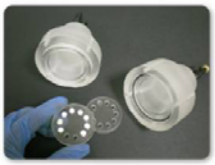 non-disposable perfusion chamber (EBERS Medical)	adMSC	-	-	-
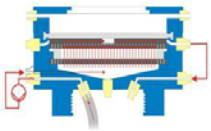 perfusion & compression bioreactor (Greiner Bio-One)	adMSC ucMSC	-	-	adMSC
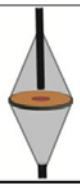 drip-perfusion bioreactor (University of Hanover)	adMSC	-	adMSC ucMSC	-

2.6.1 Improved cell distribution due to direct perfusion

As shown in section 2.3 cell distribution under static conditions is often weak, especially at the beginning of the cultivation due to the cell seeing procedure (top of the biomaterial). Only a well interconnected matrix allows the proliferation and

migration of MSC through the biomaterial. To overcome the initial limitation of cell distribution, dynamic perfusion cultivation was performed after cell seeding. For this investigation Cerasorb M was selected, which presented a very weak cell distribution under static conditions. $2*10^5$ ucMSC were seeded on the top of Cerasorb M and incubated statically under standard conditions for 2 days in culture medium. Subsequently, one matrix-cell construct was introduced into a commercially available disposable perfusion chamber P3D-10 (EBERS Medical, Zaragoza, Spain), which allows for direct perfusion of the biomaterial (Fig. 2.27). The culture chambers are designed as single-use systems to minimize the risk of contamination and reduce labor input by e.g. eluding the autoclavation process. Two dynamic cultivation experiments have been carried out in parallel. The cells were dynamically cultivated for 3 days applying a constant fluid flow of 0.2 ml/min (cp. section 5.7.3). To evaluate cell distribution, Calcein-AM staining was performed. For comparison, samples were incubated statically for 5 days in culture medium. The medium was changed (1 ml) on day 2 and 4. The results show that after dynamic cultivation of only 3 days MSC can be observed on the bottom of the biomaterial, even though significantly less than on the top of the matrix. In comparison, the static control does not display any cells on the bottom side (Fig. 2.28). Consequently, it can be stated that the use of a dynamic perfusion system can improve cell distribution.

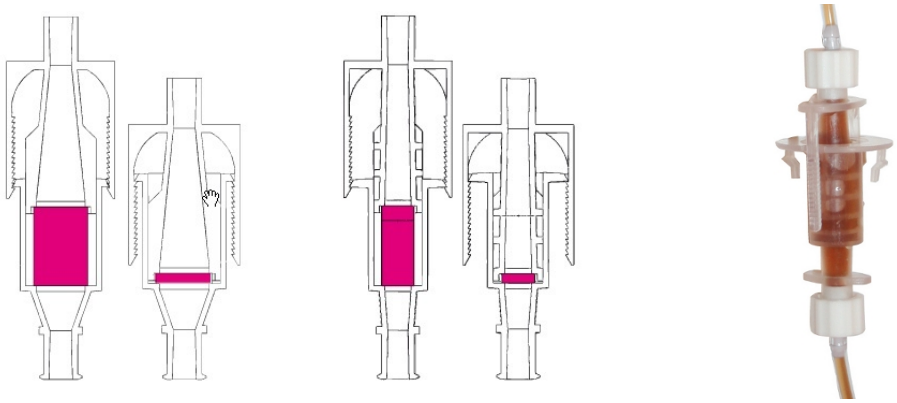

Fig. 2.27: Schematic assembly of the single-use direct perfusion bioreactor from EBERS Medical (Zaragoza, Spain), P3D-10 (left), P3D-6 (middle) and picture of the setup P3D-6 (right). Images adopted from the EBERS Medical website.

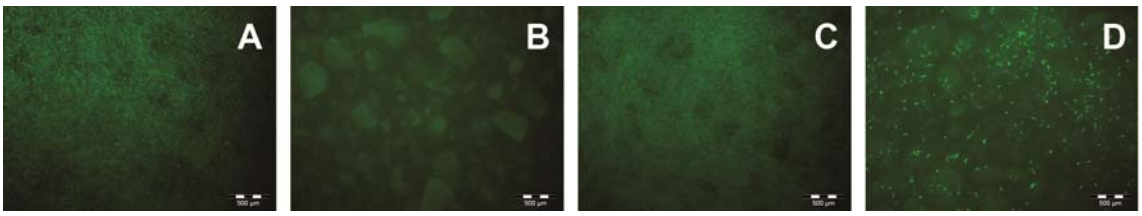

Fig. 2.28: Calcein-AM staining of ucMSC on Cerasorb M, after 5 days of static cultivation (A) top and (B) bottom of the biomaterial, and after 2 days of static cultivation followed by 3 days of dynamic cultivation (C) top and (D) bottom of the biomaterial.

2.6.2 Osteogenic differentiation of MSC in a disposable direct perfusion bioreactor

To apply direct perfusion to MSC on collagen-based biomaterials the single-use bioreactor P3D-6 (EBERS Medical, Zaragoza, Spain) was used (Fig. 2.27). In a first experiment, $2*10^5$ ucMSC were seeded on Collagen-BG (d = 8 mm) and cultivated 3 days statically in culture medium. Thereafter, three samples were transferred to each bioreactor chamber under sterile conditions. Samples were positioned on top of each other and perfused with culture medium for 5 days by either applying 0.1 or 1 ml/min of fluid flow. For detailed information see section 5.7.3. DAPI images were taken to determine cell distribution within the matrices.

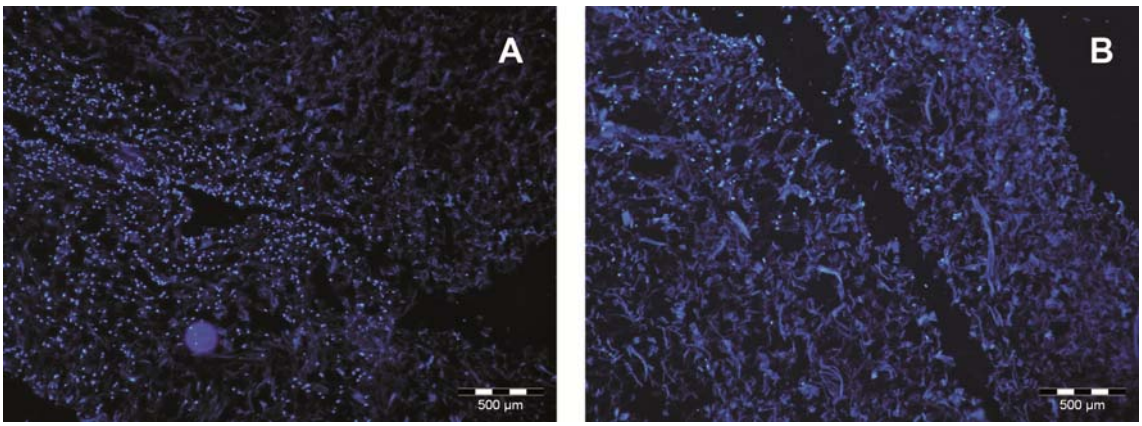

Fig. 2.29: DAPI images of ucMSC on Collagen-BG (cryosections of 25 µm) after 5 days of dynamic cultivation in the P3D-6 single-use perfusion bioreactor applying (A) 0.1 ml/min fluid flow or (B) 1 ml/min.

The cultivation of ucMSC on collagen-based biomaterials was difficult to carry out at a fluid flow of 1 ml/min in the single-use perfusion chamber. Collagen-based matrices deformed under the application of the fluid flow and were pressed into the bottom part (medium outlet) of the chamber. This effect did not occur at a fluid flow of 0.1 ml/min. The result of this effect can also be seen on DAPI images (Fig. 2.29). Only few cells can be observed on the samples cultivated at 1 ml/min. In comparison, matrices cultivated at 0.1 ml/min show nearly uniform cell distribution.

In a next approach, a dynamic long-term cultivation of ucMSC on Collagen-BG was performed in the single-use perfusion bioreactor P3D-6 to determine the influence of fluid flow on MSC differentiation. For this experiment, $2*10^5$ ucMSC were seeded on each matrix (d = 8 mm), cultivated 4 days in culture medium and 4 days in ODM-M. Thereafter, a dynamic cultivation for 3 weeks was carried out with a constant fluid flow of 0.1 ml/min using ODM-M. For comparison, cells on Collagen-BG were cultivated statically over the same time period. Mineralization of the ECM was

examined by AlizarinRed and von Kossa staining of cryosections (25 µm). The isolated amount of RNA was not sufficient to perform PCR analysis.

The DAPI image indicates a uniform cell distribution throughout Collagen-BG after 3 weeks of dynamic perfusion cultivation. Moreover, a strong ECM mineralization can be verified by AlizarinRed and von Kossa staining. Mineralization occurs almost throughout the entire matrix (**Fehler! Verweisquelle konnte nicht gefunden werden.**). On the contrary, static cultivation only reveals small mineralized areas on the edges of the matrix (cp. Tab. 2.7).

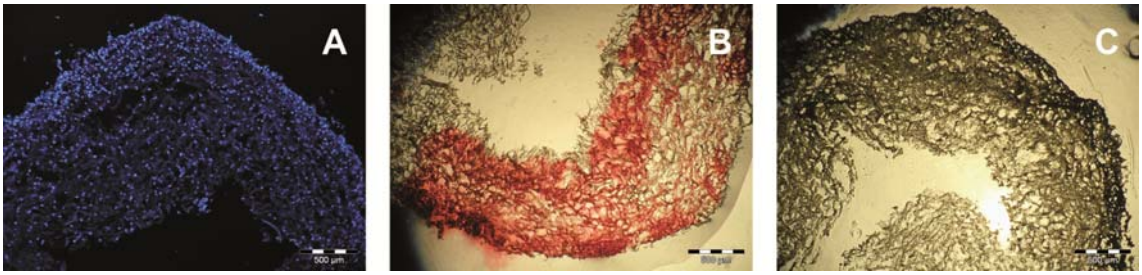

Fig. 2.30: Histological stainings of cryosections (25 µm) after cultivation of ucMSC on Collagen-BG in a single-use perfusion bioreactor for 3 weeks (A) DAPI, (B) AlizarinRed and (C) von Kossa staining.

Summing up the results, it can be stated that the design of the single-use perfusion chamber only allows for cultivation of collagen-based biomaterials at very low fluid flow rates. To overcome this limitation EBERS Medical lately designed a mesh to be positioned on the bottom of the bioreactor chamber with the function to keep soft biomaterials in its location. However, already the application of very small flow rates resulted in an enhanced osteogenic differentiation of ucMSC on Collagen-BG compared to static cultivation. Furthermore, a uniform mineralization could be observed. This is the result of an improved cell distribution and medium supply in the dynamically cultured sample.

2.6.3 Osteogenic differentiation of MSC in a non-disposable direct perfusion bioreactor

To perform 3D dynamic cultivations on ceramic biomaterials a special designed non-disposable perfusion culture chamber (EBERS Medical, Zaragoza, Spain) was used (Fig. 2.31, left). The perfusion bioreactor is constructed to apply laminar flow to eight matrices (d = 10 mm) simultaneously. It consists of two identical cylindrical parts and a disk to position eight biomaterials in the middle of the chamber. In the first approach cell performance on Sponceram-Al at different flow rates was investigated. Therefore, $2*10^5$ adMSC were seeded onto each sterile Sponceram-Al matrix and cultivated 3 days statically in culture medium. Then, samples were transferred to the perfusion culture

chamber under sterile conditions and cultivated at a constant fluid flow of 0.25, 0.5, 1, 1.5, 3 or 5 ml/min for 5 days using culture medium. The assembling of the bioreactor system is described in detail in section 5.7.4. To determine cell viability an MTT assay was performed (n = 5) and images of DAPI staining were taken. For comparison, cells on Sponceram-Al were cultivated statically over the same time period.

DAPI images (Fig. 2.32) indicate approximately the same amount of cells on Sponceram-Al after static cultivation and after dynamic cultivation with 0.25 ml/min fluid flow. Matrices are completely covered by a dense cell layer. Samples cultivated at a fluid flow of 0.5 and 1.5 ml/min show significantly less cells compared to the static control. However, after the dynamic cultivation applying 3 and 5 ml/min fluid flow only few cells can be detected via DAPI staining. The visual impression that an increasing flow rate disrupts cells from the matrix can be supported by the MTT viability assay (Fig. 2.31, right). MSC on statically cultured samples and on samples cultivated with 0.25 ml/min fluid flow exhibit identical viability. A significant decrease of cell viability can be seen by increasing the fluid flow to 0.5 ml/min. MSC on matrices cultivated with 1.5 and 0.5 ml/min fluid flow show about the same viability. Increasing the fluid flow to 3 or 5 ml/min further decreases cell viability. Taken into account the results of DAPI images, there is no reduction of cell viability, but a disruption of cells from the matrix. Cell viability is measured to indirectly compare the cell number.

Next goal was to improve osteogenic differentiation due to the application of fluid flow. For this approach, fluid flow of 1.5 ml/min was chosen. In literature a variety of fluid flow rates are described, e.g. 0.05 to 5 ml/min [178] or 5 to 20 ml/min [179]. Briefly, $2*10^5$ adMSC were seeded onto each sterile Sponceram-Al matrix, cultivated 4 days in culture medium and 4 days in ODM. Thereafter, dynamic cultivation for 3 weeks was performed applying a constant fluid flow of 1.5 ml/min using ODM. 10 ml of fresh medium were added to the medium reservoir through a septum on day 5, 10 and 15. For comparison, cells on Sponceram-Al were cultivated statically over the same time period in ODM. Osteogenic differentiation was verified by different histological stainings and PCR analysis. Moreover, the cell morphology after cultivation was observed via SEM.

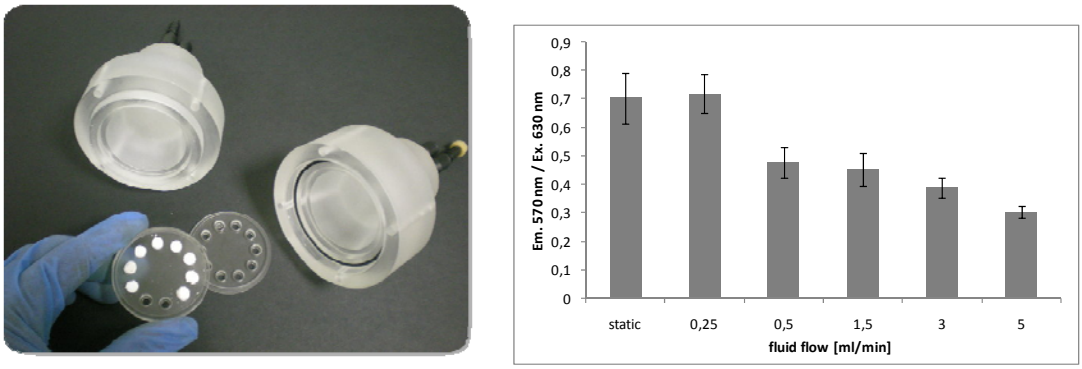

Fig. 2.31: (Left) perfusion bioreactor designed and distributed by EBERS Medical (Zaragoza, Spain) and (right) MTT viability assay of adMSC on Sponceram-Al after 8 days of static cultivation and after 3 days of static cultivation followed by 5 days of dynamic cultivation, applying different fluid flow rates. Standard deviation is given for n = 5.

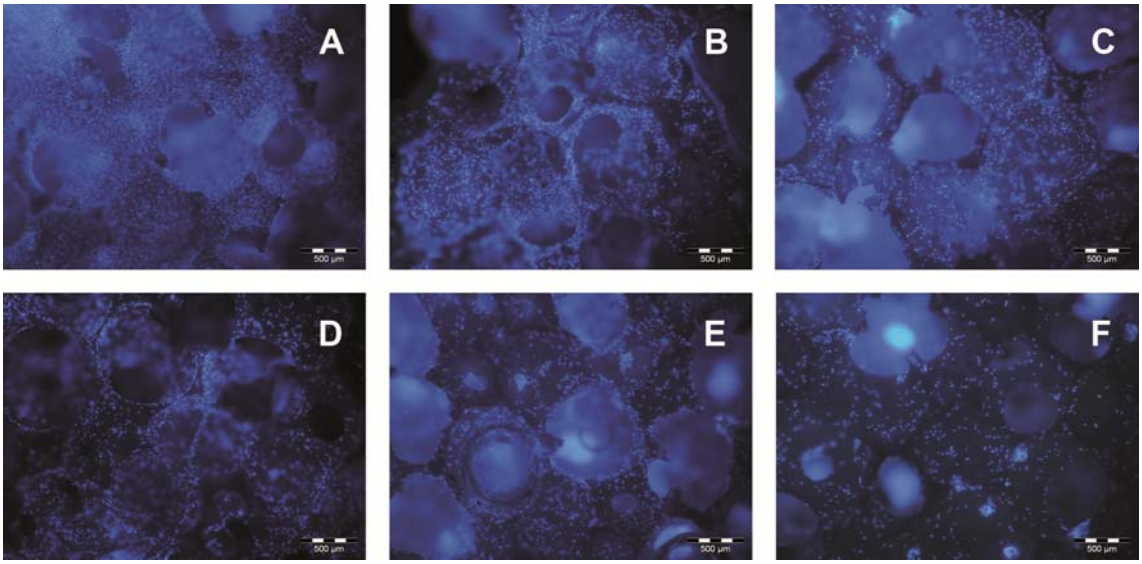

Fig. 2.32: DAPI images of adMSC on Sponceram-Al after static cultivation (A) and after 5 days of dynamic cultivation applying constant fluid flow of (B) 0.25 ml/min, (C) 0.5 ml/min, (D) 1.5 ml/min, (E) 3 ml/min and (F) 5 ml/min.

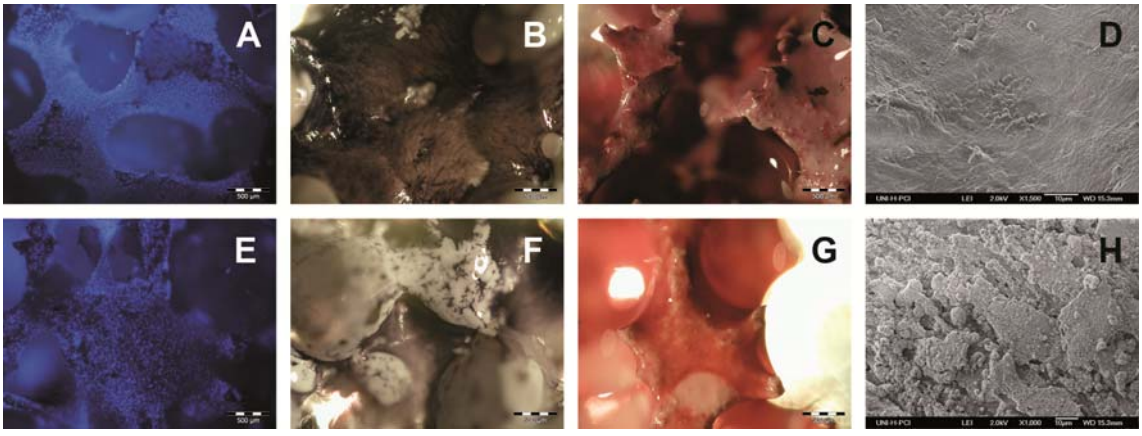

Fig. 2.33: Osteospecific histological stainings of adMSC on Sponceram-Al after dynamic cultivation in a perfusion bioreactor (A-D) and static cultivation (E-H); DAPI staining (A, E), membrane-bound AP staining (B, F), AlizarinRed staining (C, G) and SEM images (D, H).

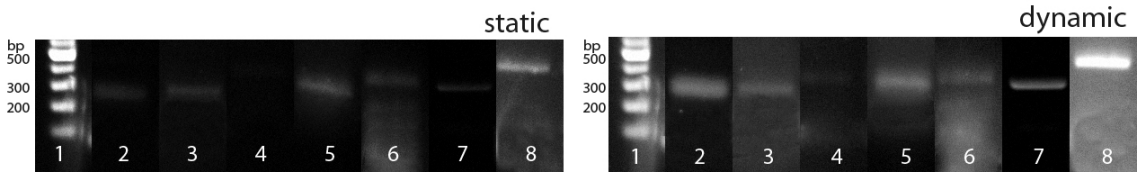

Fig. 2.34: RT-PCR of statically cultured sample (left), dynamically cultured sample (right). Lane 1: ladder, lane 2: *HPRT*, lane 3: *COL I*, lane 4: *BMP-4*, lane 5: *RUNX*, lane 6: *OC*, lane 7: *OP*, lane 8: *AP*.

DAPI images indicate a dense cell layer on Sponceram-Al after static, as well as after dynamic cultivation. The expression of membrane-bound AP is enhanced on dynamically cultivated samples. However, no significant difference can be found in the level of ECM mineralization (AlizarinRed). Static as well as dynamic samples show a beginning mineralization of their ECM. But, a clear difference can be seen in cell morphology. MSC on dynamically cultivated matrices obtain a rather smooth and flat morphology with areas showing bone nodule formation. However, cells on statically cultivated samples possess a very rough morphology, indicating an advanced osteogenic differentiation (Fig. 2.33). These results are supported by RT-PCR analysis (**Fehler! Verweisquelle konnte nicht gefunden werden.**). Electrophoretic gel images reveal the expression of osteogenic markers in the dynamic, as well as in the statically cultured sample. Only the mRNA production of *AP* is enhanced in the dynamically cultured sample (both samples of *AP* have been analyzed on one electrophoretic gel and the image has been taken with the same exposure).

In summary, it could be shown that adMSC show decreasing viability in the perfusion bioreactor with increasing fluid flow rates (up to 5 ml/min). Supposably, the strength of cell attachment is not sufficient to withstand high perfusion rates and cells detach from the substrate. Different studies revealed a cell loss of 40 to 50 % applying a shear stress of only 0.00008 to 0.002 dyn/cm² [180-182]. Therefore, a fluid flow rate of 1.5 ml/min was chosen to perform long-term cultivation. A significant cell loss could not be observed after 3 weeks of dynamic cultivation. Even though, an enhanced *AP* production could be detected on the dynamically cultured samples, no difference in ECM mineralization was obvious. However, SEM images of the cell morphology indicate a beginning differentiation of adMSC on dynamically cultivated samples and an advanced differentiation on the static control. But it shall be taken into account that fluid flow might also have an influence on cell morphology. Applying fluid flow on a 2D adMSC culture, for example, resulted in significantly elongated cell morphology (cp. section 2.1). Although, no significantly enhanced differentiation of adMSC on Sponceram-Al could be observed under dynamic conditions, the use of the bioreactor system facilitated cultivation. Labor input, for example, could be reduced, since no

medium change was necessary. Adding fresh medium into the bioreactor system may also be automated by an additional programmed peristaltic pump.

2.6.4 Osteogenic differentiation of MSC in a bioreactor system combining perfusion and compression

It is well known that mechanical loading influences new bone formation *in vivo*. To date, however, the exact mechanism of how loading evokes bone formation is not fully understood. Two main hypotheses exist: The direct transmission of mechanical loading to bone cells and the evocation of fluid shear stress mediated by mechanical loading [183]. Nevertheless, numerous studies reveal that especially cyclic pressure enhances osteoblast function *in vitro* [184], as well as osteogenic differentiation of MSC [185]. The exposure of MSC, derived from bone marrow, to perfusion and cyclic pressure, for example, resulted in an increased production of Collagen I, Collagen III, and Osteocalcin [185].

In order to study the influence of perfusion and compression on adMSC and ucMSC in a 3D environment a prototype bioreactor system developed by Greiner Bio-One (Frickenhausen, Germany) was used. The prototype was actually designed to promote chondrogenic differentiation of MSC in hydrogels (cooperation of Greiner Bio-One with Frauenhofer, Stuttgart), but was here adopted to perform cultivations of adMSC or ucMSC on either Matriderm or Sponceram-Al. Briefly, medium is pumped from the reservoir into the culture chamber. The biomaterial in the chamber is perfused from the bottom to the top. Compression of the matrix is induced by filling the headspace of the bioreactor with compressed air. Matrix and headspace are separated by an elastic membrane (Fig. 2.35). The flow of compressed air is controlled by an automatically guided magnetic valve.

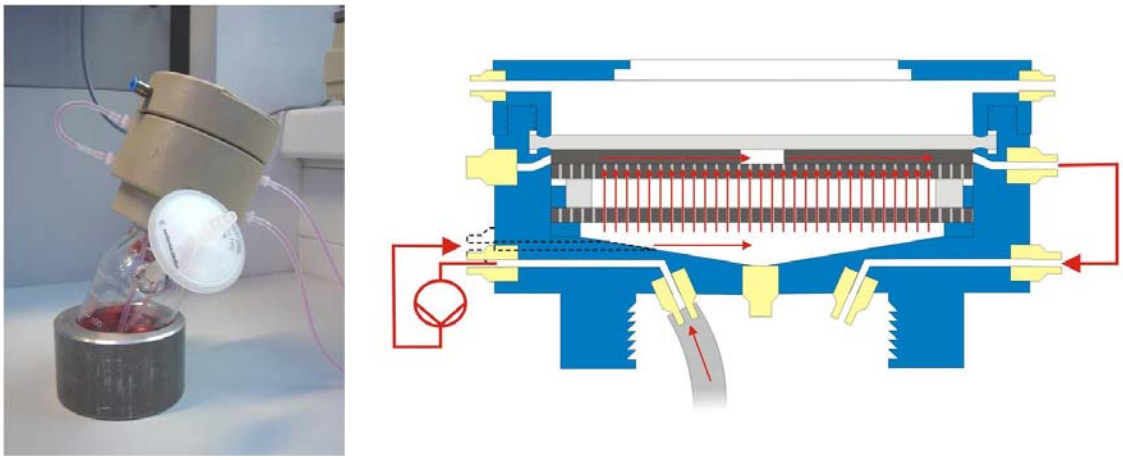

Fig. 2.35: Prototype bioreactor system designed by Greiner Bio-One (Frickenhausen, Germany) to perform dynamic cultivation applying perfusion and cyclic compression simultaneously.

2.6.4.1 *Application of perfusion and compression on MSC cultivated on a collagen-based biomaterial*

In a first approach, cultivation was performed with adMSC on Matriderm at 1.5 ml/min continuous fluid flow and applying the following compression profile: Compression over the headspace with 0.4 bar alternating 2 s on and 2 s off for 1 h, followed by a rest period of 2 h. The membrane separating the headspace and the matrix is compressing the collagen-based biomaterial. For cultivation $1.8*10^6$ adMSC were seeded evenly with a syringe onto Matriderm (d = 5 cm). Previously, Matriderm was sterilized under UV light. The cell-biomaterial construct was cultivated 3 days statically in culture medium. Then, the matrix was transferred to the bioreactor under sterile conditions. During the first 2 days of dynamic cultivation only perfusion was applied. From the third day on perfusion and compression were performed simultaneously over a period of 19 days. Dynamic cultivation was carried out using 80 ml ODM. 10 ml of fresh ODM were added to the medium reservoir on day 5, 10 and 15 using a septum and a syringe. For comparison, adMSC on Matriderm were statically cultivated in 25 ml ODM over the same time period. Medium of the statically cultured samples was changed on day 5, 10 and 15. To verify osteogenic differentiation histological stainings of cryosections (25 µm) were prepared. Moreover, RNA was isolated and PCR analysis performed.

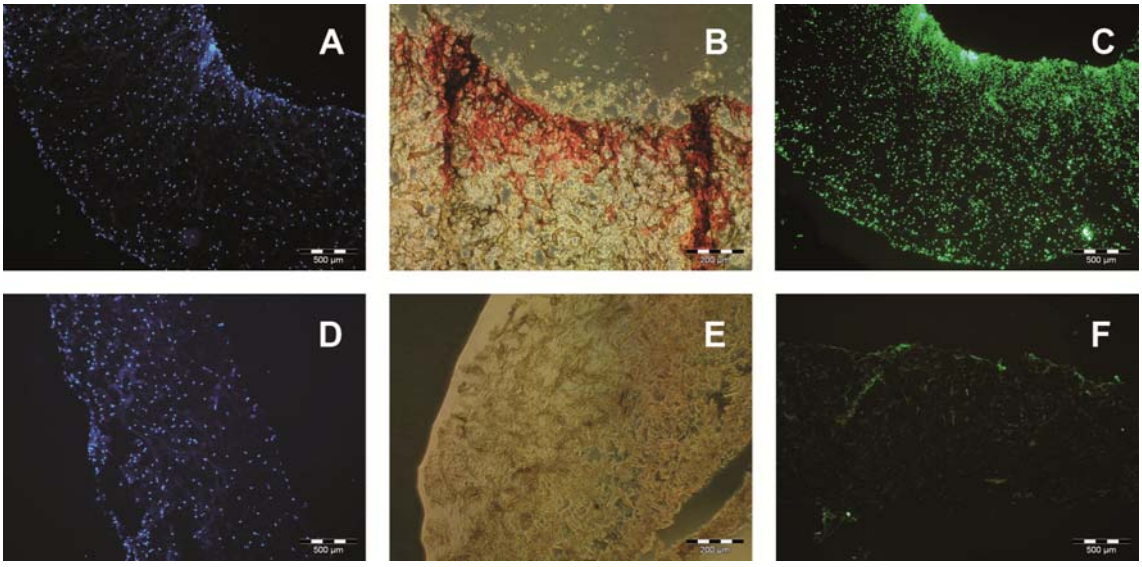

Fig. 2.36: Histological stainings of cryosections (25 µm) after dynamic cultivation of adMSC on Matriderm applying perfusion and compression (A-C) and static cultivation (D-F); DAPI (A, D), AlizarinRed (B, E) and Calcein staining (C, F).

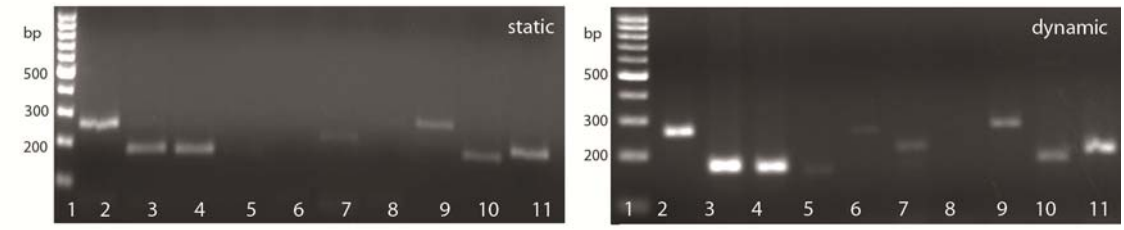

Fig. 2.37: RT-PCR of statically cultured sample (left) and dynamically cultured sample (right). Lane 1: ladder, lane 2: *HPRT*, lane 3: *COL I*, lane 4: *COL III*, lane 5: *RUNX*, lane 6: *BSP-2*, lane 7: *OP*, lane 8: *BMP-2*, lane 9: *BMP-4*, lane 10: *OC*, lane 11: *AP*.

DAPI images indicate a uniform cell distribution in dynamically as well as in statically cultivated samples. However, mineralization and calcification of the ECM could only be verified by AlizarinRed and Calcein staining in samples cultivated under dynamic conditions (Fig. 2.36). Especially, the staining with Calcein is very intense. The assumption that osteogenic differentiation of adMSC is enhanced by perfusion and cyclic compression is supported by the results of PCR analysis. mRNA expression of *RUNX* and *BSP-2* cannot be identified in the static sample, whereas these mRNAs are expressed by the cells of the dynamic sample. Additionally, in the dynamically cultivated sample the mRNA expression of *COL I* and *COL III* is enhanced (Fig. 2.37). The results reveal that constant perfusion combined with cyclic compression significantly enhances the osteogenic differentiation of adMSC in a 3D collagen-based microenvironment.

2.6.4.2 Application of perfusion and compression on MSC cultivated on a ceramic substrate

In contrast to collagen-based biomaterials, ceramic matrices cannot be squeezed by applying compression. However, cyclic compression according to the profile described above in section 2.6.4.1 will enhance fluid flow through the matrix. *In vivo* the deformation of bone evoked by mechanical loads induces cyclic movement of interstitial fluid, which generates an enhanced fluid shear stress [186]. Fluid shear stress is normally present at a constant level, which is sufficient for bone maintenance. One assumption is that enhanced shear stresses within the bone pores evoke new bone formation [183]. Also *in vitro*, especially cyclic loading is known to promote osteogenic differentiation by creating a cyclic movement of intersitial fluid [184, 185].

To investigate the assumption that cyclic loading enhances osteogenic differentiation due to creating fluid shear stress, dynamic cultivation was performed with adMSC and ucMSC on Sponceram-Al in the prototype bioreactor system of Greiner Bio-One. For implementation of this cultivation Sponceram-Al was manufactured as a disk with the dimensions d = 50 mm and ht = 3 mm. Sponceram was autoclaved and $5*10^6$ adMSC or

ucMSC were seeded evenly with a pipette on both sides of the matrix, cultivated statically for 4 days in culture medium and for 4 days in ODM and ODM-M, respectively. For ucMSC commercially available ODM-M was used. The matrix was transferred to the bioreactor under sterile conditions. In a first experiment, dynamic cultivation was performed for 21 days with either 0.1 or 1 ml/min fluid flow, but without compression. Dynamic cultivation was carried out using 80 ml ODM or ODM-M. 10 ml of fresh medium were added to the medium reservoir on day 5, 10 and 15 using a septum and a syringe. For comparison, cells were cultivated statically in 25 ml ODM or ODM-M. Medium of the statically cultured samples was changed on day 5, 10 and 15. To perform analyses the Sponceram-Al matrix was separated into small uniform pieces. MTT assay was performed to determine the cell viability (n = 3). Moreover, SEM images were taken to observe the cell distribution and morphology. In the following experiment, perfusion with 0.1 ml/min and compression were performed simultaneously according to the profile described in section 2.6.4.1 using adMSC and 80 ml ODM. The addition of fresh medium and the cultivation of a static control was performed according to the explanation given above. During the first 2 days of dynamic cultivation only perfusion was applied. Perfusion and cyclic compression were performed for 19 days. MTT assay was again carried out to determine the cell viability (n = 3). SEM images were taken and different histological stainings were performed to verify osteogenic differentiation. Moreover, RNA was isolated and PCR analysis performed.

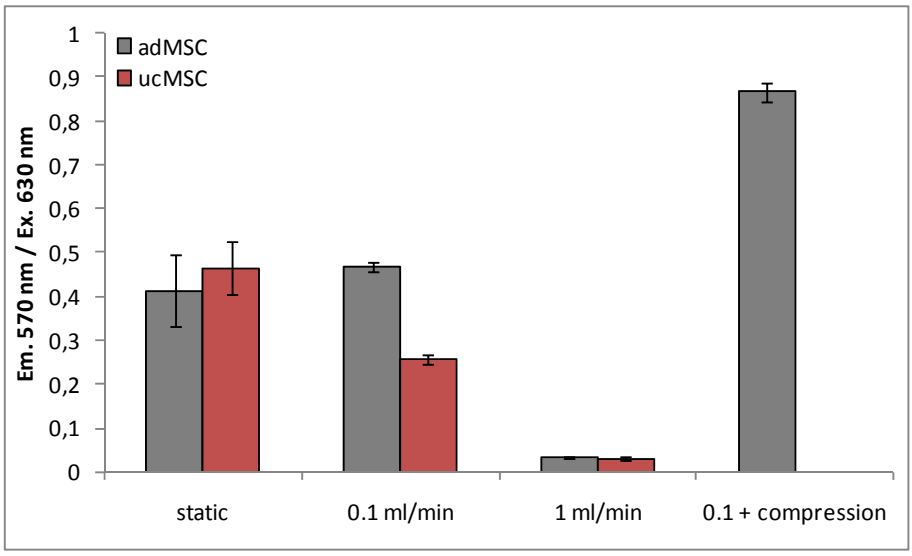

Fig. 2.38: MTT viability assay of adMSC and ucMSC on Sponceram-Al after static cultivation, dynamic cultivation applying fluid flow and dynamic cultivation combining fluid flow and cyclic compression. Standard deviation is given for n = 3.

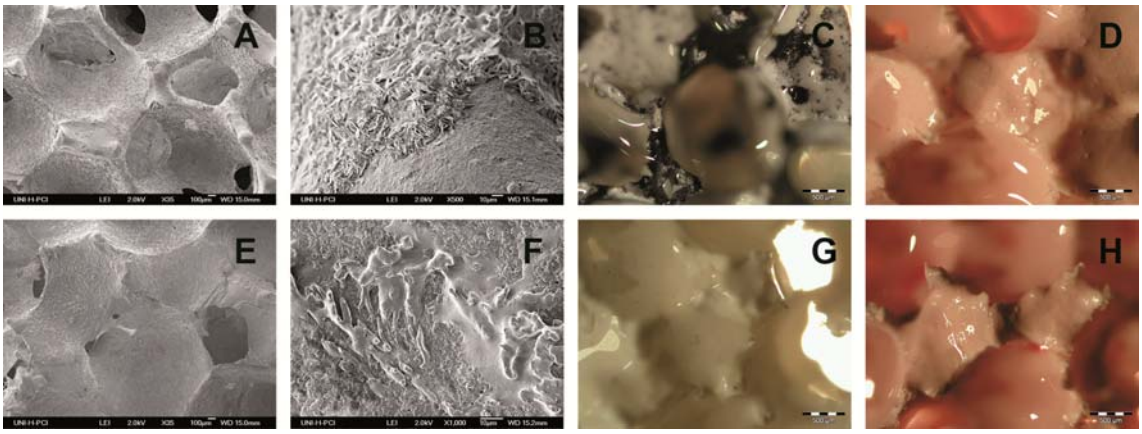

Fig. 2.39: Images of adMSC (A-D) and ucMSC (E-H) on Sponceram-Al after dynamic cultivation applying 0.1 ml/min fluid flow: (A, E) SEM image showing cell distribution, (B, F) SEM image showing cell morphology, (C, G), membrane-bound AP staining and (D, H) AlizarinRed staining.

Cultivation of adMSC and ucMSC in the bioreactor system of Greiner Bio-One using 1 ml/min fluid flow resulted in cell loss, therefore, no cell viability can be measured. AdMSC cultivated at 0.1 ml/min fluid flow show the same viability than cells on the static control. However, the viability of ucMSC is reduced. Surprisingly, adMSC on Sponceram-Al cultivated with the combination of 0.1 ml/min and cyclic compression resulted in a significantly increased cell viability (Fig. 2.38).

SEM images indicate that adMSC as well as ucMSC are distributed evenly on Sponceram-Al after 3 weeks of dynamic cultivation using 0.1 ml/min fluid flow (Fig. 2.39, A, E). However, cell morphology is significantly different. AdMSC are present in a very thick layer of ECM, which obtains a rough morphology. On the contrary, ucMSC still present a rather smooth and elongated morphology (Fig. 2.39, B, F). Histological stainings indicate a strong membrane-bound AP production of adMSC after dynamic cultivation, which cannot be detected for ucMSC (Fig. 2.39, C, G). Mineralization of the ECM can neither be observed for adMSC nor for ucMSC (Fig. 2.39, D, H). However, strong mineralization can be verified for adMSC, via AlizarinRed and von Kossa staining, after dynamic cultivation applying 0.1 ml/min fluid flow and cyclic compression (Fig. 2.40, C, D). In addition cells present a rough cell morphology and the production of membrane-bound AP. Histological stainings indicate an enhanced EMC mineralization in the dynamically cultured sample compared to the static control (cp. **Fehler! Verweisquelle konnte nicht gefunden werden.**, F-H). This result can be supported by PCR analysis. Especially the production of *OC* mRNA is enhanced by perfusion, but even more by combining perfusion and cyclic compression (all samples of *OC* have been analyzed on one electrophoretic gel and the image has been taken with the same exposure). Also the production of *AP* is

increased by the combination of perfusion and compression, as well as by only applying perfusion (Fig. 2.41).

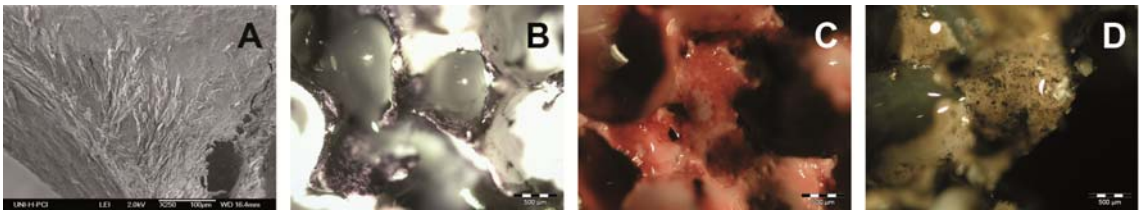

Fig. 2.40: Images of adMSC on Sponceram-Al after dynamic cultivation combining 0.1 ml/min fluid flow and cyclic compression: (A) SEM image, (B) membrane-bound AP staining, (C) AlizarinRed staining and (D) von Kossa staining.

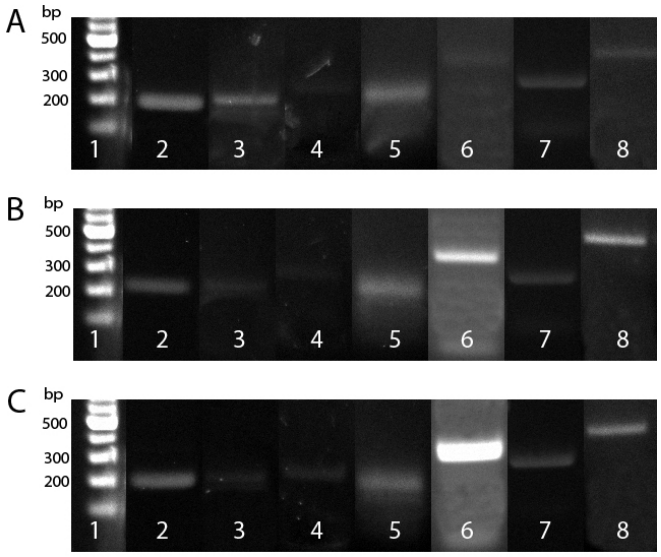

Fig. 2.41: RT-PCR of statically cultured sample (A), dynamically cultured sample applying 0.1 ml/min perfusion (B) and dynamically cultured sample combining 0.1 ml/min perfusion and cyclic compression. Lane 1: ladder, lane 2: *HPRT*, lane 3: *COL I*, lane 4: *BMP-4*, lane 5: *RUNX*, lane 6: *OC*, lane 7: *OP*, lane 8: *AP*.

It can be concluded that ucMSC are not suitable for the dynamic cultivation on Sponceram-Al in the Greiner Bio-One prototype bioreactor system. Their viability was already at a fluid flow rate of 0.1 ml/min significantly reduced compared to adMSC. Dynamically cultivating adMSC under the same conditions resulted in a rough cell morphology and membrane-bound AP production, but no ECM mineralization could be revealed via staining procedures. Only the combination of 0.1 ml/min fluid flow and cyclic compression significantly enhanced osteogenic differentiation of adMSC on Sponceram-Al compared to the static control. However, this dynamic cultivation procedure not only improved osteogenic differentiation, but also resulted in increased cell viability (cp. [187]).

Tab. 2.9 summarizes the experiments carried out with MSC on a ceramic substrate using the prototype bioreactor designed by Greiner Bio-One. It can be seen that only the cultivation of ucMSC combining 0.1 ml/min fluid flow and compression has not

been performed. This decision was based on the weak viability of ucMSC on Sponceram-Al applying only 0.1 ml/min fluid flow without compression (Tab. 2.10). Furthermore, Tab. 2.10 summarizes the results of MSC viability and differentiation under different cultivation conditions. It is obvious that adMSC presented strongest osteogenic differentiation by combining 0.1 ml/min fluid flow and compression.

Tab. 2.9: Overview on the performed dynamic experiments using the prototype bioreactor of Greiner Bio-One and Sponceram-Al (**+** labels experiments performed and **-** experiments not performed)

	static	**1 ml/min**	**0.1 ml/min**	**0.1 ml/min + compression**
adMSC	+	+	+	+
ucMSC	+	+	+	-

Tab. 2.10: Summary of the proliferation and differentiation results of MSC cultivated on Sponceram-Al in the dynamic bioreactor of Greiner Bio-One [level of osteogenic differentiation from **-** (no differentiation) to **+++** (strong differentiation)].

	Viability	**AP**	**AlizarinRed**	**Von Kossa**	**Osteocalcin**
adMSC static	++	+	+	N/A	+
adMSC 0.1 ml/min	++	++	-	N/A	++
adMSC 0.1 ml/min and compression	+++	++	++	++	+++
ucMSC static	++	-	-	N/A	N/A
ucMSC 0.1 ml/min	+	-	-	N/A	N/A

2.6.5 Osteogenic differentiation of MSC in a drip-perfusion bioreactor

For further investigation of cell differentiation under perfusion conditions, a drip-perfusion bioreactor has been developed at the Institute of Technical Chemistry at the Leibniz University of Hanover. The system is designed for the 3D dynamic cultivation of MSC. It consists of a cylindrical culture chamber with a mesh and a disk in the middle to keep the biomaterial in the centre of the chamber (Fig. 2.42). Medium is pumped at a very low flow rate from the reservoir into the culture chamber using a peristaltic pump. A tube is located in the middle of the chamber with a short distance to the matrix in order to directly position droplets of medium on the top center of the biomaterial. Applying this technique, the biomaterial is constantly kept moisturized, but the matrix is not entirely surrounded by medium. The biomaterial is slowly perfused with medium only by the force of gravity. The medium is collected on the bottom of the culture chamber and pumped back to the reservoir using a second peristaltic pump.

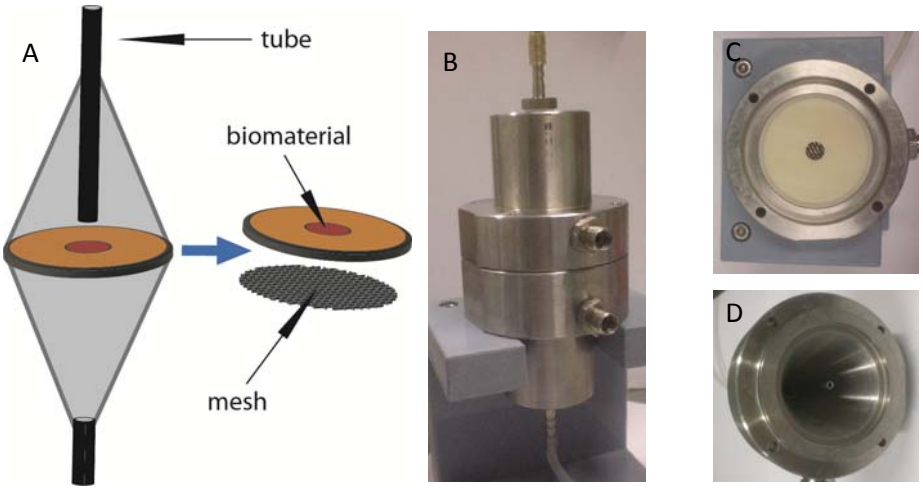

Fig. 2.42: Drip-Perfusion bioreactor for 3D dynamic cultivation of MSC designed at the Institute of Technical Chemistry at the Leibniz University of Hanover: (A) Schematic assembly, (B) complete drip-perfusion bioreactor, (C) fixing to center the biomaterial and (D) tube in the culture chamber.

First task was to examine cell viability in the newly developed drip-perfusion bioreactor system. Therefore, $2*10^5$ adMSC or ucMSC were seeded onto Collagen-BG (d = 10 mm) and cultivated statically for 2 days in culture medium. Then, three matrices were transferred into the autoclaved bioreactor under sterile conditions. The matrices were positioned on top of each other. Dynamic cultivation was performed for either 4, 10 or 21 days at a fluid flow of 0.1 ml/min. Cell viability after dynamic cultivation was determined by CellTiter Blue assay (n = 3) and compared to static controls (n = 3).

There is no significant difference in cell viability between the statically and dynamically cultured samples at day 4 and 10. Moreover, ucMSC viability on day 10 is enhanced compared to adMSC. This effect can be explained with the different cell size of adMSC and ucMSC. AdMSC obtain a larger cell size than ucMSC, whereas the biomaterials surface area remains the same. Therefore, ucMSC can further proliferate on the biomaterial. However, on day 21 cell viability of adMSC and the viability of dynamically cultured ucMSC samples remain equal. In contrast, the viability of statically cultivated ucMSC is reduced compared to data at day 10 (Fig. 2.43). UcMSC in static conditions might not optimally be supplied with nutrients. In summary, it can be stated that cultivation of MSC in the designed drip-perfusion bioreactor does not inhibit cell proliferation or reduce cell viability in comparison to a static control.

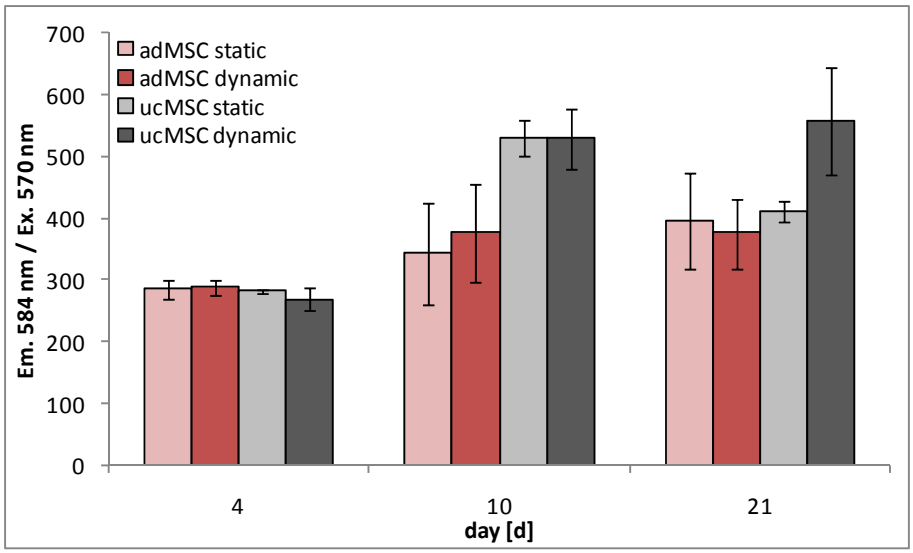

Fig. 2.43: CellTiter Blue viability assay of adMSC and ucMSC after 4, 10 or 21 days of static or dynamic cultivation in the drip-perfusion bioreactor using culture medium. Standard deviation is given for n = 3.

Next task was the performance of MSC differentiation in the drip-perfusion bioreactor. Nevertheless, the size of the biomaterial (d = 10 mm) was only sufficient for the implementation of histological stainings, but not for the isolation of RNA to carry out PCR analysis. Hence, the inner fixing of the biomaterial at the centre of the bioreactor chamber was scaled up. At the same time, the complete bioreactor chamber was modified and miniaturized. The new fixing was designed to hold three collagen-based biomaterials with a diameter of 16 mm (Fig. 2.44). Another future goal was the parallelization of bioreactor cultivation; therefore, four equal mini-drip-perfusion bioreactors have been constructed (cp. section 2.7).

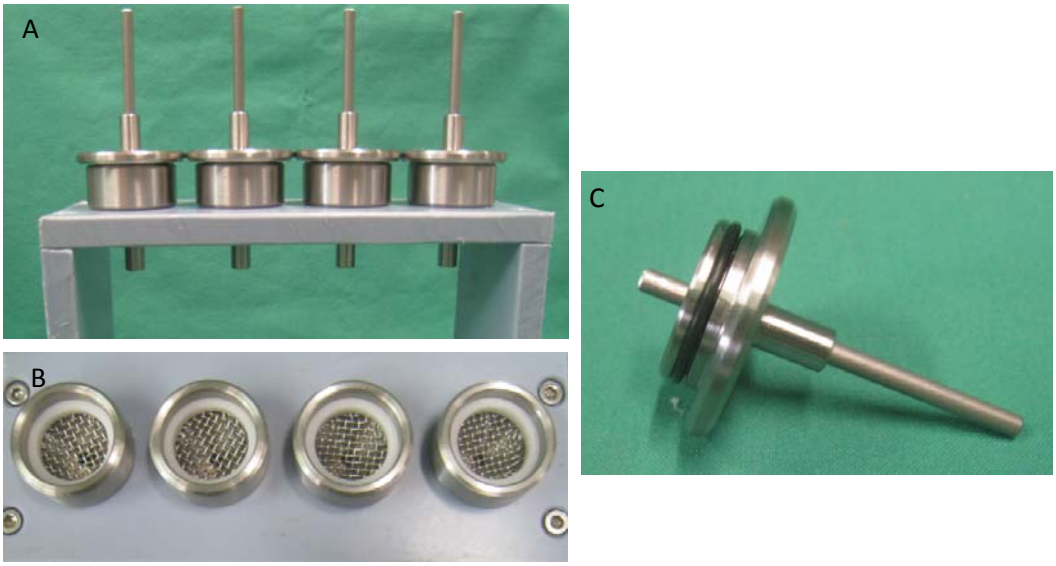

Fig. 2.44: Miniaturization of the drip-perfusion bioreactor and modification of the fixing: (A) Four equally designed drip-perfusion bioreactors, (B) fixing to hold biomaterials with a diameter of 16 mm and (C) upper part of the drip-perfusion bioreactor chamber.

To perform dynamic differentiation experiments, $4*10^5$ adMSC or ucMSC were seeded onto Collagen-BG (d = 16 mm), cultivated statically for 4 days in culture medium and for 4 days in ODM or ODM-M. For cultivation of ucMSC commercially available ODM-M was used. After static cultivation three samples were introduced into one culture chamber under sterile conditions. Dynamic cultivation was performed at 0.1 ml/min constant fluid flow for 21 days in 80 ml ODM or ODM-M. About 10 ml of fresh ODM or ODM-M were added into the reservoir at day 5, 10 and 15 using a syringe and a septum. For comparison, cells on Collagen-BG were cultivated statically in 2 ml ODM or ODM-M. Medium of the statically cultured samples was changed (2 ml) on day 1, 3 and 5 of every week. To verify osteogenic differentiation histological stainings of cryosections (25 µm) and PCR analysis were performed.

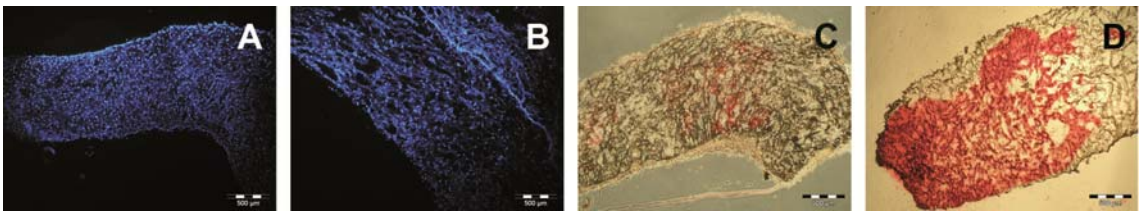

Fig. 2.45: DAPI and AlizarinRed staining of adMSC on Collagen-BG (cryosections of 25 µm); (A, C) statically cultured sample and (B, D) dynamically cultured sample.

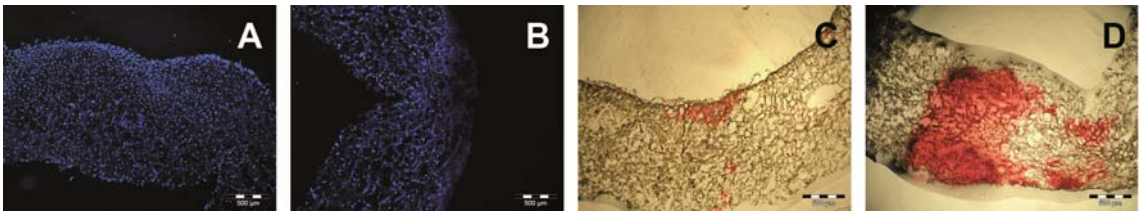

Fig. 2.46: DAPI and AlizarinRed staining of ucMSC on Collagen-BG (cryosections of 25 µm); (A, C) statically cultured sample and (B, D) dynamically cultured sample.

After the dynamic cultivation on Collagen-BG in the drip-perfusion bioreactor less adMSC, as well as ucMSC, are present on the matrix, compared to the static control (verified by DAPI staining). But in contrast, a stronger ECM mineralization (AlizarinRed) can be identified (Fig. 2.45 and Fig. 2.46). Cell death is caused by strong ECM production. This effect has also been observed in 2D differentiation experiments by Antonina Lavrentieva (Institute of Technical Chemistry, Leibniz University of Hanover) and will be further discussed in section 2.7. The impression given by the histological stainings that MSC differentiation is enhanced due to dynamic cultivation in the drip-perfusion bioreactor is supported by PCR analysis, exemplarily shown for ucMSC (Fig. 2.47). Expression of *OC* cannot be detected in the statically cultured sample, but clearly be identified after the cultivation under dynamic conditions.

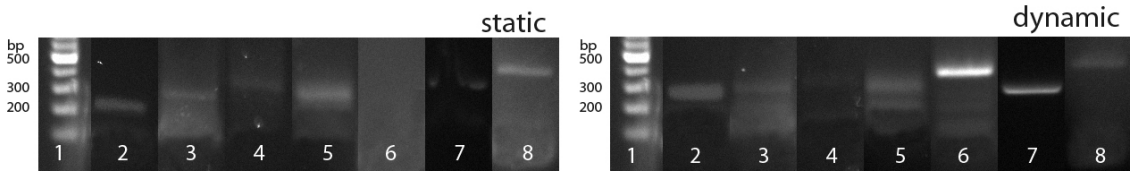

Fig. 2.47: RT-PCR of statically cultured sample (left), dynamically cultured sample (right). Lane 1: ladder, lane 2: *HPRT*, lane 3: *COL I*, lane 4: *BMP-4*, lane 5: *RUNX*, lane 6: *OC*, lane 7: *OP*, lane 8: *AP*.

The drip-perfusion bioreactor was not only developed for 3D dynamic cultivation of MSC on collagen-based biomaterials, but also on ceramic biomaterials. For this purpose, the design of the fixture in the culture chamber was changed. The fixture consists of an autoclaveable plastic ring (d = 10 mm) to position a ceramic biomaterial in the center of the chamber (Fig. 2.48, A). To check the performance of MSC on ceramic biomaterials in this culture system, $2*10^5$ adMSC were seeded onto each Sponceram-Al matrix, cultivated statically for 2 days in culture medium and for 2 days in ODM. Static cultivation in ODM was performed to initiate the production of ECM and consequently stabilize the cells on the matrix. Earlier experiments without static cultivation in ODM resulted in complete cell loss under dynamic conditions (not illustrated). After static cultivation, each matrix was transferred into one drip-perfusion bioreactor (n = 4) and parallel dynamic cultivation was performed for 3 days at 0.1 ml/min fluid flow using two multichannel peristaltic pumps. Cell performance was shown by DAPI staining.

DAPI images indicate a weak performance of adMSC on Sponceram-Al under dynamic conditions. Significantly less cells can be observed compared to the static control (Fig. 2.48, B and C). Moreover, dynamically cultivated MSC on Sponceram-Al form cell colonies. A homogeneous cell layer cannot be detected. Cultivation of MSC on ceramic biomaterials in the drip-perfusion bioreactor system has to be optimized further. Maybe, an advanced medium distribution system might help to minimize shear forces and therefore reduce cell detachment. Due to the weak performance of adMSC on ceramic biomaterials under dynamic conditions using this bioreactor system, differentiation experiments have not been performed.

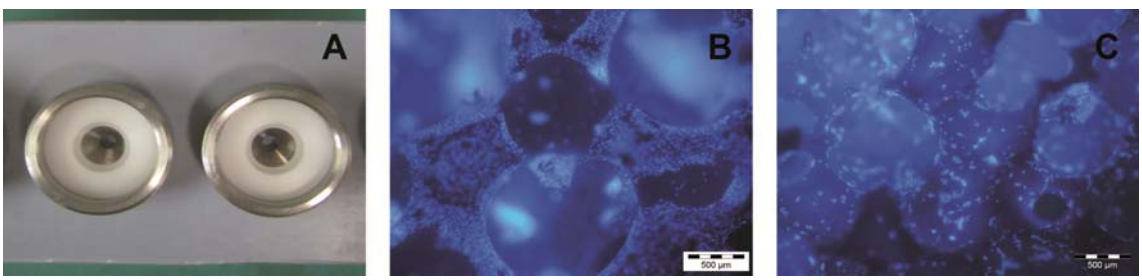

Fig. 2.48: (A) Design of the drip-perfusion bioreactor to culture MSC on ceramic biomaterials; (B) adMSC on Sponceram-Al after static cultivation and (C) after 3 days of dynamic cultivation.

2.6.6 Summary of 3D dynamic MSC cultivation and differentiation

3D dynamic cultivation and differentiation of MSC was performed in different bioreactor systems. Initially, it could be shown that the use of direct perfusion bioreactors can improve cell distribution within the matrix. This effect is also described by Keogh *et al.*, who already observed homogenous cell distribution after applying only three hours of perfusion, using a collagen glycosaminoglycan matrix [188]. For the investigation and improvement of cell distribution a single-use bioreactor system P3D-10 from EBERS Medical (Zaragoza, Spain) and Cerasorb M was used, which contains very small pores and showed weak cell distribution under static conditions. Dynamic cultivation for 3 days using 0.2 ml/min fluid flow already improved cell distribution. However, a uniform cell distribution within the matrix could not be achieved. The cell seeding process may be optimized by performing internal dynamic seeding procedures. Therefore, a matrix is placed in a bioreactor under sterile conditions or even positioned in the culture chamber prior to autoclaving. Internal dynamic cell seeding is, for example, performed by applying direct perfusion. Consequently, the cell suspension is distributed evenly within the matrix. Nevertheless, one major drawback is the low efficiency of cell attachment. Cells may also attach to the walls of the bioreactor or the tubing system. In order to obtain a sufficient amount of cells on the matrix, the application of high density cell suspensions is required. Wendt *et al.*, for example, used $1.3*10^7$ cells in 2.5 ml medium to seed one matrix of 8 mm diameter and 4.3 mm thickness using a perfusion bioreactor system [189].

To create a microenvironment which is known to evoke osteogenic differentiation, a direct perfusion bioreactor (EBERS Medical) was tested. This bioreactor system applies laminar fluid flow to eight matrices (d = 10 mm) simultaneously. First, cell viability was investigated at different flow rates. Then, long-term cultivation with adMSC on Sponceram-Al applying 1.5 ml/min fluid flow was performed. However, dynamically cultured samples did not show significant improved MSC differentiation, compared to the static control. Only the production of membrane-bound AP could be enhanced by applying perfusion. Moreover, this perfusion bioreactor system was not suitable for the cultivation of MSC on collagen-based biomaterials. To enhance osteogenic differentiation on these matrices, dynamic perfusion experiments in the single-use bioreactor P3D-6 were performed using ucMSC and applying a fluid flow of 0.1 ml/min. These cultivation conditions resulted in a strong ECM mineralization throughout the entire matrix. In comparison, the static control only revealed mineralization at the edges of the biomaterial. This might be the result of a limited nutrient supply, since medium distribution and exchange in the statically cultured

sample is only caused by diffusion. Perfusion bioreactors overcome this limitation and consequently differentiation in the core of the matrix is improved.

Based on these results a prototype bioreactor combining the mechanical forces of perfusion and compression, designed by Greiner Bio-One (Frickenhausen, Germany), was tested to further increase osteogenic differentiation. In a first trail, it could be shown that 1.5 ml/min fluid flow and cyclic compression with 0.4 Pa significantly enhanced osteogenic differentiation of adMSC on a collagen-based matrix. Mechanical stimulation evoked amongst others the mRNA expression of the osteospecific genes *RUNX* and *BSP-2*. Further experiments using Sponceram-Al and only perfusion of either 0.1 or 1 ml/min indicated that ucMSC are not suitable for this reactor system in combination with ceramic materials. However, high viability of adMSC could only be shown at 0.1 ml/min fluid flow. Combining 0.1 ml/min fluid flow and cyclic compression of 0.4 Pa resulted in an improved proliferation and osteogenic differentiation of adMSC on Sponceram-Al compared to the static control. Especially the expression of *OC* was significantly enhanced.

Finally, a drip-perfusion bioreactor was developed by the Institute of Technical Chemistry at the Leibniz University of Hanover. In contrast to conventional direct perfusion bioreactors, the samples are not surrounded by medium; they are simply kept moistened by the application of medium droplets. Moreover, perfusion is only caused by gravity. No reduction of viability for dynamically cultivated MSC on Collagen-BG in this newly designed bioreactor could be revealed by CellTiter Blue assay, compared to the static control. Long-term cultivations in the drip-perfusion bioreactor using ODM or ODM-M presented a very strong osteogenic differentiation of adMSC and ucMSC, respectively. Once more, mineralization occurred throughout the complete matrix, compared to statically cultivated samples.

It can be concluded that generally dynamic cultivation systems, in this case especially perfusion systems, are suitable to enhance osteogenic differentiation of MSC in a 3D microenvironment. However, ucMSC on ceramic biomaterials cannot be cultivated under equal conditions. Cell detachment and therefore a reduction of viability could be observed, compared to adMSC. Cultivation conditions and/or the substrate surface of ceramic matrices have to be optimized. In addition it could be shown that the application of dynamic cultivations systems can improve cell proliferation and distribution within the matrix. Besides these positive effects of 3D dynamic cultivation, bioreactors enabled the reduction of labor input (e.g. no regularly exchange of medium) and decreased the risk of contaminations. Once a bioreactor system was set up, it had not been reopened. Change of medium was not necessary. Only the addition

of fresh medium during long-term cultivations was performed manually. This step can be automated by integrating an additional peristaltic pump (cp. section 2.7).

2.7 Controlled and regulated conditions for the dynamic cultivation of MSC

Connecting dynamic bioreactors to a control unit allows the cultivation outside the incubator. Cultivations carried out in a customary incubator are liable to changes of the standard parameters, temperature, pH and pO_2, due to opening the incubator several times per day. This disadvantage can be overcome by regulating cultivation parameters via a control unit. Moreover, control units allow a proper documentation of cultivation parameters over the complete time period (Fig. 2.53). This process is indispensible to satisfy GMP requirements. The main goal of combining dynamic bioreactors with a control unit is the reproducible production of artificial tissue constructs with good and constant quality.

For the controlled production of an artificial bone tissue construct the drip-perfusion bioreactor was connected to the control unit Biostat B-DCU (Sartorius-Stedim Biotech, Goettingen, Germany). Using this system, medium is conditioned in a stirred tank bioreactor (STR), to 37°C, pH 7,2 and pO_2 100 %. A value of 100 % pO_2 refers here to a partial pressure of 160 mmHg, which corresponds to 0.22 mmol O_2/l. Medium is tempered by a heating plate, positioned under the STR. The cultivation parameters pH and pO_2 are adjusted by controlling the gas flow (N_2, CO_2 and air) into the STR. A uniform gas and temperature distribution in the STR is generated by a gas sparger and a stirrer. Moreover, the weight of the STR can be documented by a balance positioned below the STR. For cultivation, conditioned medium is pumped over an automatically guided peristaltic pump into the drip-perfusion bioreactor, which is positioned under a heating cabin to guarantee an optimal temperature of 37°C. Medium passes the matrix by gravity, is collected on the bottom of the culture chamber and pumped back into the STR via a second peristaltic pump. Fresh medium is added to the STR every day via a third automatically guided peristaltic pump (Fig. 2.49). Main focus during the development was the adjustment of the pumps to very low flow rates and the adjustment of the pH by a controlled and very low gas flow. Moreover, the sterile setup of the system was examined carefully.

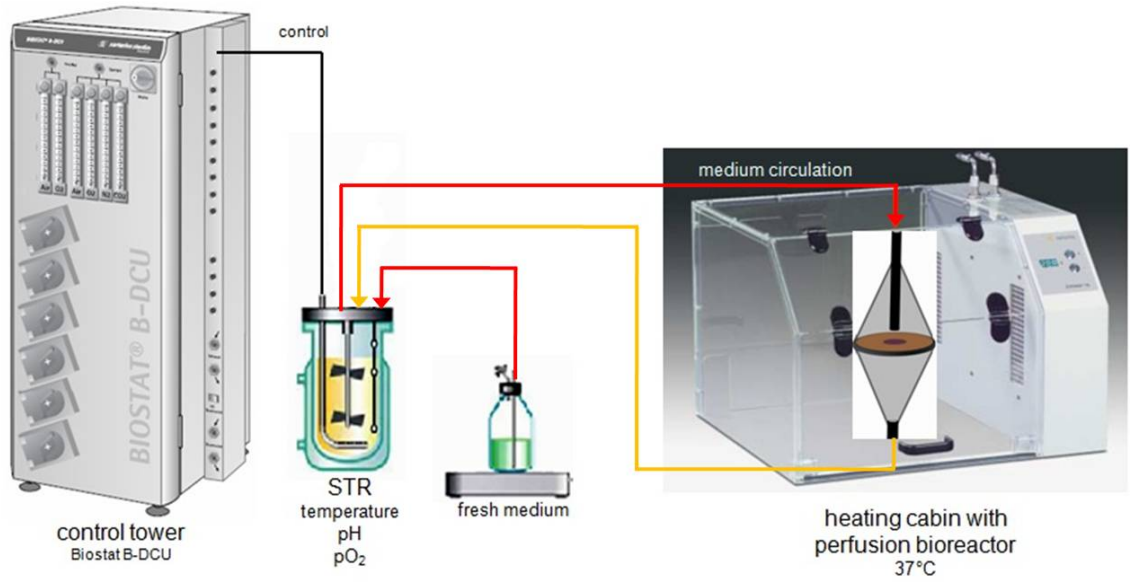

Fig. 2.49: Setup to automatically regulate the cultivation and differentiation of MSC in a perfusion bioreactor system. Temperature, pH and pO_2 of the medium are adjusted in the STR via the control unit. The medium is circulated by using two peristaltic pumps. Fresh medium is added to the STR using a third automatically guided peristaltic pump.

For dynamic cultivation under regulated conditions $4*10^5$ adMSC were seeded onto Collagen-BG (d = 16 mm), cultivated statically for 4 days in culture medium and for 4 days in ODM. Thereafter, three matrices were transferred into one mini-drip-perfusion bioreactor under sterile conditions. The bioreactor was connected via luer-lock connectors to the previously autoclaved tubing system. The tubing system was autoclaved together with the STR (cp. section 5.7.5 for detailed information). The STR was filled with 200 ml ODM under sterile conditions or via the third peristaltic pump. Cultivation was carried out for either 10 or 21 days applying 0.12 ml/min fluid flow and standard cultivation parameters (37°C, pH = 7.2 and pO_2 = 100 %). A fluid flow rate below 0.12 ml/min could not be achieved using this setup. The cultivation parameters were automatically regulated and documented via the control unit during the complete cultivation period. After cultivation histological stainings of cryosections (25 µm) and PCR analysis were performed.

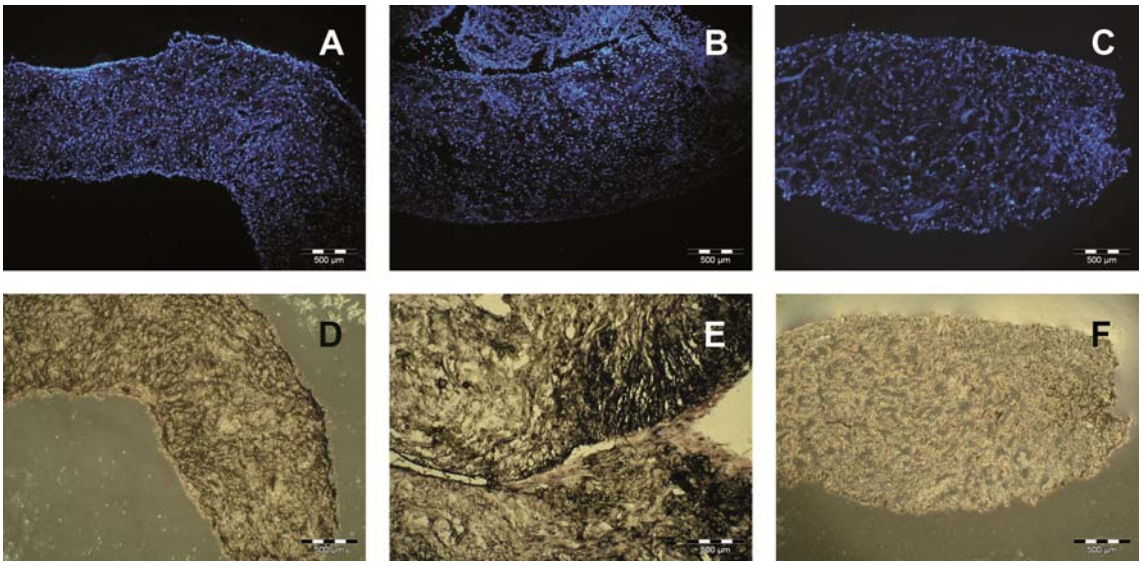

Fig. 2.50: DAPI staining (A-C) and membrane-bound AP staining (D-F) of adMSC on Collagen-BG (cryosections of 25 µm) after 21 days of static cultivation (A, D), 10 days of dynamic cultivation in a mini-drip-perfusion bioreactor (B, E) and 21 days of dynamic cultivation (C, F).

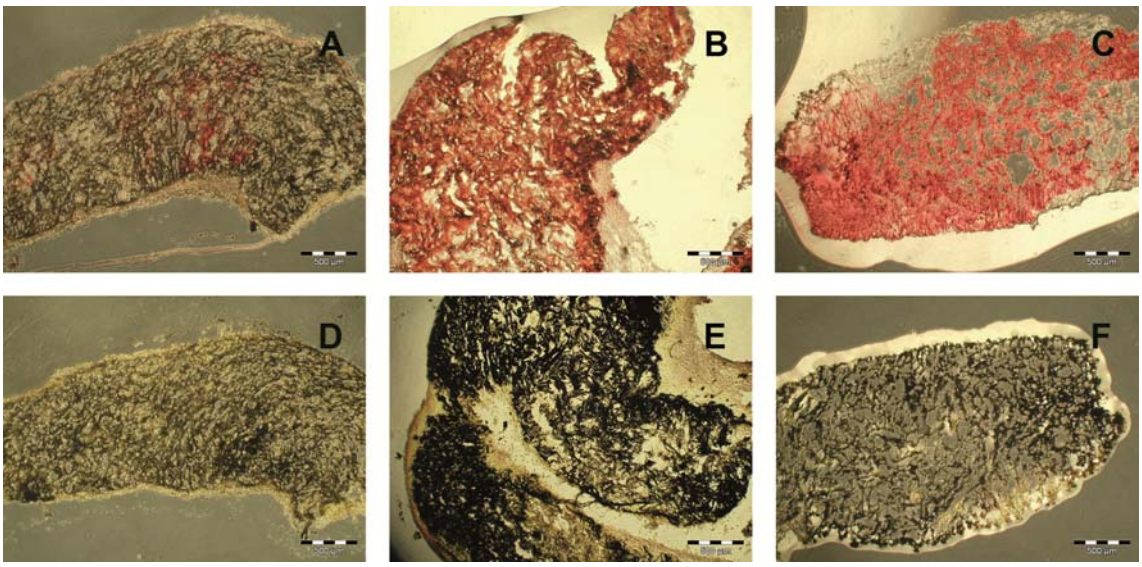

Fig. 2.51: AlizarinRed staining (A-C) and von Kossa staining (D-F) of adMSC on Collagen-BG (cryosections of 25 µm) after 21 days of static cultivation (A, D), 10 days of dynamic cultivation in a mini-drip-perfusion bioreactor (B, E) and 21 days of dynamic cultivation (C, F).

Histological stainings already indicate a very strong ECM mineralization (AlizarinRed, von Kossa) after 10 days of dynamic cultivation. Mineralization can be observed throughout the entire collagen matrix, whereas mineralization in the statically cultured sample only occurs in some small areas. After 21 days of dynamic cultivation also strong mineralization can be detected (Fig. 2.51). However, it is conspicuous that DAPI images show after 21 days of dynamic cultivation only few cells in the matrix and thus no membrane-bound AP can be detected. On the contrary, after 10 days of dynamic cultivation the amount of cells in the matrix is comparable to the static control and an

intensive staining of membrane-bound AP is visible (Fig. 2.50). This effect has already been observed in sections 2.6.5 and in 2D differentiation experiments by Antonina Lavrentieva (Institute of Technical Chemistry, Leibniz University of Hanover, Germany). Cell death is caused by a strong ECM mineralization, since the artificial tissue construct does not obtain vascularization, which is necessary to further provide the cells with nutrients.

Next challenge was the parallelization of two mini-drip-perfusion bioreactors and the simultaneous cultivation under controlled conditions. In the following setup, medium is not circulated, but pumped from the STR over a multichannel peristaltic pump in two mini-drip-perfusion bioreactors and then over a second multichannel peristaltic pump into two individual waste containers. In order to provide a sufficient amount of conditioned medium, a third automatically guided peristaltic pump added each day about 200 ml fresh medium to the STR. The waste containers were changed via luer-lock connectors on a regularly base (Fig. 2.52). In main focus was the parallelization of very low fluid flow rates.

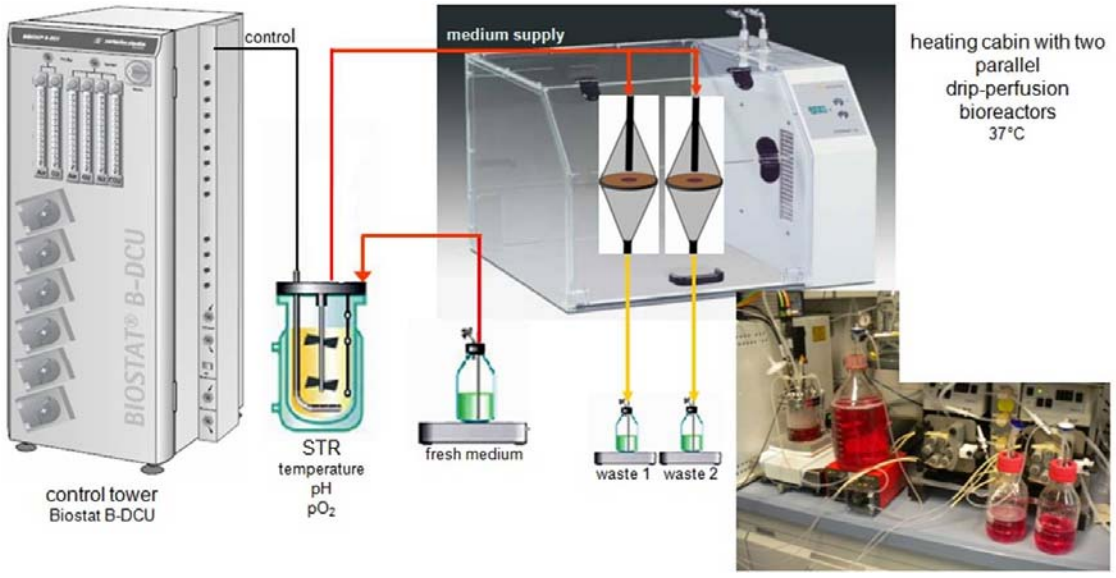

Fig. 2.52: Setup to automatically regulate the parallel cultivation and differentiation of MSC in two drip-perfusion bioreactors. Temperature, pH and pO_2 of the medium is adjusted in the STR via the control unit. The medium is pumped into the bioreactors using a multichannel peristaltic pump. Then, the medium is pumped from the bioreactor chambers into two separate waste bottles. Fresh medium is added to the STR using a third automatically guided peristaltic pump.

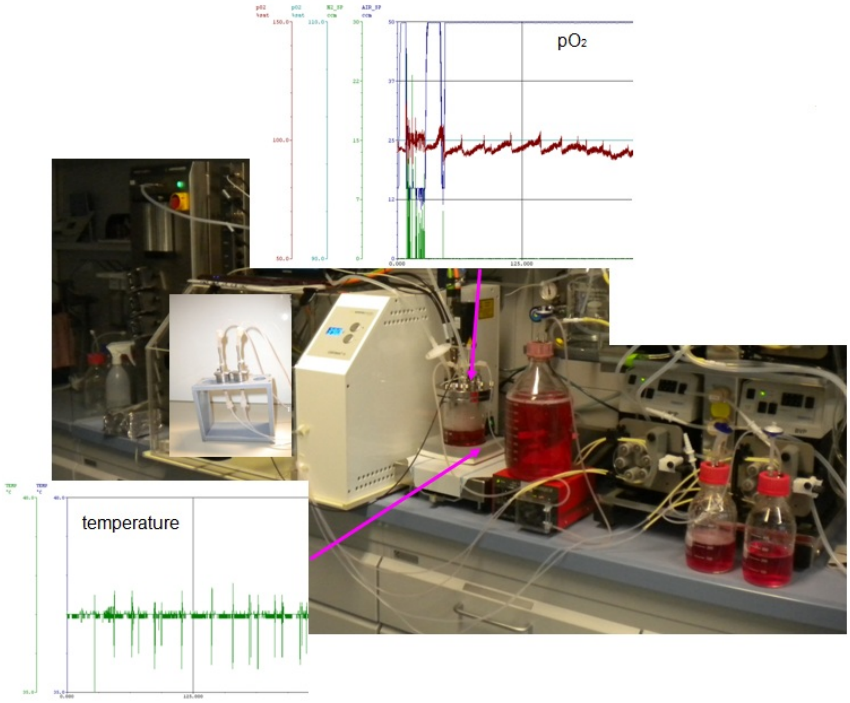

Fig. 2.53: Documentation of pO_2 and temperature in the STR during the cultivation of adMSC in two parallel drip-perfusion bioreactors over 10 days.

Cell seeding and static cultivation prior to dynamic cultivation were carried out according to the experiments above. Cultivations parameters remained the same. The dynamic cultivation of adMSC in two mini-parallel drip-perfusion bioreactors was performed and documented for 10 days (Fig. 2.53). Thereafter, mineralization was revealed by AlizarinRed and von Kossa staining. Furthermore, PCR analysis was performed.

Samples of bioreactor one, as well as samples of bioreactor two show an enhanced mineralization compared to the static control. However, mineralization does not occur throughout the entire matrix, as this was the case after controlled and regulated dynamic cultivation using only one mini-drip-perfusion bioreactor (Fig. 2.54). Moreover, RT-PCR analysis does not reveal an equal degree of osteogenic differentiation of adMSC in bioreactor one and two. The mRNA expression of *OC* is, for example, enhanced in the sample of bioreactor one (both samples of *OC* have been analyzed on one electrophoretic gel and the image has been taken with the same exposure). Furthermore, mRNA expression of *BMP-4* and *AP* cannot be identified in the samples of bioreactor two (Fig. 2.55).

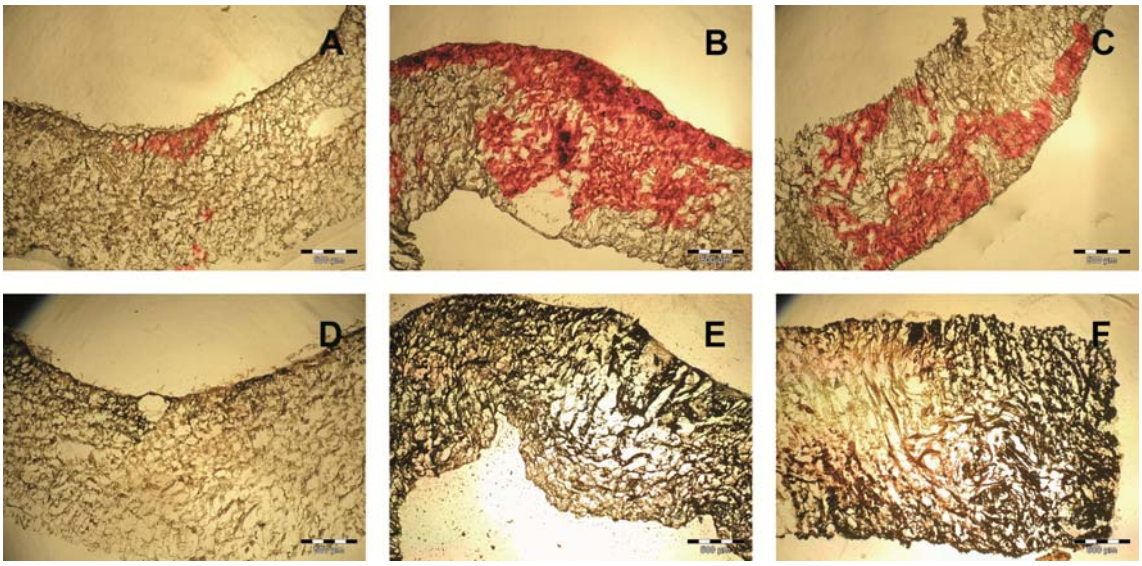

Fig. 2.54: AlizarinRed staining (A-C) and von Kossa staining (D-F) of adMSC on Collagen-BG (cryosections of 25 µm) after 10 days of static cultivation (A, D) and 10 days of dynamic cultivation in two parallel mini-drip-perfusion bioreactors: Bioreactor 1 (B, E) and bioreactor 2 (C, F).

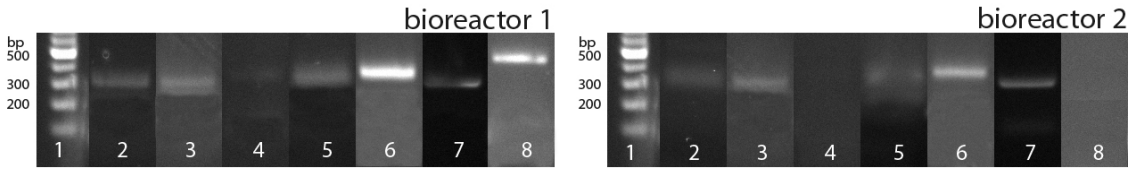

Fig. 2.55: RT-PCR of adMSC on Collagen-BG after dynamic cultivation in two parallel mini-drip-perfusion bioreactors. Lane 1: ladder, lane 2: *HPRT*, lane 3: *COL I*, lane 4: *BMP-4*, lane 5: *RUNX*, lane 6: *OC*, lane 7: *OP*, lane 8: *AP*.

The connection of the mini-drip-perfusion bioreactor to a control unit presents several advantages. The regulation of cultivation parameters enables 3D dynamic cultivations under reproducible conditions and guarantees constant quality of artificial tissue products. Variations of environmental cultivation factors, as they occur in standard incubators, were eliminated. Consequently, the osteogenic differentiation of MSC could be enhanced. Parallelization of two cultivation chambers allows the simultaneous production of two tissue transplants. Within this process cells from the same or two different donors can be used, since the assembly of the system avoids cross-contaminations. However, already RT-PCR analysis revealed that the tissue constructs of the two parallel bioreactors do not obtain similar quality (degree of osteogenic differentiation). Detailed information about matrix quality can only be gained by performing real-time PCR experiments. But, it can be stated that the level of differentiation was lower than using only one bioreactor. This may be the result of difficulties in the parallelization of the flow rates. Using a very low fluid flow rate of 0.12 ml/min and two parallel tubings occasionally stopped the rotation of the

multichannel peristaltic pump. This effect caused a non-continuous fluid flow and consequently a reduced medium supply.

2.8 Regulations concerning Advanced Therapy Medicinal Products

In this chapter a brief overview about the legislation for a potential approval of the cell-matrix construct Sponceram-Al/human adMSC as a bone transplant will be given. A cell-matrix construct used in regenerative medicine is considered as a tissue engineered product, which are classified as Advanced Therapy Medicinal Products (ATMPs). The legislation defines three types of ATMPs [190]:

1. Gene therapy products, used to treat genetic diseases, e.g. inserting genes (DNA) into cells, in order to regulate, repair, replace, add or delete a genetic sequence, which may help slow down or cure a disease. Excluding vaccines against infectious diseases.
2. Somatic cell therapy products containing cells or tissues, manipulated to change their biological function, in order to cure, diagnose or prevent a disease.
3. Tissue engineered products containing cells or tissues, modified to repair, regenerate or replace tissues.

The cell-matrix construct of Sponceram-Al and human adMSC is regarding to this definition not a classical ATMP. Cell-matrix constructs are considered as "Combined ATMPs". The 3D matrix is classified as a medical device and the cell component as an ATMP. Therefore, the medical device has to fulfill the requirements of the Directive 93/42/EEC (06/14/1993) on medical devices and the Directive 90/385/EEC (06/20/1990) regarding active implantable medical devices [191, 192]. These directives are valid within the European Union (EU). The approval of medical products has to be performed by so called "notified bodies". A "notified body" has to be accredited by an EU member state and controls weather the device fulfills the requirements of the directives. With the "Declaration of Conformity" the producer can label the device with the CE Mark (European Conformity), which is necessary for the distribution of the product within the EU. The "notified body" may not be directly involved in the design, construction, marketing or maintenance of the devices. An example for a "notified body" is the company "mdc medical device certification GmbH" located in Stuttgart and Berlin (Germany), which has e.g. approved the medical device Cerasorb M. In order to approve a cell-matrix construct as an ATMP, the isolation and cultivation of human MSC have to be performed according to the Directive 2004/23/EC (03/31/2004) on setting standards of quality and safety for the donation, procurement, testing,

processing, preservation, storage and distribution of human tissues and cells [193]. Moreover, in "Combined ATMPs" the component with the major influence on the human body is the cell or tissue component. Therefore, the cell-matrix construct also has to accomplish the requirements of the Regulation (EC) No 1394/2007 (11/13/2007) on advanced therapy medicinal products and amending Directive 2001/83/EC and Regulation (EC) No 726/2004 [194]. The approval of combined ATMPs is carried out by the European Medicines Agency (EMA), which is a EU agency, established in 1995 and located in London (United Kingdom). If the medical device has not been approved in advance, as in the case of Sponceram-Al, the EMA selects together with the applicant a "nominated body" for the certification [195]. Annex I shows the presubmission request form of the EMA, filled in with the available data to approve Sponceram-Al with human adMSC as a "Combined ATMP".

Finally, to ensure maximum safety, it is important that all procedures of ATMP production satisfy the GMP guidelines, which are stated in the Directive 2003/94/EC (10/08/2003) laying down the principles and guidelines of good manufacturing practice in respect of medicinal products for human use and investigational medicinal products for human use [196]. This concerns the starting material, cell cultivation, devices for cell cultivation and quality control [197].

Detailed information on the regulatory aspects of ATMPs is given in the Bachelor Thesis of Anne Stamm [198] (Institute of Technical Chemistry, Leibniz University Hanover, Germany).

Bioreactors and control units used to create tissue engineered products, in this context a "Combined ATMP", gained importance over the last decades, as they help to accomplish many requirements stated in the Directive 2003/94/EC (guidelines for GMP) [196]. Closed and disposable bioreactor systems, for example, fulfill the requirements written in:

> *Article 8/2 "Premises and manufacturing equipment shall be laid out, designed and operated in such a way as to minimize the risk of error and to permit effective cleaning and maintenance in order to avoid contamination, cross contamination and, in general, any adverse effect on the quality of the product."*
>
> *and*
>
> *Article 10/2 "Appropriate technical or organizational measures shall be taken to avoid cross contamination and mix-ups."*

The use of a control unit while producing tissue engineered products makes it possible to fulfill the following requirements of the GMP guideline:

Article 9/1 "The manufacturer shall establish and maintain a documentation system based upon specifications..."

Article 9/2: "... The electronically stored data shall be protected, by methods such as duplication or back-up and transfer on to another storage system, against loss or damage of data, and audit trails shall be maintained."

Article 10/1: "... All process deviations and product defects shall be documented and thoroughly investigated."

Article 10/4: "... All steps in the design and development of the manufacturing process shall be fully documented."

Article 11/3: "... essential information such as the production conditions, the results of in-process controls, the examination of the manufacturing documents and the conformity of the product..."

As stated earlier, the application of bioreactors and control units not only minimizes the risk of contamination and allows a proper documentation, it also reduces labor input by automating the process. Highly automated processes generally require less qualified staff, which reduces the personal expenses and consequently the product costs. This refers to the following articles of the GMP guideline:

Article 7/1: "At each manufacturing site, the manufacturer shall have a sufficient number of competent and appropriately qualified personnel at his disposal to achieve the pharmaceutical quality assurance objective."

and

Article 7/4 "The personnel shall receive initial and ongoing training, the effectiveness of which shall be verified, covering in particular the theory and application of the concept of quality assurance..."

3 Summary and outlook

Until today, many osteogenic differentiation experiments using MSC are still performed in a 2D environment. Based on the origin of MSC and the for transplantation desired 3D tissue structure, there is a high demand for 3D cultivation experiments. Existing literature reveals that especially the 3D biomaterials' porosity, pore size, stiffness and topography has a high impact on MSC differentiation. In this context four different 3D ceramic biomaterials (Sponceram-Al, Osseolive, Cerasorb M and 45S5-Bioglass) and three different collagen-based matrices (Matriderm, Collagen-Bioglass and Collagen-Silk) have been analyzed in detail. Their surface texture, 3D architecture, permeability and biomechanical stability were investigated.

In conclusion only Sponceram-Al fulfilled the requirements for bone TE in this work. A porosity of about 67 % and an average pore size of 510 µm could be determined. These values are known to allow for optimal cell migration, mass transportation and vascularization. In addition, Sponceram-Al only showed a low intra-batch variability of these parameters, which is important to guarantee constant matrix quality and satisfy GMP requirements. Furthermore, the highly rough aluminum oxide coating may improve cell attachment and adhesion. However, for Sponceram-Al, as well as for all other ceramic biomaterials a highly unequal fluid flow distribution within the matrix has been verified. This implies that cells on the biomaterials' surface are exposed to different intensities of shear stress (chapter 2.2.1 to 2.2.5).

Static 3D cell culture experiments have been performed with ad- and ucMSC, respectively. Especially adMSC showed good proliferation and differentiation capacity on Sponceram-Al. The suggestion that the 3D architecture of Sponceram-Al allows superior cell migration could be supported by the static cell culture experiments. Moreover, the cultivation of adMSC on 45S5-Bioglass resulted in very strong differentiation. However, 45S5-Bioglass could not be applied for further experiments due to its very brittle characteristics. In conclusion, 3D matrix geometry has an influence on MSC differentiation behavior (chapter 2.3 and 2.4). Though, it has to be taken into account, that MSC of different origin might favor different 3D microenvironments.

All tested collagen-based biomaterials revealed a similar 3D architecture. Their matrix is mainly composed by a dense mesh of collagen fibers. Compared to ceramic biomaterials their stability was shown to be very weak. Strongest ECM mineralization

under static conditions has been achieved by using adMSC and Collagen-Silk. Nevertheless, due to the softness of collagen-based biomaterials, these cannot be implanted into load bearing areas (chapter 2.2.1 to 2.2.5 and 2.3 to 2.4).

Previous findings reveal that not only the biomaterials' 3D geometry, but also the exposure of MSC to mechanical stimulations significantly influences differentiation. Especially fluid flow stimulation is described to enhance osteogenic differentiation of MSC. This effect has first been investigated for adMSC and ucMSC in a 2D microenvironment. An exposure of ucMSC to two stimulation periods of 4 hours each already resulted in a significant higher production of membrane-bound AP. The cultivation of adMSC and ucMSC for seven days with a specific stimulation pattern indicated a beginning ECM mineralization. However, an entire ECM mineralization could not be achieved, as MSC detached from the 2D surface by extending the cultivation period (chapter 2.1).

Therefore, a combination of 3D biomaterials with dynamic bioreactor systems is desired. Various innovative bioreactors have been tested. Bioreactor systems based on direct perfusion (developed by EBERS Medical, Zaragoza, Spain) were shown to improve cell distribution within the matrix. This was exemplarily presented for Cerasorb M, which indicated a weak cell distribution under static conditions (chapter 2.6.1). Moreover, direct perfusion of Sponceram-Al containing adMSC resulted in enhanced membrane-bound AP production. Nevertheless, an improved ECM mineralization could not be verified (chapter 2.6.3). Direct perfusion experiments of ucMSC on collagen-based biomaterials were carried out using Collagen-BG, since MSC on this matrix did not show an entire ECM mineralization under static conditions. On the contrary, applying fluid flow stimulation to ucMSC seeded on Collagen-BG, osteogenic differentiation occurred throughout the complete matrix (chapter 2.6.2).

Another prototype bioreactor system developed by Greiner Bio-One (Frickenhausen, Germany), which combines perfusion and cyclic compression has also been shown to be advantageous for bone TE application. AdMSC presented compared to the static control significantly enhanced osteogenic differentiation on Collagen-BG, as well as on Sponceram-Al applying a defined stimulation pattern. In addition, the combination of perfusion and cyclic compression increased cell viability on Sponceram-Al (chapter 2.6.4).

Further investigation of osteogenic differentiation under perfusion conditions led to the development of a drip-perfusion bioreactor, designed and constructed at the Institute of Technical Chemistry at the Leibniz University of Hanover. Applying this bioreactor system, the biomaterial is slowly perfused with medium only by the force of

gravity. Experiments with adMSC and ucMSC on Collagen-BG revealed an advanced ECM mineralization compared to the static control. However, first attempts cultivating and differentiating adMSC on Sponceram-Al in the dip-perfusion bioreactor system failed (chapter 2.6.5).

Last goal of the present work was the production of bone tissue structures in a dynamic microenvironment, which can be transferred to GMP-conform conditions. In order to achieve this goal a high degree of automation is required. The drip-perfusion bioreactor has been combined with a control unit from Sartorius-Stedim Biotech (Goettingen, Germany). This system not only allows preconditioning the medium in terms of temperature, pH and oxygen, but also guarantees a complete documentation of all cultivation parameters. Moreover, all cultivation processes are automatically guided, by creating and loading different protocols. The production of bone tissue structures under controlled and regulated conditions could be realized by using adMSC on Collagen-BG and connecting the drip-perfusion bioreactor to the control unit. The parallel cultivation and differentiation of adMSC in two drip-perfusion bioreactors under GMP-conform conditions has also been performed. Specific analysis for osteogenic differentiation revealed a high degree of MSC differentiation in the two parallel bioreactors (chapter 2.7). However, in order to completely fulfill GMP requirements the bioreactors would need to be produced as a closed disposable system.

In summary it can be concluded that special designed 3D biomaterials and dynamic bioreactor systems are a potent combination for the production of artificial bone tissue structures. The 3D architecture allows creating a natural microenvironment to improve MSC differentiation. In addition, the application of mechanical stimuli, such as fluid flow or cyclic compression, further enhances the mineralization of the ECM. Moreover, the connection of dynamic bioreactors to a control unit allows for the production of bone tissue structures under GMP-conform conditions, by automating and documenting the cultivation process.

There is a high potential for further optimization of 3D biomaterial design. Current manufacturing processes, such as freeze-drying or salt-leaching, result in a non-homogenous matrix architecture. The consequence of irregular matrix geometries are non-uniform shear stress profiles when applying fluid flow. An example has been presented in chapter 2.2.4. This problem could be solved by using rapid prototyping, a method to design complex 3D structures with defined pore sizes layer-by-layer [79, 80]. Consequently this design allows for an equal distribution of shear stress within the

matrix, which is beneficial for osteogenic differentiation. Only homogeneous shear stress can guarantee a uniform differentiation over the complete matrix, without cell disruption caused by too high fluid flow.

Furthermore, a detailed investigation on composite biomaterials would be advantageous for the improvement of osteogenic differentiation. It could successfully been shown that MSC favor a collagen microenvironment and present a high degree of osteogenic differentiation on these matrices. However, these materials do not possess the ability to withstand forces in the area of transplantation. Beneficial could be the design of a composite material consisting of a strong 3D framework with the desired porosity and pore size, covered by a collagen coating. This combination would on the one hand allow for vascularization and could withstand loads in the area of transplantation; on the other hand it would improve cell attachment and favor differentiation.

Until today, dynamic cell seeding procedures have rarely been performed. Nevertheless, this process implies many advantages. The biomaterials can be sterilized within the bioreactor chamber, which has not to be reopened for cell seeding, hence the risk of contamination would be reduced. Moreover, it could be shown that a homogenous cell distribution is the result of dynamic cell seeding [150]. Homogenous cell distribution is a basic requirement for entire and uniform differentiation.

A more intense investigation and application of single-use bioreactors could further reduce the risk of bacterial-, fungal- and cross-contamination. Besides, single-use systems decrease labor effort. These systems can already be produced with the complete tubing system and are generally gamma-sterilized prior to application. In addition, a high degree of automation and parallelization is not only required to fulfill GMP conditions, but also to minimize human errors. Consequently, the application of disposable bioreactors in the future can reduce the prize for the production of high quality tissue transplants, which is one of the key factors influencing the spread of this new therapy.

4 Literature

1. Grayson, W.L., et al., *Biomimetic approach to tissue engineering.* Semin Cell Dev Biol, 2009. **20**(6): p. 665-73.
2. McCoy, R.J. and F.J. O'Brien, *Influence of Shear Stress in Perfusion Bioreactor Cultures for the Development of Three-Dimensional Bone Tissue Constructs: A Review.* Tissue Engineering Part B-Reviews, 2010. **16**(6): p. 587-601.
3. Scheper, T., ed. *Bioreactor Systems for Tissue Engineering*. ed. C. Kasper, Griensven van, M., Pörtner, R. 2009, Springer-Verlag: Berlin, Heidelberg.
4. Kohara, H. and Y. Tabata, *Review: Tissue Engineering Technology to Enhance Cell Recruitment for Regeneration Therapy.* Journal of Medical and Biological Engineering, 2010. **30**(5): p. 267-276.
5. Calori, G.M., et al., *Bone morphogenetic proteins and tissue engineering: future directions.* Injury-International Journal of the Care of the Injured, 2009. **40**: p. 67-76.
6. Porter, J.R., T.T. Ruckh, and K.C. Popat, *Bone tissue engineering: a review in bone biomimetics and drug delivery strategies.* Biotechnol Prog, 2009. **25**(6): p. 1539-60.
7. Mauney, J.R., V. Volloch, and D.L. Kaplan, *Role of adult mesenchymal stem cells in bone tissue-engineering applications: Current status and future prospects.* Tissue Engineering, 2005. **11**(5-6): p. 787-802.
8. Quarto, R., et al., *Repair of large bone defects with the use of autologous bone marrow stromal cells.* New England Journal of Medicine, 2001. **344**(5): p. 385-386.
9. Lavrentieva, A., *Strategies in umbilical cord-derived mesenchymal stem cells expansion.* Disseration, Leibniz University Hannover, Technical Chemistry, 2012.
10. Ma, P.X., *Scaffolds for tissue fabrication.* Materials Today, 2004. **7**(5): p. 30-40.
11. Colley, H.E., et al., *Plasma Polymer Coatings to Support Mesenchymal Stem Cell Adhesion, Growth and Differentiation on Variable Stiffness Silicone Elastomers.* Plasma Processes and Polymers, 2009. **6**(12): p. 831-839.
12. Takezawa, T., *A strategy for the development of tissue engineering scaffolds that regulate cell behavior.* Biomaterials, 2003. **24**(13): p. 2267-2275.
13. Kim, B.S. and D.J. Mooney, *Development of biocompatible synthetic extracellular matrices for tissue engineering.* Trends in Biotechnology, 1998. **16**(5): p. 224-230.
14. Eisenbarth, E., *Biomaterials for tissue engineering.* Advanced Engineering Materials, 2007. **9**(12): p. 1051-1060.
15. Stiehler, M., et al., *Bioreactor Systems for Bone Tissue Engineering.* Tissue Engineering Part B-Reviews, 2011. **17**(4): p. 263-280.

16. Kawahara, H., et al., *In vitro study on bone formation and surface topography from the standpoint of biomechanics.* Journal of Materials Science-Materials in Medicine, 2004. **15**(12): p. 1297-1307.

17. Fisher, J.P. and A.B. Yeatts, *Bone tissue engineering bioreactors: Dynamic culture and the influence of shear stress.* Bone, 2011. **48**(2): p. 171-181.

18. Wolff, J., *The law of bone remodelling*. 1986, Berlin ; New York: Springer-Verlag. xii, 126 p.

19. Hutmacher, D.W., *Scaffold design and fabrication technologies for engineering tissues - state of the art and future perspectives.* Journal of Biomaterials Science-Polymer Edition, 2001. **12**(1): p. 107-124.

20. Cao, Y., et al., *Scaffolds, stem cells, and tissue engineering: A potent combination!* Australian Journal of Chemistry, 2005. **58**(10): p. 691-703.

21. Arinzeh, T.L., et al., *A comparative study of biphasic calcium phosphate ceramics for human mesenchymal stem-cell-induced bone formation.* Biomaterials, 2005. **26**(17): p. 3631-3638.

22. Wang, M., *Composite Scaffolds for Bone Tissue Engineering.* American Journal of Biochemistry and Biotechnology, 2006. **2**(2): p. 80-84.

23. Lovell, C.S., et al., *Analysis and modeling of the mechanical properties of novel thermotropic polymer biomaterials.* Polymer, 2010. **51**(9): p. 2013-2020.

24. Sung, H.J., et al., *Poly(ethylene glycol) as a sensitive regulator of cell survival fate on polymeric biomaterials: the interplay of cell adhesion and pro-oxidant signaling mechanisms.* Soft Matter, 2010. **6**(20): p. 5196-5205.

25. Shalumon, K.T., et al., *Preparation, Characterization and Cell Attachment Studies of Electrospun Multi-scale Poly(caprolactone) Fibrous Scaffolds for Tissue Engineering.* Journal of Macromolecular Science Part a-Pure and Applied Chemistry, 2011. **48**(1): p. 21-30.

26. da Silva, M.L.A., et al., *Cartilage Tissue Engineering Using Electrospun PCL Nanofiber Meshes and MSCs.* Biomacromolecules, 2010. **11**(12): p. 3228-3236.

27. Woodruff, M.A. and D.W. Hutmacher, *The return of a forgotten polymer-Polycaprolactone in the 21st century.* Progress in Polymer Science, 2010. **35**(10): p. 1217-1256.

28. Koch, M.A., et al., *Perfusion cell seeding on large porous PLA/calcium phosphate composite scaffolds in a perfusion bioreactor system under varying perfusion parameters.* J Biomed Mater Res A. **95**(4): p. 1011-8.

29. Gupta, B., N. Revagade, and J. Hilborn, *Poly(lactic acid) fiber: An overview.* Progress in Polymer Science, 2007. **32**(4): p. 455-482.

30. Stevanovic, M. and D. Uskokovic, *Poly(lactide-co-glycolide)-based Micro and Nanoparticles for the Controlled Drug Delivery of Vitamins.* Current Nanoscience, 2009. **5**(1): p. 1-14.

31. Lu, J.M., et al., *Current advances in research and clinical applications of PLGA-based nanotechnology.* Expert Review of Molecular Diagnostics, 2009. **9**(4): p. 325-341.

32. Barrere, F., C.A. van Blitterswijk, and K. de Groot, *Bone regeneration: molecular and cellular interactions with calcium phosphate ceramics.* International Journal of Nanomedicine, 2006. **1**(3): p. 317-332.

33. Emadi, R., et al., *Nanostructured Forsterite Coating Strengthens Porous Hydroxyapatite for Bone Tissue Engineering.* Journal of the American Ceramic Society, 2010. **93**(9): p. 2679-2683.

34. Chen, J.G., et al., *In situ grown fibrous composites of poly(DL-lactide) and hydroxyapatite as potential tissue engineering scaffolds.* Polymer, 2010. **51**(26): p. 6268-6277.

35. Uskokovic, V. and D.P. Uskokovic, *Nanosized hydroxyapatite and other calcium phosphates: Chemistry of formation and application as drug and gene delivery agents.* Journal of Biomedical Materials Research Part B-Applied Biomaterials, 2011. **96B**(1): p. 152-191.

36. Swetha, M., et al., *Biocomposites containing natural polymers and hydroxyapatite for bone tissue engineering.* Int J Biol Macromol. **47**(1): p. 1-4.

37. Bellucci, D., et al., *Potassium based bioactive glass for bone tissue engineering.* Ceramics International, 2010. **36**(8): p. 2449-2453.

38. Mourino, V., P. Newby, and A.R. Boccaccini, *Preparation and Characterization of Gallium Releasing 3-D Alginate Coated 45S5 Bioglass (R) Based Scaffolds for Bone Tissue Engineering.* Advanced Engineering Materials, 2010. **12**(7): p. B283-B291.

39. Mullen, L.M., et al., *Binding and Release Characteristics of Insulin-Like Growth Factor-1 from a Collagen-Glycosaminoglycan Scaffold.* Tissue Engineering Part C-Methods, 2010. **16**(6): p. 1439-1448.

40. Yuan, T., et al., *Chondrogenic Differentiation and Immunological Properties of Mesenchymal Stem Cells in Collagen Type I Hydrogel.* Biotechnology Progress, 2010. **26**(6): p. 1749-1758.

41. Zorlutuna, P., P. Vadgama, and V. Hasirci, *Both sides nanopatterned tubular collagen scaffolds as tissue-engineered vascular grafts.* Journal of Tissue Engineering and Regenerative Medicine, 2010. **4**(8): p. 628-637.

42. Zheng, W.F., W. Zhang, and X.Y. Jiang, *Biomimetic Collagen Nanofibrous Materials for Bone Tissue Engineering.* Advanced Engineering Materials, 2010. **12**(9): p. B451-B466.

43. Lee, C.H., A. Singla, and Y. Lee, *Biomedical applications of collagen.* International Journal of Pharmaceutics, 2001. **221**(1-2): p. 1-22.

44. Kosmala, J.D., D.B. Henthorn, and L. Brannon-Peppas, *Preparation of interpenetrating networks of gelatin and dextran as degradable biomaterials.* Biomaterials, 2000. **21**(20): p. 2019-2023.

45. Tripathi, A., N. Kathuria, and A. Kumar, *Elastic and macroporous agarose-gelatin cryogels with isotropic and anisotropic porosity for tissue engineering.* Journal of Biomedical Materials Research Part A, 2009. **90A**(3): p. 680-694.

46. Leddy, H.A., H.A. Awad, and F. Guilak, *Molecular diffusion in tissue-engineered cartilage constructs: Effects of scaffold material, time, and culture conditions.* Journal

of Biomedical Materials Research Part B-Applied Biomaterials, 2004. **70B**(2): p. 397-406.

47. Bensaid, W., et al., *A biodegradable fibrin scaffold for mesenchymal stem cell transplantation.* Biomaterials, 2003. **24**(14): p. 2497-2502.

48. Kim, S.H., et al., *Recent Research Trends of Fibrin Gels for the Applications of Regenerative Medicine.* Tissue Engineering and Regenerative Medicine, 2009. **6**(1-3): p. 273-286.

49. Oliveira, J.T., et al., *Novel Melt-Processable Chitosan-Polybutylene Succinate Fibre Scaffolds for Cartilage Tissue Engineering.* Journal of Biomaterials Science-Polymer Edition, 2011. **22**(4-6): p. 773-788.

50. Jayakumar, R., et al., *Biomedical applications of chitin and chitosan based nanomaterials-A short review.* Carbohydrate Polymers, 2010. **82**(2): p. 227-232.

51. Venkatesan, J. and S.K. Kim, *Chitosan composites for bone tissue engineering--an overview.* Mar Drugs. **8**(8): p. 2252-66.

52. VandeVord, P.J., et al., *Evaluation of the biocompatibility of a chitosan scaffold in mice.* Journal of Biomedical Materials Research, 2002. **59**(3): p. 585-590.

53. Eiselt, P., et al., *Porous carriers for biomedical applications based on alginate hydrogels.* Biomaterials, 2000. **21**(19): p. 1921-1927.

54. Choi, M.S., et al., *Chondrogenic Differentiation of Human Adipose-derived Stem Cells in Alginate Sponge Scaffolds.* Tissue Engineering and Regenerative Medicine, 2008. **5**(4-6): p. 842-848.

55. Ebraheim, N.A., A.O. Mekhail, and M. Darwich, *Open reduction and internal fixation with bone grafting of clavicular nonunion.* Journal of Trauma-Injury Infection and Critical Care, 1997. **42**(4): p. 701-704.

56. Kretlow, J.D., et al., *Uncultured Marrow Mononuclear Cells Delivered Within Fibrin Glue Hydrogels to Porous Scaffolds Enhance Bone Regeneration Within Critical-Sized Rat Cranial Defects.* Tissue Engineering Part A, 2010. **16**(12): p. 3555-3568.

57. Staiger, M.P., et al., *Magnesium and its alloys as orthopedic biomaterials: A review.* Biomaterials, 2006. **27**(9): p. 1728-1734.

58. Brar, H.S., et al., *Magnesium as a biodegradable and bioabsorbable material for medical implants.* Jom, 2009. **61**(9): p. 31-34.

59. Zeng, R.C., et al., *Progress and challenge for magnesium alloys as biomaterials.* Advanced Engineering Materials, 2008. **10**(8): p. B3-B14.

60. Luo, W., S.R. Jones, and M.N. Yousaf, *Geometric Control of Stem Cell Differentiation Rate on Surfaces.* Langmuir, 2008. **24**(21): p. 12129-12133.

61. Roosa, S.M.M., et al., *The pore size of polycaprolactone scaffolds has limited influence on bone regeneration in an in vivo model.* Journal of Biomedical Materials Research Part A, 2010. **92A**(1): p. 359-368.

62. Tsuruga, E., et al., *Pore size of porous hydroxyapatite as the cell-substratum controls BMP-induced osteogenesis.* Journal of Biochemistry, 1997. **121**(2): p. 317-324.

63. Shor, L., et al., *Fabrication of three-dimensional polycaprolactone/hydroxyapatite tissue scaffolds and osteoblast-scaffold interactions in vitro.* Biomaterials, 2007. **28**(35): p. 5291-7.

64. Hulbert, S.F.e.a., *Potential of Ceramic Materials as Permanently Implantable Skeletal Prostheses.* J. Biomed. Mater. Res., 1970. **4**: p. 433-456.

65. Kasten, P., et al., *Porosity and pore size of beta-tricalcium phosphate scaffold can influence protein production and osteogenic differentiation of human mesenchymal stem cells: An in vitro and in vivo study.* Acta Biomaterialia, 2008. **4**(6): p. 1904-1915.

66. Karageorgiou, V. and D. Kaplan, *Porosity of 3D biornaterial scaffolds and osteogenesis.* Biomaterials, 2005. **26**(27): p. 5474-5491.

67. Yannas, I., *Tissue Regeneration by Use of Collagen-Glycosaminoglycan Copolymers.* Clinical Materias, 1992. **9**: p. 179-187.

68. Khoda, A.K.M.B., I.T. Ozbolat, and B. Koc, *Engineered Tissue Scaffolds With Variational Porous Architecture.* Journal of Biomechanical Engineering-Transactions of the Asme, 2011. **133**(1): p. -.

69. Oh, S.H., et al., *Investigation of Pore Size Effect on Chondrogenic Differentiation of Adipose Stem Cells Using a Pore Size Gradient Scaffold.* Biomacromolecules, 2010. **11**(8): p. 1948-1955.

70. Kuboki, Y., Q.M. Jin, and H. Takita, *Geometry of carriers controlling phenotypic expression in BMP-induced osteogenesis and chondrogenesis.* Journal of Bone and Joint Surgery-American Volume, 2001. **83A**: p. S105-S115.

71. Cyster, L.A., et al., *The influence of dispersant concentration on the pore morphology of hydroxyapatite ceramics for bone tissue engineering.* Biomaterials, 2005. **26**(7): p. 697-702.

72. http://www.engin.umich.edu/class/bme456/bonestructure/bonestructure.htm. *Bone Structure*. [cited 2011 15th of March].

73. Grimm, M.J. and J.L. Williams, *Measurements of permeability in human calcaneal trabecular bone.* J Biomech, 1997. **30**(7): p. 743-5.

74. Benninghoff, D., ed. *Anatomie*. 16. ed. Zellen- und Gewebelehre, Entwicklungslehre, Skelett- und Muskellehre, Atemsystem, Verdauungssystem, Harn- und Genitalsystem, ed. D. Drenckhahn. 2003, Urban & Fischer: München, Jena.

75. Hakulinen, M.A., et al., *Ultrasonic characterization of human trabecular bone microstructure.* Physics in Medicine and Biology, 2006. **51**(6): p. 1633-1648.

76. Hsu, Y.Y., et al., *Effect of polymer foam morphology and density on kinetics of in vitro controlled release of isoniazid from compressed foam matrices.* Journal of Biomedical Materials Research, 1997. **35**(1): p. 107-116.

77. Mikos, A.G., et al., *Preparation and Characterization of Poly(L-Lactic Acid) Foams.* Polymer, 1994. **35**(5): p. 1068-1077.

78. McCoy, R.J. and F.J. O'Brien, *Influence of shear stress in perfusion bioreactor cultures for the development of three-dimensional bone tissue constructs: a review.* Tissue Eng Part B Rev, 2010. **16**(6): p. 587-601.

79. Kellomaki, M., et al., *A review of rapid prototyping techniques for tissue engineering purposes.* Annals of Medicine, 2008. **40**(4): p. 268-280.

80. Chua, C.K., et al., *Rapid prototyping in tissue engineering: challenges and potential.* Trends in Biotechnology, 2004. **22**(12): p. 643-652.

81. Chen, F.L., et al., *Bone graft in the shape of human mandibular condyle reconstruction via seeding marrow-derived osteoblasts into porous coral in a nude mice model.* Journal of Oral and Maxillofacial Surgery, 2002. **60**(10): p. 1155-1159.

82. Mygind, T., et al., *Mesenchymal stem cell ingrowth and differentiation on coralline hydroxyapatite scaffolds.* Biomaterials, 2007. **28**(6): p. 1036-1047.

83. van den Dolder, J., et al., *Bone tissue reconstruction using titanium fiber mesh combined with rat bone marrow stromal cells.* Biomaterials, 2003. **24**(10): p. 1745-1750.

84. Diederichs, S., et al., *Dynamic Cultivation of Human Mesenchymal Stem Cells in a Rotating Bed Bioreactor System Based on the Z (R) RP Platform.* Biotechnology Progress, 2009. **25**(6): p. 1762-1771.

85. Roker, S., et al., *Novel 3D biomaterials for tissue engineering based on collagen and macroporous ceramics (vol 40, pg 54, 2009).* Materialwissenschaft Und Werkstofftechnik, 2009. **40**(3): p. 224-225.

86. Yuan, J., et al., *Repair of canine mandibular bone defects with bone marrow stromal cells and porous beta-tricalcium phosphate.* Biomaterials, 2007. **28**(6): p. 1005-1013.

87. Kim, H.J., J.H. Lee, and G.I. Im, *Chondrogenesis using mesenchymal stem cells and PCL scaffolds.* Journal of Biomedical Materials Research Part A, 2010. **92A**(2): p. 659-666.

88. Yamane, S., et al., *Effect of pore size on in vitro cartilage formation using chitosan-based hyaluronic acid hybrid polymer fibers.* Journal of Biomedical Materials Research Part A, 2007. **81A**(3): p. 586-593.

89. Lee, S.J., et al., *Response of human chondrocytes on polymer surfaces with different micropore sizes for tissue-engineered cartilage.* Journal of Applied Polymer Science, 2004. **92**(5): p. 2784-2790.

90. Chia, S.L., et al., *Biodegradable elastomeric polyurethane membranes as chondrocyte carriers for cartilage repair.* Tissue Engineering, 2006. **12**(7): p. 1945-1953.

91. Cho, S.W., et al., *Smooth muscle-like tissues engineered with bone marrow stromal cells.* Biomaterials, 2004. **25**(15): p. 2979-2986.

92. Wang, M., et al., *Hepatogenesis of Adipose-Derived Stem Cells on Poly-Lactide-co-Glycolide Scaffolds: In Vitro and In Vivo Studies.* Tissue Engineering Part C-Methods, 2010. **16**(5): p. 1041-1050.

93. Pelham, R.J. and Y.L. Wang, *Cell locomotion and focal adhesions are regulated by substrate flexibility.* Proceedings of the National Academy of Sciences of the United States of America, 1997. **94**(25): p. 13661-13665.

94. Ni, Y. and M.Y.M. Chiang, *Cell morphology and migration linked to substrate rigidity.* Soft Matter, 2007. **3**(10): p. 1285-1292.

95. Schneider, A., et al., *Polyelectrolyte multilayers with a tunable Young's modulus: Influence of film stiffness on cell adhesion.* Langmuir, 2006. **22**(3): p. 1193-1200.

96. Yeung, T., et al., *Effects of substrate stiffness on cell morphology, cytoskeletal structure, and adhesion.* Cell Motility and the Cytoskeleton, 2005. **60**(1): p. 24-34.

97. McBeath, R., et al., *Cell shape, cytoskeletal tension, and RhoA regulate stem cell lineage commitment.* Developmental Cell, 2004. **6**(4): p. 483-495.

98. Wang, H.B., M. Dembo, and Y.L. Wang, *Substrate flexibility regulates growth and apoptosis of normal but not transformed cells.* American Journal of Physiology-Cell Physiology, 2000. **279**(5): p. C1345-C1350.

99. Engler, A.J., et al., *Matrix elasticity directs stem cell lineage specification.* Cell, 2006. **126**(4): p. 677-689.

100. Rowlands, A.S., P.A. George, and J.J. Cooper-White, *Directing osteogenic and myogenic differentiation of MSCs: interplay of stiffness and adhesive ligand presentation.* American Journal of Physiology-Cell Physiology, 2008. **295**(4): p. C1037-C1044.

101. Wang, L.S., et al., *The role of stiffness of gelatin-hydroxyphenylpropionic acid hydrogels formed by enzyme-mediated crosslinking on the differentiation of human mesenchymal stem cell.* Biomaterials, 2010. **31**(33): p. 8608-8616.

102. Wan, Y.Q., et al., *Adhesion and proliferation of OCT-1 osteoblast-like cells on micro- and nano-scale topography structured pply(L-lactide).* Biomaterials, 2005. **26**(21): p. 4453-4459.

103. D.M., B., ed. *Titanium in medicine*. Principles of cell behavior on titanium surfaces and their application to implanted devices, ed. T.P. Brunette D.M., Textor M., Thomsen P.,. 2001, Springer: Berlin and Heidelberg. 485-512.

104. Boyan, B.D., et al., *Osteoblast-mediated mineral deposition in culture is dependent on surface microtopography.* Calcified Tissue International, 2002. **71**(6): p. 519-529.

105. Perizzolo, D., W.R. Lacefield, and D.M. Brunette, *Interaction between topography and coating in the formation of bone nodules in culture for hydroxyapatite- and titanium-coated micromachined surfaces.* Journal of Biomedical Materials Research, 2001. **56**(4): p. 494-503.

106. Castellani, R., et al., *Response of rat bone marrow cells to differently roughened titanium discs.* Clinical Oral Implants Research, 1999. **10**(5): p. 369-378.

107. ter Brugge, P.J., J.G.C. Wolke, and J.A. Jansen, *Effect of calcium phosphate coating crystallinity and implant surface roughness on differentiation of rat bone marrow cells.* Journal of Biomedical Materials Research, 2002. **60**(1): p. 70-78.

108. Cavalcanti-Adam, E.A., et al., *Cell spreading and focal adhesion dynamics are regulated by spacing of integrin ligands.* Biophysical Journal, 2007. **92**(8): p. 2964-2974.

109. Zhao, L.Z., et al., *Suppressed primary osteoblast functions on nanoporous titania surface.* Journal of Biomedical Materials Research Part A, 2011. **96A**(1): p. 100-107.

110. Arnold, M., et al., *Activation of integrin function by nanopatterned adhesive interfaces.* Chemphyschem, 2004. **5**(3): p. 383-8.

111. McNamara, *Nanotopographical Control of Stem Cell Differentiation.* Journal of Tissue Engineering 2010: p. 13.

112. Dalby, M.J., et al., *Investigating the limits of filopodial sensing: a brief report using SEM to image the interaction between 10 nm high nano-topography and fibroblast filopodia.* Cell Biol Int, 2004. **28**(3): p. 229-36.

113. Li, J.J., et al., *Surface characterization and biocompatibility of micro- and nano-hydroxyapatite / chitosan-gelatin network films.* Materials Science & Engineering C-Biomimetic and Supramolecular Systems, 2009. **29**(4): p. 1207-1215.

114. Dalby, M.J., et al., *The control of human mesenchymal cell differentiation using nanoscale symmetry and disorder.* Nat Mater, 2007. **6**(12): p. 997-1003.

115. Oh, S., et al., *Stem cell fate dictated solely by altered nanotube dimension.* Proc Natl Acad Sci U S A, 2009. **106**(7): p. 2130-5.

116. Oh, S., et al., *Significantly accelerated osteoblast cell growth on aligned TiO2 nanotubes.* Journal of Biomedical Materials Research Part A, 2006. **78A**(1): p. 97-103.

117. Yim, E.K., S.W. Pang, and K.W. Leong, *Synthetic nanostructures inducing differentiation of human mesenchymal stem cells into neuronal lineage.* Experimental Cell Research, 2007. **313**(9): p. 1820-9.

118. Jiang, X., et al., *Directing cell migration with asymmetric micropatterns.* Proc Natl Acad Sci U S A, 2005. **102**(4): p. 975-8.

119. Thery, M., et al., *Anisotropy of cell adhesive microenvironment governs cell internal organization and orientation of polarity.* Proceedings of the National Academy of Sciences of the United States of America, 2006. **103**(52): p. 19771-19776.

120. Wan, L.Q., et al., *Geometric control of human stem cell morphology and differentiation.* Integrative Biology, 2010. **2**(7-8): p. 346-353.

121. Gerber, I., Gwynn I., *Infuence of Cell Isolation, Cell Culture Density, and Cell Nutrition on Differentiation of Rat Calvarial Osteoblast-like Cells in vitro.* European Cells and Materials, 2001. **2**: p. 10-20.

122. Röker, S., *Herstellung funktionaler Kompositmaterialien für das Tissue Engineering von Knochen.* Leibniz University of Hannover, 2009.

123. Cohen, S., et al., *Controlled Delivery Systems for Proteins Based on Poly(Lactic Glycolic Acid) Microspheres.* Pharmaceutical Research, 1991. **8**(6): p. 713-720.

124. Benoit, J.P., et al., *Development of microspheres for neurological disorders: From basics to clinical applications.* Journal of Controlled Release, 2000. **65**(1-2): p. 285-296.

125. Young, S., et al., *Gelatin as a delivery vehicle for the controlled release of bioactive molecules.* Journal of Controlled Release, 2005. **109**(1-3): p. 256-274.

126. Gombotz, W.R. and D.K. Pettit, *Biodegradable Polymers for Protein and Peptide Drug-Delivery.* Bioconjugate Chemistry, 1995. **6**(4): p. 332-351.

127. Schense, J.C., et al., *Enzymatic incorporation of bioactive peptides into fibrin matrices enhances neurite extension.* Nature Biotechnology, 2000. **18**(4): p. 415-419.

128. Kim, H.W., J.C. Knowles, and H.E. Kim, *Development of hydroxyapatite bone scaffold for controlled drug release via poly(epsilon-caprolactone) and hydroxyapatite hybrid coatings.* J Biomed Mater Res B Appl Biomater, 2004. **70**(2): p. 240-9.

129. Arcos, D., et al., *Ibuprofen release from hydrophilic ceramic-polymer composites.* Biomaterials, 1997. **18**(18): p. 1235-42.

130. Chan, L.W., H.Y. Lee, and P.W.S. Heng, *Production of alginate microspheres by internal gelation using an emulsification method.* International Journal of Pharmaceutics, 2002. **242**(1-2): p. 259-262.

131. Zhang, Y. and M.Q. Zhang, *Three-dimensional macroporous calcium phosphate bioceramics with nested chitosan sponges for load-bearing bone implants.* Journal of Biomedical Materials Research, 2002. **61**(1): p. 1-8.

132. Shin, H., S. Jo, and A.G. Mikos, *Biomimetic materials for tissue engineering.* Biomaterials, 2003. **24**(24): p. 4353-4364.

133. Craig, W.S., et al., *Concept and progress in the development of RGD-containing peptide pharmaceuticals.* Biopolymers, 1995. **37**(2): p. 157-75.

134. Massia, S.P. and J.A. Hubbell, *Covalent surface immobilization of Arg-Gly-Asp- and Tyr-Ile-Gly-Ser-Arg-containing peptides to obtain well-defined cell-adhesive substrates.* Anal Biochem, 1990. **187**(2): p. 292-301.

135. Yu, J.S., et al., *The use of human mesenchymal stem cells encapsulated in RGD modified alginate microspheres in the repair of myocardial infarction in the rat.* Biomaterials, 2010. **31**(27): p. 7012-7020.

136. Ranieri, J.P., et al., *Neuronal Cell Attachment to Fluorinated Ethylene-Propylene Films with Covalently Immobilized Laminin Oligopeptides Yigsr and Ikvav .2.* Journal of Biomedical Materials Research, 1995. **29**(6): p. 779-785.

137. Massia, S.P. and J.A. Hubbell, *Vascular Endothelial-Cell Adhesion and Spreading Promoted by the Peptide Redv of the Iiics Region of Plasma Fibronectin Is Mediated by Integrin Alpha-4-Beta-1.* Journal of Biological Chemistry, 1992. **267**(20): p. 14019-14026.

138. Biggs, M.J.P. and M.J. Dalby, *Focal adhesions in osteoneogenesis.* Proceedings of the Institution of Mechanical Engineers Part H-Journal of Engineering in Medicine, 2010. **224**(H12): p. 1441-1453.

139. Klees, R.F., et al., *Laminin-5 induces osteogenic gene expression in human mesenchymal stem cells through an ERK-dependent pathway.* Mol Biol Cell, 2005. **16**(2): p. 881-90.

140. Kon, E., et al., *Orderly Osteochondral Regeneration in a Sheep Model Using a Novel Nano-Composite Multilayered Biomaterial.* Journal of Orthopaedic Research, 2010. **28**(1): p. 116-124.

141. Samuel, R.E., et al., *Delivery of plasmid DNA to articular chondrocytes via novel collagen-glycosaminoglycan matrices.* Human Gene Therapy, 2002. **13**(7): p. 791-802.

142. Meinel, L., et al., *Bone tissue engineering using human mesenchymal stem cells: Effects of scaffold material and medium flow.* Annals of Biomedical Engineering, 2004. **32**(1): p. 112-122.

143. Sikavitsas, V.I., G.N. Bancroft, and A.G. Mikos, *Formation of three-dimensional cell/polymer constructs for bone tissue engineering in a spinner flask and a rotating wall vessel bioreactor.* Journal of Biomedical Materials Research, 2002. **62**(1): p. 136-148.

144. Wartella, K.A. and J.S. Wayne, *Bioreactor for Biaxial Mechanical Stimulation to Tissue Engineered Constructs.* Journal of Biomechanical Engineering-Transactions of the Asme, 2009. **131**(4).

145. Goldstein, A.S., et al., *Effect of convection on osteoblastic cell growth and function in biodegradable polymer foam scaffolds.* Biomaterials, 2001. **22**(11): p. 1279-1288.

146. Sailon, A.M., et al., *A Novel Flow-Perfusion Bioreactor Supports 3D Dynamic Cell Culture.* Journal of Biomedicine and Biotechnology, 2009.

147. Wendt, D., et al., *Bioreactors in tissue engineering: scientific challenges and clinical perspectives.* Adv Biochem Eng Biotechnol, 2009. **112**: p. 1-27.

148. Lavrentieva, A., *Strategie in umbilical cord-derived mesenchymal stem cell expansion.* Dissertation, 2012. **Leibniz Universität Hannover, Germany**.

149. Justice, C., et al., *Online- and offline- monitoring of stem cell expansion on microcarrier.* Cytotechnology, 2011. **63**(4): p. 325-335.

150. Martin, I., D. Wendt, and M. Heberer, *The role of bioreactors in tissue engineering.* Trends in Biotechnology, 2004. **22**(2): p. 80-86.

151. Sikavitsas, V.I., J.S. Temenoff, and A.G. Mikos, *Biomaterials and bone mechanotransduction.* Biomaterials, 2001. **22**(19): p. 2581-2593.

152. Porter, B.D., et al., *Noninvasive image analysis of 3D construct mineralization in a perfusion bioreactor.* Biomaterials, 2007. **28**(15): p. 2525-2533.

153. Bernhardt, A., et al., *Mineralised collagen - an artificial, extracellular bone matrix - improves osteogenic differentiation of bone marrow stromal cells.* Journal of Materials Science-Materials in Medicine, 2008. **19**(1): p. 269-275.

154. Neidlinger-Wilke, C., Wilke, H.J., Claes, L., *Cyclic stretching of human osteoblasts affects proliferation and metabolism: a new experimental method and its applications.* Journal of Orthopeadic Research, 1994. **12**: p. 70.

155. Bodamyali, T., et al., *Pulsed electromagnetic fields simultaneously induce osteogenesis and upregulate transcription of bone morphogenetic proteins 2 and 4 in rat osteoblasts in vitro.* Biochemical and Biophysical Research Communications, 1998. **250**(2): p. 458-461.

156. Schwartz, Z., et al., *Pulsed electromagnetic fields enhance BMP-2 dependent osteoblastic differentiation of human mesenchymal stem cells.* Journal of Orthopaedic Research, 2008. **26**(9): p. 1250-1255.

157. Bok, M., et al., *The dynamics of surface acoustic wave-driven scaffold cell seeding.* Biotechnol Bioeng, 2009. **103**(2): p. 387-401.

158. Zhang, Z.Y., et al., *A comparison of bioreactors for culture of fetal mesenchymal stem cells for bone tissue engineering.* Biomaterials, 2010. **31**(33): p. 8684-8695.

159. Ishaug, S.L., et al., *Bone formation by three-dimensional stromal osteoblast culture in biodegradable polymer scaffolds.* Journal of Biomedical Materials Research, 1997. **36**(1): p. 17-28.

160. McGarry, J.G., et al., *A comparison of strain and fluid shear stress in stimulating bone cell responses--a computational and experimental study.* Faseb Journal, 2005. **19**(3): p. 482-4.

161. Kim, J. and T. Ma, *Perfusion regulation of hMSC microenvironment and osteogenic differentiation in 3D scaffold.* Biotechnology and Bioengineering, 2012. **109**(1): p. 252-261.

162. Zhang, Z.Y., et al., *A biaxial rotating bioreactor for the culture of fetal mesenchymal stem cells for bone tissue engineering.* Biomaterials, 2009. **30**(14): p. 2694-2704.

163. Waked, E., et al., *Bone Specific Alkaline Phosphatase and Cardiovascular Morbidity among Patients on Maintenance Hemodialysis.* Life Science Journal-Acta Zhengzhou University Overseas Edition, 2011. **8**(4): p. 1078-1087.

164. Harris, M.T., et al., *Mesenchymal stem cells used for rabbit tendon repair can form ectopic bone and express alkaline phosphatase activity in constructs.* Journal of Orthopaedic Research, 2004. **22**(5): p. 998-1003.

165. Martino, S., et al., *Stem cell-biomaterial interactions for regenerative medicine.* Biotechnology Advances, 2012. **30**(1): p. 338-351.

166. Sadir, S., Kadir, S. R. A., Oechsner, A., Harun, M. N., *Modeling of Bio Scaffolds: Structural and Fluid Transport Characterization.* World Academy of Science, Engineering and Technology, 2011. **74**: p. 621-626.

167. Acosta Santamaria, V.A., *Ingeniería de tejidos del cartílago articular: caracterización y modelado del comportamiento mecánico.* Dissertation, 2011. **Universidad de Zaragoza, Spain**.

168. Chen, J.P., S.H. Chen, and G.J. Lai, *Preparation and characterization of biomimetic silk fibroin/chitosan composite nanofibers by electrospinning for osteoblasts culture.* Nanoscale Res Lett, 2012. **7**(1): p. 170.

169. Kearns, V., MacIntosh, A.C., Crawford, Hatton, P.V., *Silk-based Biomaterials for Tissue Engineering.* Topics in Tissue Engineering, 2008. **4**: p. Chapter 1.

170. Bosetti, M. and M. Cannas, *The effect of bioactive glasses on bone marrow stromal cells differentiation.* Biomaterials, 2005. **26**(18): p. 3873-3879.

171. Alno, N., et al., *Development of a three-dimensional model for rapid evaluation of bone substitutes in vitro: Effect of the 45S5 bioglass.* Journal of Biomedical Materials Research Part A, 2010. **95A**(1): p. 137-145.

172. Hu, X., et al., *The influence of elasticity and surface roughness on myogenic and osteogenic-differentiation of cells on silk-elastin biomaterials.* Biomaterials, 2011. **32**(34): p. 8979-8989.

173. Lozito, T.P., Kolf, C.M., Tuan, R.S., ed. *Microenvironmental Regulation of Adult Mesenchymal Stem Cells*. Regulatory Networks in Stem Cells, ed. V.K. Rajasekhar, Vemuri, M.C. 2009, Humana Press.

174. Pattappa, G., et al., *The Metabolism of Human Mesenchymal Stem Cells During Proliferation and Differentiation.* Journal of Cellular Physiology, 2011. **226**(10): p. 2562-2570.

175. Yeatts, A.B. and J.P. Fisher, *Bone tissue engineering bioreactors: Dynamic culture and the influence of shear stress.* Bone, 2011. **48**(2): p. 171-181.

176. Hillsley, M.V. and J.A. Frangos, *Bone Tissue Engineering - the Role of Interstitial Fluid-Flow - Review.* Biotechnology and Bioengineering, 1994. **43**(7): p. 573-581.

177. Nagatomi, J., et al., *Cyclic pressure affects osteoblast functions pertinent to osteogenesis.* Annals of Biomedical Engineering, 2003. **31**(8): p. 917-923.

178. McCoy, R.J., C. Jungreuthmayer, and F.J. O'Brien, *Influence of flow rate and scaffold pore size on cell behavior during mechanical stimulation in a flow perfusion bioreactor.* Biotechnol Bioeng, 2012. **109**(6): p. 1583-94.

179. Liu, L., et al., *Three-dimensional dynamic culture of pre-osteoblasts seeded in HA-CS/Col/nHAP composite scaffolds and treated with alpha-ZAL.* Acta Biochim Biophys Sin (Shanghai), 2012. **44**(8): p. 669-77.

180. Jaasma, M.J. and F.J. O'Brien, *Mechanical stimulation of osteoblasts using steady and dynamic fluid flow.* Tissue Engineering Part A, 2008. **14**(7): p. 1213-1223.

181. Partap, S., et al., *Stimulation of osteoblasts using rest periods during bioreactor culture on collagen-glycosaminoglycan scaffolds.* Journal of Materials Science-Materials in Medicine, 2010. **21**(8): p. 2325-2330.

182. Plunkett, N.A., S. Partap, and F.J. O'Brien, *Osteoblast Response to Rest Periods During Bioreactor Culture of Collagen-Glycosaminoglycan Scaffolds.* Tissue Engineering Part A, 2010. **16**(3): p. 943-951.

183. Hillsley, M.V. and J.A. Frangos, *Bone tissue engineering: the role of interstitial fluid flow.* Biotechnol Bioeng, 1994. **43**(7): p. 573-81.

184. Nagatomi, J., et al., *Cyclic pressure affects osteoblast functions pertinent to osteogenesis.* Ann Biomed Eng, 2003. **31**(8): p. 917-23.

185. Jagodzinski, M., et al., *Influence of perfusion and cyclic compression on proliferation and differentiation of bone marrow stromal cells in 3-dimensional culture.* J Biomech, 2008. **41**(9): p. 1885-91.

186. Luo, W., et al., *Laminar shear stress delivers cell cycle arrest and anti-apoptosis to mesenchymal stem cells.* Acta Biochim Biophys Sin (Shanghai), 2011. **43**(3): p. 210-6.

187. Liu, C.X., et al., *Influence of perfusion and compression on the proliferation and differentiation of bone mesenchymal stromal cells seeded on polyurethane scaffolds.* Biomaterials, 2012. **33**(4): p. 1052-1064.

188. Keogh, M.B., et al., *Three Hours of Perfusion Culture Prior to 28 days of Static Culture, Enhances Osteogenesis by Human Cells in a Collagen GAG Scaffold.* Biotechnology and Bioengineering, 2011. **108**(5): p. 1203-1210.

189. Wendt, D., et al., *Oscillating perfusion of cell suspensions through three-dimensional scaffolds enhances cell seeding efficiency and uniformity.* Biotechnol Bioeng, 2003. **84**(2): p. 205-14.

190. http://www.ema.europa.eu/ema/index.jsp?curl=pages/regulation/q_and_a/q_and_a_detail_000081.jsp&murl=menus/regulations/regulations.jsp&mid=WC0b01ac05800862bf. ATMPs. [cited 2012 5th of Sep.].

191. *Directive 93/42/EEC (06/14/1993) on medical devices*.

192. *Directive 90/385/EEC (06/20/1990) regarding active implantable medical devices*.

193. *Directive 2004/23/EC (03/31/2004) on setting standards of quality and safety for the donation, procurement, testing, processing, preservation, storage and distribution of human tissues and cells*

194. *Regulation (EC) No 1394/2007 (11/13/2007) on advanced therapy medicinal products and amending Directive 2001/83/EC and Regulation (EC) No 726/2004*.

195. Kloth, S., *Aktuelle regulatorische Aspekte der Marktzulassung im Bereich Tissue Engineering.* Regenerative Medizin 2008. **1**(1): p. 28-29.

196. *Directive 2003/94/EC (10/08/2003) laying down the principles and guidelines of good manufacturing practice in respect of medicinal products for human use and investigational medicinal products for human use*.

197. Sensebe, L. and P. Bourin, *Producing MSC according GMP: process and controls.* Biomed Mater Eng, 2008. **18**(4-5): p. 173-7.

198. Stamm, A., *Grundlagen und Gesetzgebung für Advanced Therapy Medicinal Products (ATMPs).* Bachelorarbeit, 2011. **Technical Chemistry, Leibniz University of Hannover**.

199. Lavrentieva, A., et al., *Effects of hypoxic culture conditions on umbilical cord-derived human mesenchymal stem cells.* Cell Commun Signal. **8**: p. 18.

200. Moretti, P., et al., *Mesenchymal stromal cells derived from human umbilical cord tissues: primitive cells with potential for clinical and tissue engineering applications.* Adv Biochem Eng Biotechnol. **123**: p. 29-54.

201. Majore, I., et al., *Growth and Differentiation Properties of Mesenchymal Stromal Cell Populations Derived from Whole Human Umbilical Cord.* Stem Cell Reviews and Reports, 2011. **7**(1): p. 17-31.

202. Hatlapatka, T., *Entwicklung von Expansionsstrategien für Misch- und Subpopulationen mesenchymaler Stromazellen aus dem Nabelschnurgewebe unter xeno-freien Kultivierungsbedingungen.* Dissertation, 2011. **Leibniz University of Hannover**.

203. Wolbank, S., et al., *Dose-dependent immunomodulatory effect of human stem cells from amniotic membrane: a comparison with human mesenchymal stem cells from adipose tissue.* Tissue Eng, 2007. **13**(6): p. 1173-83.

204. Wolbank, S., et al., *Labelling of human adipose-derived stem cells for non-invasive in vivo cell tracking.* Cell Tissue Bank, 2007. **8**(3): p. 163-77.

205. Bedini, R., et al., *The use of microtomography in bone tissue and biomaterial three-dimensional analysis.* Ann Ist Super Sanita, 2009. **45**(2): p. 178-84.

206. Moriguchi, T., et al., *Elucidation of adsorption mechanism of bone-staining agent alizarin red S on hydroxyapatite by FT-IR microspectroscopy.* J Colloid Interface Sci, 2003. **260**(1): p. 19-25.

5 Appendix

5.1 Chemicals

Chemical/Reagent	Manufacturer
10*PCR buffer	Peq Biotechnology GmbH, Erlangen, Germany
5*RT buffer	Peq Biotechnology GmbH, Erlangen, Germany
Accutase	PAA Laboratories GmbH, Pasching, Austria
Alizarin Red S	Roth GmbH + Co. KG, Karlsruhe, Germany
cacodyl acid sodium-trihydrate	Sigma Aldrich Chemie GmbH, Munich, Germany
Calcein	Sigma Aldrich Chemie GmbH, Munich, Germany
Calcein-AM	Promega GmbH, Mannheim, Germay
calcium chloride	Sigma Aldrich Chemie GmbH, Munich, Germany
Celltiter blue	Promega BioScience, San Luis Obispo, USA
Chloroform	Sigma Aldrich Chemie GmbH, Munich, Germany
CICP ELISA	Teco Medical AG, Sissach, Switzerland
cryosection medium	Thermo Scientific, Karlsruhe, Germany
DAPI	Roth GmbH + Co. KG, Karlsruhe, Germany
DAPI Roti®-Mount FluorCare	Roth GmbH + Co. KG, Karlsruhe, Germany
dexamethason-21	Honeywell Riedel-de Haen, Seelze, Germany
Directred 80	Sigma Aldrich Chemie GmbH, Munich, Germany
di-sodium-phosphate	Applichem, Darmstadt, Germany
DMSO	Sigma Aldrich Chemie GmbH, Munich, Germany
DNA ladder "Gene RulerTM"	Fermentas GmbH, St. Leon-Rot, Germany
DNA-Polymerase GoTaq	Promega GmbH, Mannheim, Germany
dNTPs	Fermentas GmbH, St. Leon-Rot, Germany
ethanol 96 %	Carl Roth GmbH & Co KG, Karlsruhe, Germany
ethidium bromide	Sigma Aldrich Chemie GmbH, Munich, Germany
Formaldehyde	Sigma Aldrich Chemie GmbH, Munich, Germany
GeneRuler 100 bp DNA-Ladder	Fermentas GmbH, St. Leon-Rot, Germany
Gentamycine	PAA Laboratories GmbH, Pasching, Austria
Glutaraldehyde	Sigma Aldrich Chemie GmbH, Munich, Germany
human serum	Medical School Hanover, Germany
Isopropanole	Merck KGaA, Darmstadt, Germany
loading buffer	Fermentas GmbH, St. Leon-Rot, Germany
MTT	Sigma Aldrich Chemie GmbH, Munich, Germany
NH OsteoDiff Medium	Miltenyi Biotec GmbH, Bergisch Gladbach, Germany
oligo(dT) Primer	Invitrogen GmbH, Darmstadt, Germany
Picricacid	Sigma Aldrich Chemie GmbH, Munich, Germany
Reverse Transkriptase Superscript III	Invitrogen GmbH, Darmstadt
RNA-tidy	Applichem, Darmstadt, Germany

SDS	Sigma Aldrich Chemie GmbH, Munich, Germany
SIGMAFAST™ BCIP®/NBT	Sigma Aldrich Chemie GmbH, Munich, Germany
silver nitrate solution	Roth GmbH + Co. KG, Karlsruhe, Germany
sodium-bi-carbonate	Sigma Aldrich Chemie GmbH, Munich, Germany
tris-base	Sigma Aldrich Chemie GmbH, Munich, Germany
α-Ascorbate	Sigma Aldrich Chemie GmbH, Munich, Germany
α-Minimum Essential Medium (MEM)	GIBCO Invitrogen GmbH, Darmstadt, Germany
β-Glycerolphosphate	Sigma Aldrich Chemie GmbH, Munich, Germany

5.2 Devices

Device	Model	Manufacturer
Analytical balance	ED 224S	Sartorius AG, Göttingen, Germany
Biostat	B-DCU	Sartorius-Stedium Biotech, Göttingen, Germany
Cell counter	TC-10	Bio-Rad Laboratories GmbH, Munich, Germany
Centrifuge for conical tubes	Centrifuge 5702	Eppendorf AG, Hamburg, Germany
Compression instrument		Instron, Pfungstadt, Germany
Cryostat		
Gel iX Imager		Intas Science Imaging Instruments GmbH, Goettingen
Gelstation		Roth GmbH + Co. KG, Karlsruhe, Germany
Glucose/Lactate analysis	YSI2700 Select	YSI Incorporated, Ohio, USA
Incubator	Heracell 240i	Thermo Scientific GmbH, Langenselbold, Germany
Laminar flow cabinet	Technoflow 2F150-II GS	Integra Biosciences AG, Zurich, Switzerland
Microscope	IX 50, Olympus	Europa Holding GmbH, Hamburg, Germany
Microscope Camera	Camedia C-4040	Olympus, Hamburg, Germany
Mini centrifuge	MiniSpin	Eppendorf AG, Hamburg, Germany
nanoCT	system phoenix nanotom	GE Healthcare, Solingen, Germany
PCR-Thermocycler	Doppio	VWR International GmbH, Darmstadt, Germany
Perfusion bioreactor		EBERS Medical Technology, Zaragoza, Spain
Peristaltic pump	IPC-4	Ismatec, Wertheim-Mondfeld, Germany
Fluoroscan Ascent microplate reader		Thermo Scientific GmbH, Langenselbold, Germany
Pipetting aid	Easypet	Eppendorf AG, Hamburg, Germany
Platereader	Model 680	Bio-Rad Laboratories GmbH, Munich, Germany
Scanning electron microscope	JSM-6700F	JEOL GmbH, Munich, Germany
Single-use perfusionchamber	P3D-6/P3D-10	EBERS Medical Technology, Zaragoza, Spain
Ultra pure water system	Arium 611	Sartorius AG, Göttingen, Germany
Ultra-Turrax	T-10	IKA, Staufen, Germany

UV/Vis-Spectralphotometer	Nanodrop ND-1000	PeqLab-Biotechnologie GmbH, Erlangen, Germany
ortex		VWR International GmbH, Darmstadt, Germany
Water bath	WNB	Memmert GmbH & Co KG, Schwabach, Germany

5.3 Materials

Material	Manufacturer
µ-Slide I0.8 Luer, Collagen IV coated	IBIDI GmbH, Martinsried, Germany
Cell culture flasks (T25, T75, T175)	Sarstedt AG & Co, Numbrech, Germany
Cell culture plates (6-, 12-, 24-, 96-Wells)	Sarstedt AG & Co, Numbrech, Germany
Conical tubes (15 ml, 50 ml)	Greiner Bio-One GmbH, Frickenhausen, Germany
Cryo Pure Tubes	Sarstedt AG & Co, Nümbrecht, Germany
Cryosection glass slides	Thermo Scientific GmbH, Langenselbold, Germany
Lab flasks (100 ml, 250 ml,1 l)	VWR International GmbH, Darmstadt, Germany
Latex gloves, Diamond Grip Plus	Microflex, Reno, USA
Needles	B. Braun Melsungen AG, Melsungen, Germany
Nitril gloves, Rotiprotect Nitril	Carl Roth GmbH & Co KG, Karlsruhe, Germany
PCR Plates	Fisher Scienctific GmbH, Schwerte, Germany
PCR Tubes, 0.2 ml	Kisker Biotech GmbH & Co. KG, Steinfurt, Germany
Peristaltic pump tubing	VWR International GmbH, Darmstadt, Germany
Pipette tips (20, 200,1000 µl)	Brand GmbH & CO KG, Wertheim, Germany
Reaction tubes (1.5 ml, 2 ml)	Sarstedt AG & Co, Nümbrecht, Germany
Serologic Pipetts (5, 25, 50, 100 ml)	Sarstedt AG & Co, Nümbrecht, Germany
Syringe filter, Minisart NY25, 0.25 µl	Sartorius AG, Göttingen, Germany
Syringes	Becton Dickinson GmbH, Heidelberg, Germany
Tube connectors	Carl Roth GmbH & Co KG, Karlsruhe, Germany
Tubes	VWR International GmbH, Darmstadt, Germany

5.4 Solutions and buffers

Solutions	Formation
agarose gel	TAE running buffer with 2 % Agarose + 0.002 % Ethidium bromide
Calcein stock solution	200 µg/ml Calcein in ddH_2O
Calcein working solution	2.5 ml Calcein-Stock solution + 97.5 ml ddH_2O
cryomedium	α-MEM Medium + 20 % Human serum + 10 % DMSO
DAPI stock solution	0.5 mg/ml DAPI in ddH_2O
DAPI buffer	100 mM Tris pH 7, 150 mM NaCl, 1 mM CaCl2, 0.5 $MgCl_2$, 0,1 % Nonidet
agarose gelelectrophoresis loading buffer (2x)	95 % Formamide; 0.025 % SDS; 0.025 % Bromphenol blue; 0.025 % Xylene cyanol FF; 0.025 % EtBr; 0.5 mM EDTA
PBS	137 mM NaCl; 2.7 mM KCl; 8.1 mM Na_2HPO_4 * 2 H_2O; 1.8 mM KH_2PO_4; pH 7.4
primer solutions	1 pmol/µl forward primer + 1/µl pmol reverse primer in ddH_2O

TAE Running buffer	40 mM Tris Base; 20 mM Acetic acid; 1 mM EDTA; in ddH_2O; pH 8
von Kossa $AgNO_3$ solution	5% $AgNO_3$ in ddH_2O
von Kossa formaldehyde solution	5%Na_2CO_3 + 0.2% formaldehyde in ddH_2O

5.5 Cell isolation and proliferation

Experiments were carried out with primary human mesenchymal stem cell obtained from adipose or umbilical cord (UC) tissue. AdMSC were isolated by the Austrian Red Cross in Linz. The donor is unknown. UcMSC were obtained from the Wharton's jelly of the whole UC. Isolation was carried out at the Institute of Technical Chemistry at the Leibniz University of Hanover. UCs were provided by the Clinic for Gynaecology and Maternity, Research Group Biochemistry and Tumour Biology at the Hanover Medical School.

5.5.1 Isolation of ucMSC

As previously described [199-201] ucMSC (Fig. 5.2, B) were obtained using a protocol to isolate MSC from the whole human UC tissue in an explant culture approach (Fig. 5.1). UC were obtained from term-delivery (38 to 40 weeks) by Cesarean section. For the transportation from the operating room to the laboratory the UC was stored in a transportation buffer containing saline, antibiotics and fungicides. In a first step, blood from arteries and the vein was removed by flushing the UC with PBS enriched with 5 g/l glucose, 50 µg/ml gentamicine, 2.5 µg/ml amphotericin B, 100 U/ml penicillin and 100 µg/ml streptomycin, in order to minimize the risk of contaminations. The UC was manually cut in pieces of about 0.5 cm^3. After this process, the small tissue pieces were transferred into a 175 cm^2 culture flask and incubated under standard conditions (37°C in a humidified atmosphere with 5 % CO_2) in αMEM supplemented with 10 to 15 % of human serum and 50 µg/ml gentamicine. The medium was changed every second day. A beginning outgrowth of adherent cells from several tissue pieces could be observed after approx. 10 days. After 2 weeks UC tissue pieces were removed and the adherent cells were harvested by using accutase enzymatic treatment. The cell suspension was centrifuged at 200 g for 5 min, the cell pellet was resuspended in culture medium and subcultured until 80 % of confluence at 37°C and 5 % CO_2. Cells were frozen in aliquots of $1*10^6$ cells/ml in αMEM enriched with 20 % human serum and 10 % DMSO in liquid nitrogen.

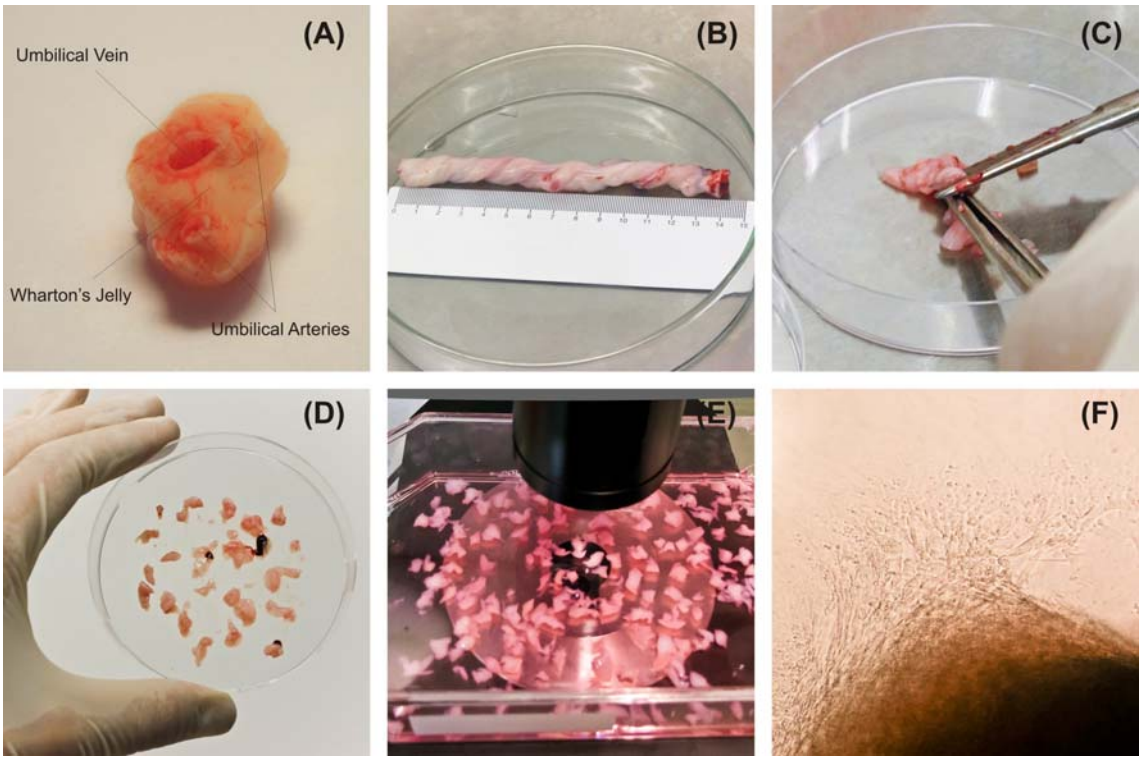

Fig. 5.1: Isolation of ucMSC from the Warton's jelly of the umbilical cord: (A) UC cross section, (B) whole UC, (C) preparation of the UC, (D) UC tissue pieces, (E) UC tissue pieces in a 175 cm^2 culture flask containing culture medium, explant culture, (F) ucMSC growing out of a UC tissue piece after approx. 10 days (adopted from [202]).

5.5.2 Isolation of adMSC

AdMSC (Fig. 5.2, A) were isolated by the Austrian Red Cross in Linz according to the existing protocols [203, 204]. The isolation method is described in detail by Wolbank *et al*. Briefly, adMSC were isolated from subcutaneous adipose tissue. The tissue was rinsed with PBS and thereafter digested with collagenase for 60 min at 37°C under vigorous shaking. The suspension was centrifuged and the obtained cell pellet treated with erythrocyte lysis buffer. PBS was added and the cell suspension filtrated in order to obtain adMSC. Cells were cultivated in Endothelial Cell Growth Medium-2 at 37°C and 5 % CO_2. Cells were frozen in aliquots of $1*10^6$ cells in liquid nitrogen. Subcultivation was carried out in culture medium until 80 % of confluence.

5.5.3 Culture medium

Culture medium for ucMSC and adMSC contained α-MEM (10.08 g α-MEM powder and 2.2 g sodium-bi-carbonate in 1 l ddH_2O, filtrated sterile) enriched with 5 % human serum and 50 µg/ml gentamicine.

5.5.4 Osteogenic differentiation medium

Osteogenic differentiation medium (ODM) for adMSC applied in bioreactor experiments contained α-MEM (10.08 g α-MEM powder and 2.2 g sodium-bi-carbonate in 1 l ddH_2O, filtrated sterile) enriched with 5 % human serum and 50 µg/ml gentamicine. Additionally, 10 nM dexamethasone, 50 mg/ml α-ascorbate and 10 mM β-glycerolphosphate were added. Osteogenic differentiation medium from Miltenyi Biotec (ODM-M) was used for static differentiation experiments and dynamic cultivations applying ucMSC. The exact composition of ODM-M is unknown.

5.5.5 2D cell expansion

Cell expansion was carried out in culture medium. 1000 cells/cm² were seeded in a 175 cm² culture flask containing 25 ml medium. Cells were cultivated 3 to 4 days until 80 % of confluence. Then, cells were subcultured. For this process, the cell layer was washed once with 5 ml of PBS and thereafter incubated in 3 ml Accutase for about 5 min. Accutase contains enzymes to perform gentile cell detachment. Next, 5 ml of culture medium was added and the suspension transferred to a 50 ml falcon tube. The suspension was centrifuged 5 min at 300 g. Supernatant was discarded and the pellet resolved in a defined volume of culture medium, depending on the amount of cells. For expansion purposes once more 1000 cells/cm² were seeded into each 175 cm² culture flask. Subcultivation was only performed until passage eight.

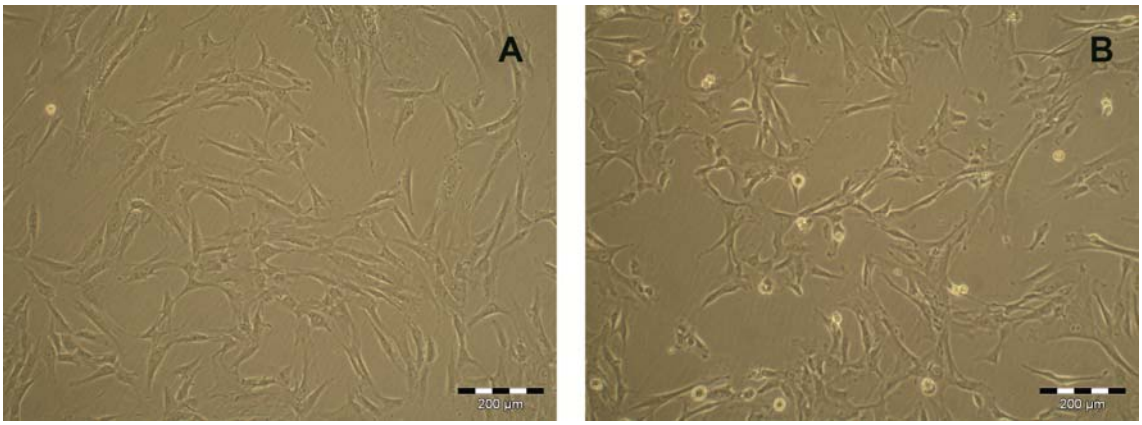

Fig. 5.2: Phase contrast images of isolated adMSC (A) and ucMSC (B)

5.5.6 Determination of the cell number

Cell number was either determined by using a cell counter or counted manually. For determination of viable cells 20 µl of cell suspension was mixed with 20 µl of trypan blue. Viable cells do not absorb trypan blue; however, the dye can pass the membrane of dead cells. Dead cells appear blue and can be detected by the cell counter and under

the microscope. For the determination of the cell number by the cell counter about 5 µl of the cell-dye-suspension was introduced in a µ-slide and inserted into the cell counter. For manually counting of the cells the cell-dye-suspension was introduced to a haemocytometer with a specific pattern of squares. Each square has an area of 1 mm^2. A cover glass was placed on the pattern with a distance of 0.1 mm, so that each square has a fix volume. The counted cell number was multiplied by 10^4 to obtain the cell number per milliliter.

5.6 Characterization of biomaterials

5.6.1 Scanning electron microscopy

With the scanning electron microscopy (SEM) high magnification images of biomaterials can be realized. Biomaterials are scanned by a high-energy beam of electrons. Signals produced by the interaction of electrons and atoms contain information about the topology of the biomaterial.

SEM images of the ceramic biomaterials were taken with a JEOL JSM-6700F at 2 kV acceleration at a working distance of 15 mm. Biomaterials containing cells were treated with Karnovsky buffer (5 mg calcium chloride, 10 ml Cacodylate buffer, 20 µl glutaraldehyde and 2.5 ml ddH_2O) for 24 h at 4°C to fix the cells on the matrix. The following day the matrices were washed three times with Cacodylate buffer (0.2 M Cacodyl Acid sodium-trihydrate in ddH_2O) and then dried for at least one week at room temperature.

5.6.2 Micro computed tomography

The 3D geometry of biomaterials was characterized and evaluated in detail by a high resolution nanofocus computed tomography (nanoCT) technique (Fig. 5.3). NanoCT analyses allow a detailed non-invasive and non-destructive visualization of the 3D architecture of biomaterials. Different methods of data processing can help to identify the following quantitative parameters [205]: Surface area, total volume, void space volume, matrix porosity, pore wall thickness, interconnectivity, pore diameter distribution, average pore diameter, average pore wall thickness.

Five different samples of each ceramic biomaterial, Sponceram-Al, Osseolive, Cerasorb M and 45S5-Bioglass, were scanned using a nanoCT system phoenix nanotom by GE. All samples were measured with 90 kV and 90 µA. For quantitative analysis of the data one mm^3 of each sample was analyzed with the Avizo software by VSG. The

calculations are based the 3D volume, which is approximated by the number of pixels, and on the grey values in the image.

One sample of each collagen-based biomaterial, Matriderm, Collagen-BG and Collagen-Silk was analyzed. The samples were measured with 70 kV and 220 µA. Quantitative data analysis was not performed for collagen-based biomaterials.

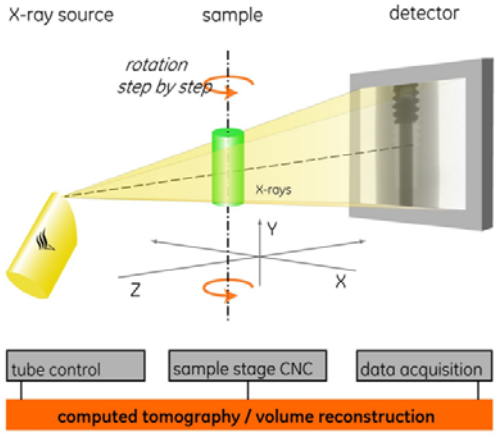

Fig. 5.3: Setup of the nanoCT system phoenix nanotom (adopted from GE Healthcare).

5.6.3 Permeability

The permeability (k) is a parameter, which describes the interconnectivity of the pores and the capacity of the material to absorb fluids, without changing its structure. Moreover, the average porosity, pore size and pore size distribution, as well as the orientation of the pores have an influence on the permeability. To determine the ratio between the porosity and the pore size a permeability test under Darcy's Law was carried out (Formula 2). To calculate the permeability, the fluid flow rate across the biomaterial was varied (50, 100, 150, 200, 300, 400 ml/min) and in each case the pressure difference was measured. The used equipment is shown in Fig. 5.4 and schematically displayed in Fig. 5.5. In order to determine the average permeability five samples of each ceramic biomaterial were used. The average pressure difference was calculated for each fluid flow rate and afterwards the specific permeability k was evaluated using Formula 2.

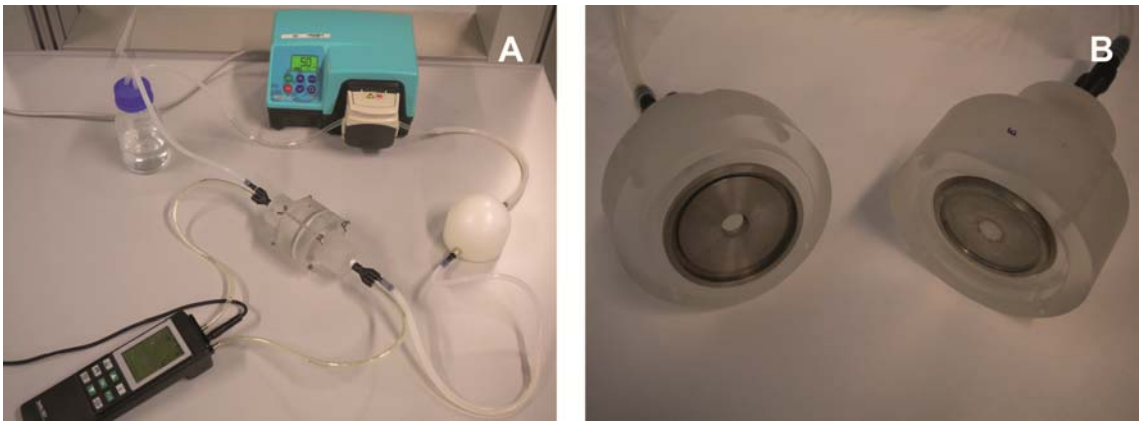

Fig. 5.4: Setup to determine the biomaterials permeability: (A) complete assembling, (B) permeability chamber with a biomaterial.

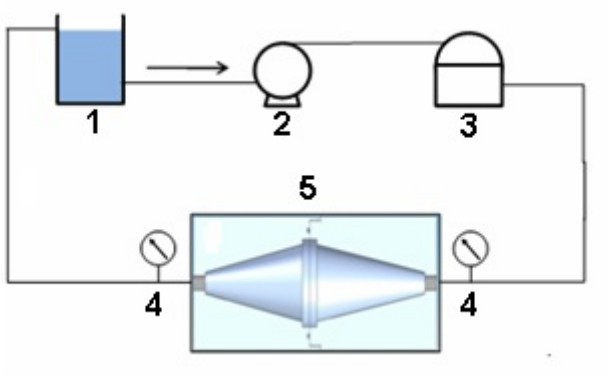

1. Reservoir
2. Pump
3. Fluid flow damper
4. Differential pressure instrument
5. Permeability chamber

Fig. 5.5: Schematic assembling to determine the biomaterials permeability (adopted from dissertation Victor Acosta Santamaría [167], University of Zaragoza, Spain).

5.6.4 Compression test

In order to determine the stability of the biomaterials uniaxial static unconfined (UC) and confined (CC) compression test were carried out (Fig. 2.16). During the UC test, the biomaterial can laterally be deformed as load is applied to the material. On the contrary, during the CC test the lateral deformation is avoided by a fixed volume. Furthermore, the fluid flow behaves differently in the UC and CC test. In the UC test the liquid moves freely through the biomaterial and its walls. However, in the CC test a porous metal plate is fixed under the sample, whereby, combined with the fixed volume, the liquid can only flow from the top to the bottom through the biomaterial.

During each UC and CC test the stress-strain-curve was plotted (Fig. 5.6). The curve can be divided into three areas. In the first area the strain deforms the pores temporally; they can return to their actual state after loading. In the second area a stronger strain is applied to the biomaterial, so that the pores deform permanently, whereas the third area describes the collapse of the pores. The Young Modulus (Es) is

calculated from the UC data and the Aggregate Modulus (HA) from the CC data. Therefore, in each stress-strain-curve the linear slope of the first area was chosen.

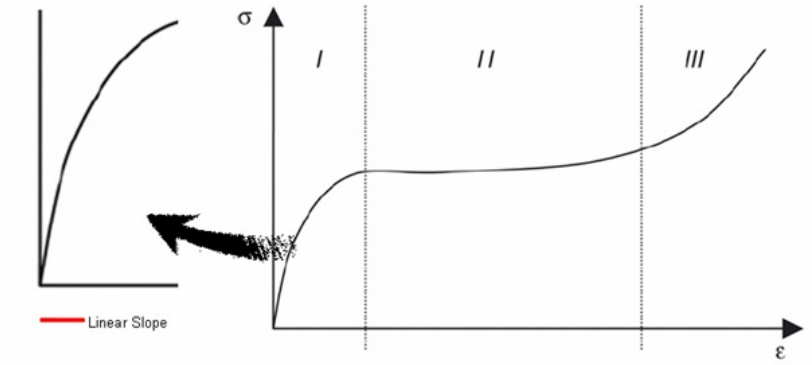

Fig. 5.6: Theoretical stress-strain-curve: From the linear slope the Young Modulus (Es) and Aggregate Modulus (HA) can be calculated (adopted from dissertation Victor Acosta Santamaría [167], University of Zaragoza, Spain).

Es can directly be calculated from the lateral displacement of the biomaterial. On the contrary, the deformation in the CC test only accrues in y-direction, as the lateral deformation is avoided by the fixed volume. Nevertheless, the CC test is described as a multiaxial test, because the inner wall of the equipment bears a strain on the lateral surface of the biomaterial. The applied lateral force defines HA.

Before carrying out each compression test, the biomaterials were moistened with PBS. At the beginning of each experiment it has to be assured that the test tool is in contact with the biomaterial. This is necessary to eliminate measurement inaccuracy, which can occur due to a non planar geometry of the biomaterial. Furthermore, the contact is needed to set an initial reference point. For this reason all tests begin with a prestrain of 5 % at 0.001 mm/s. In order to start each test with at the same reference point, the first contact of the test tool with the sample is performed by taking a reference force between 0.01 N and 0.02 N. The experiments were carried out with the instrument Instron Micro Tester 5548, which performs monotonic steps of 0.01 mm/s and applies a final force of 50 N. Moreover, the equipment has a precision of 0.0001 N in force and 0.001 mm in displacement. The dimension of each biomaterial (thickness and diameter) was measured before each experiment. The experimentally obtained stress-strain curves were treated using a code implemented in MatLab to fit each curve by the least square approximation in order to determine E_s and HA. Moreover, the mean average and the standard deviation were calculated. Five samples of each material were used in the UC- and CC-test, respectively.

5.7 Cultivation experiments

5.7.1 Fluid flow stimulation of 2D MCS cultures

To apply fluid flow to 2D MSC cultures a commercially available cell culture system (Fig. 2.1) was used (IBIDI µ-slide $I^{0.8}$ Luer, collagen IV coated). Cell seeding is performed with $2.8*10^4$ cells in 200 µl culture medium. The suspension is slowly pipetted into the channel, bubbles are removed by gently shaking the culture chamber. The cells are cultivated statically under standard conditions for two days (cp. literature 24 to 72 h of static cultivation prior to stimulation [78]) until about 100 % of confluence (Fig. 5.7). The medium is changed completely every day.

Cultivation over 7 days in the IBIDI µ-slide chamber was performed according to the stimulation pattern indicated in Fig. 5.8. Fluid flow stimulation was applied for 4 hours, followed by a 4 hour break and followed by 4 hours stimulation. After a break of 12 hours this pattern was repeated with an increased stimulation (0.1 dyn/cm² to 1.2 dyn/cm²). 20 ml of either culture medium or osteogenic differentiation medium were circulated using a peristaltic pump and a medium reservoir. The µ-slide and the medium reservoir were placed in the incubator during the cultivation period, however, the peristaltic pump was located outside. For comparison, cells were cultivated under static conditions in µ-slide chambers and the medium exchanged every day. In order to perform histological stainings, cells were fixed in the µ-slides with cold ethanol (96 %) for 10 min. Then, the cell layer was washed twice with PBS.

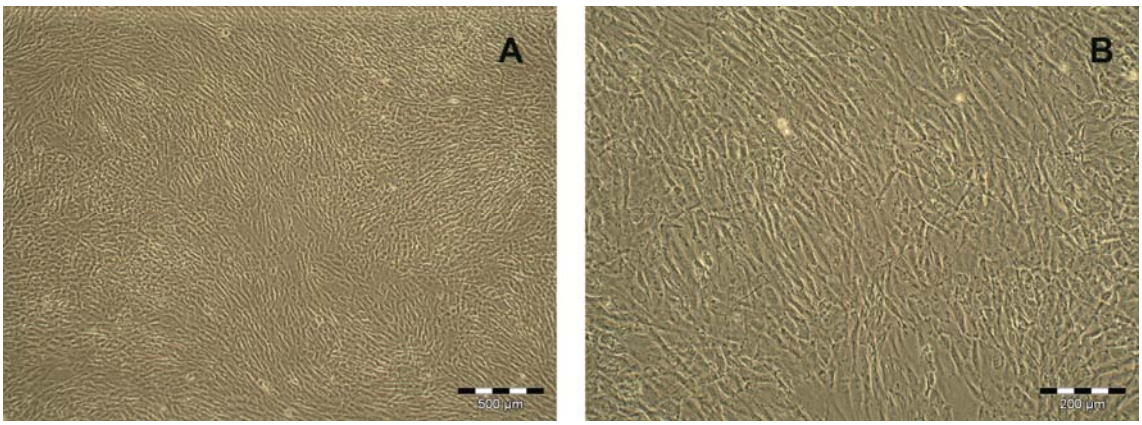

Fig. 5.7: Phase contrast images of adMSC in the IBIDI µ-Slide $I^{0.8}$ chamber after 2 days of static cultivation, before applying fluid flow: (A) 20-times magnification, (B) 100-times magnification.

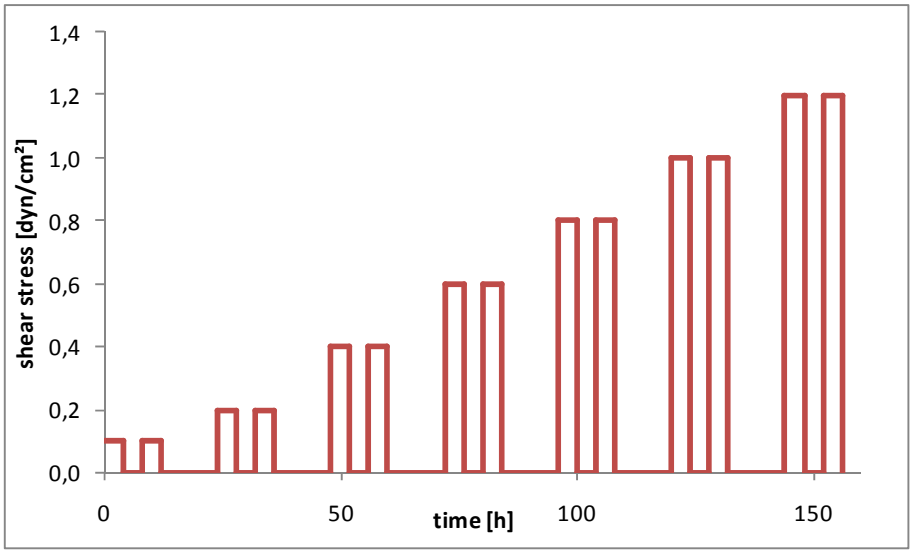

Fig. 5.8: Stimulation pattern for 2D MSC cultures over a time period of 7 days. MSC are stimulated twice a day for 4 hours with a 4 hour break in-between, followed by a break of 12 hours. The stimulation intensity increases from 0.1 dyn/cm² to 1.2 dyn/cm².

5.7.2 Static cultivation of MSC on 3D biomaterials

Prior to cell seeding ceramic biomaterials were autoclaved at 121°C for 30 min. The size of collagen-based biomaterials was determined by using a hollow punch and a hammer. Each side of the collagen-based biomaterials was sterilized for 30 min under UV light. Thereafter, biomaterials were transferred to a 24-well-plate. Each biomaterial was seeded with a cell suspension of about 30 µl containing $6*10^4$ ucMSC or adMSC. The biomaterial-cell construct was incubated for 45 min at 37°C and 5 % CO_2 in the incubator. In order to prevent drying-out, twice about 20-30 µl culture medium was pipetted onto each biomaterial. After 45 min 1 ml of culture medium was added to each well. For proliferation purposes, cultivation was performed in culture medium during the first week. To evoke differentiation, medium was switched to ODM-M. Cultivation in ODM-M was performed for 4 weeks. The medium was changed three times per week (1 ml). During each change of medium three samples of three different wells of each biomaterial were collected and combined to measure the glucose consumption and lactate production, as well as the collagen I production. In order to determine biocompatibility and perform proliferation experiments biomaterial-cell constructs were cultivated for 5 weeks in culture medium. Medium change was carried out according to the instructions above.

5.7.3 Cultivation of MSC in a disposable direct perfusion bioreactor

The single use perfusion chambers have been developed by EBERS Medical (Zaragoza, Spain) and are commercially available (Fig. 2.27). To date, two different models are

distributed: The model P3D-6 for the cultivation of matrices with a diameter of about 6 mm, and the model P3D-10 to position matrices of about 10 mm. The bioreactor chamber was designed to apply direct perfusion and consists of 2 parts, the male part (upper part) and the female part (lower part), which can be connected via clip lock. Tubing can be connected to the bioreactor chamber via luer-lock connectors.

These chambers were used in the experimental part of this work to perform two different experiments: (1) Improve the cell distribution on Cerasorb M and (2) dynamically cultivate MSC on collagen-based biomaterials.

1. To improve the cell distribution on Cerasorb M $2*10^5$ ucMSC were seeded on the top of the matrix and cultivated 2 days statically in culture medium. Then, the Cerasorb M matrix was transferred with a forceps under sterile conditions to the female part (bottom part) of a P3D-10 single-use perfusion culture chamber. The chamber was closed with the male part (upper part), thereby the biomaterial was fixed. About 15 ml of culture medium were circulated for 3 days with 200 µl/min, using a peristaltic pump and a medium reservoir. Air in the culture chamber was removed during the first minutes of dynamic cultivation, by turning the culture chamber upside down.
2. For dynamic cultivation of ucMSC on collagen-based biomaterials $2*10^5$ ucMSC were seeded on collagen-BG (d = 8 mm), cultivated statically for 4 days in culture medium and for 4 days in ODM-M. Thereafter, 3 matrices were transferred with a forceps under sterile conditions to the female part of a P3D-6 single-use perfusion chamber. In order to remove the air, female part (bottom part) was filled completely with ODM-M before closing the chamber with male part. In a first approach, about 15 ml culture medium were circulated for 1 week with either 0.1 or 1 ml/min, using a peristaltic pump and a medium reservoir. In a next approach, 15 ml ODM-M was circulated for 3 weeks with 0.1 ml/min. In this experiment, about 5 ml ODM-M were added to the medium reservoir through a sterile septum on day 5, 10 and 15 using a syringe.

During both approaches the single-use perfusion bioreactors and the medium reservoir were placed in the incubator during the cultivation period, however, the peristaltic pump was located outside.

5.7.4 Cultivation of MSC in a non-disposable direct perfusion bioreactor

To perform dynamic 3D cultivations on ceramic biomaterials a special designed perfusion culture chamber was used (EBERS Medical, Zaragoza, Spain). It consists of two identical cylindrical parts and a disk to position eight biomaterials in the middle of

the chamber. For cultivation $2*10^5$ adMSC were seeded onto each sterile Sponceram-Al matrix and cultivated 4 days in culture medium and 4 days in ODM. The bioreactor was autoclaved and eight matrices transferred with a forceps under sterile conditions to the disk. The disk was positioned in the middle of the culture chamber. The chamber was slowly filled with ODM under displacement of air using a peristaltic pump. Thereafter, medium was circulated for 3 weeks with 1.5 ml/min and an initial medium amount of 100 ml using a peristaltic pump and a medium reservoir. The bioreactor and the medium reservoir were placed in the incubator during the cultivation period, however, the peristaltic pump was located outside. On day 5, 10 and 15 about 10 ml ODM were added to the medium reservoir through a sterile septum with a syringe. Medium of the statically cultured samples (1 ml) was changed three times a week.

5.7.5 Setup for the cultivation under controlled and regulated conditions

In order to perform MSC cultivation and differentiation under controlled and regulated conditions a stirred tank bioreactor (STR) was used as a medium reservoir (cp. section 2.7). The STR was connected to a control unit to allow for documentation and regulation of cultivation parameters, such as temperature, pH and pO_2. Prior to autoclaving the sparger of the STR was equipped with a tube and a filter for the sterile connection to the gas supply. Moreover, two air filters were fixed for exhaust emission. The STR was connected to the tubing system of the drip-perfusion bioreactor. The pH electrode was calibrated prior autoclaving. The pO_2 and pH electrodes were implemented to the STR and, to prevent drying out, the STR was filled with approximately 300 ml ddH_2O. The drip-perfusion reactor was sterilized separately. After the sterilization procedure, the ddH_2O of the STR was removed under sterile conditions. About 200 ml ODM were added to the STR either under the laminar flow cabin or by using a peristaltic pump. In order to calibrate the pO_2 electrode the medium was heated up to 37°C and 30 ccm/min air were pumped into the STR for about 1 hour. Then the motor was set to 100 rpm. After another 30 min the pO_2 value was set to 100 %. Now, the biomaterials were transferred to the drip-perfusion bioreactor under sterile conditions and then connected to the tubing system using luer-lock connectors.

5.8 Analytical methods

5.8.1 Glucose and lactate measurement

Medium samples collected during the cultivations were measured at YSI2700 Select in order to determine the glucose consumption and the lactate production. These factors can indirectly be used as an indicator for cell survival and cell proliferation.

5.8.2 MTT viability assay

Cell viability on the ceramic biomaterials was determined using the MTT viability test. The yellow MTT (3-(4,5-dimethylthiazol-2-yl)-2,5-diphenyl-tetrazolium-bromid) is metabolized to violet formazan by dehydrogenases in the mitochondria of living cells. The concentration of the formazan (measured by its absorption of the yellow light) is used as an indicator of the viability and proliferation respectively. Ceramic matrices were washed three times with warm PBS and afterwards transferred in a solution of 495 µl α-MEM and 55 µl MTT-solution. After an incubation period of 4 h under standard conditions 500 µl SDS-solution (10 % in 0.01 N HCl) was added. The samples were incubated over night. On the following day the solution of each sample was divided into 4 wells of a 96-well-plate (200 µl each) and the formazan concentration was measured by the extinction at 570 nm with a reference wave length of 630 nm. The average value of the 4 wells was calculated. The blank (495 µl α-MEM, 55 µl MTT, 500 µl SDS) was deducted from the data.

5.8.3 CellTiter-Blue viability assay

CellTiter-Blue assay allows for the monitoring of cell viability. Only living cells can convert the redox dye (resazurin) into the fluorescent product (resorufin). Resorufin is pink and can be detected at extinction of 589 nm and emission of 584 nm. To determine the viability of cells on collagen-based biomaterials, each matrix was placed in a mixture of 300 µl αMEM and 60 µl CellTiter-Blue and incubated under standard conditions for 3 h. Then, the solution of each sample was divided into 3 wells of a 96-well-plate (100 µl each) and measured at a plate-reading fluorometer. The average value of the 3 wells was calculated. The blank (300 µl αMEM and 60 µl CellTiter-Blue) was deducted from the data.

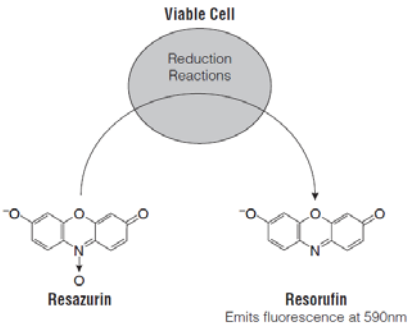

Fig. 5.9: Mechanism of the CellTiter-Blue viability assay. Viable cells transform the blue dye resazurin into the pink fluorescent dye resorufin (adopted from the instruction manual of the manufacturer).

5.8.4 Collagen I ELISA

Collagen I is the main component of the ECM of osteogenic differentiated MSC and can be quantified via CICP-ELISA. CICP signifies the C-terminal of type I collagen. The level of CICP is indicative of collagen production *in vivo*. As the primary organic constituent of bone, type I collagen levels are linked to bone growth and formation. CICP-ELISA was performed with the samples of each medium change during the static differentiation of MSC on different biomaterials. ELISA was carried out according to instructions given by the manufacturer. Briefly, the assay is based on the sandwich enzyme immunoassay principle using a monoclonal anti-CICP antibody, which is coated on a 96-microtiter-well-plate. Moreover, rabbit anti-CICP antiserum is used, which binds specifically to the CICP bound to the antibody. For detection a goat anti-rabbit alkaline phosphatase conjugate and the substrate pNPP (Para-nitrophenyl phosphate) is used. The yellow dye was measured at a wave length of 405 nm.

5.8.5 RNA isolation

Ceramic matrices were frozen in liquid nitrogen directly after the end of the cultivation period. For RNA isolation, they were smashed with a mortar in liquid nitrogen. Thereafter, the smashed sample was collected in a 2 ml vial and 500 µl of RNA-tidy was added. Collagen samples were frozen in 500-1000 µl RNA-tidy (depending on the size of the sample) at -20°C directly after cultivation. For RNA isolation samples were thawed and treated three times about 3-5 s by Ultra-Turrax.

Ceramic materials as well as collagen materials were centrifuged 10 min at 12000 rpm and 4°C. Supernatant was transferred to a new vial, adding 200 µl of chloroform. Samples were shaken and then centrifuged 15 min at 12000 rpm and 4°C, resulting in a three-phase solution. The upper liquid phase containing the RNA was transferred into a new vial and 500 µl of isopropanol was added. The interphase, containing proteins and DNA, and the phenol-chloroform phase were discarded. The vial containing the

liquid phase and isopropanol was shaken and centrifuged 10 min at 12000 rpm and 4°C. The supernatant was discarded, resulting a white pallet containing RNA. The pellet was resolved in 1 ml ethanol (75 %) and again centrifuged 5 min at 12000 rpm and 4°C. The pellet was dried and then resolved in DEPC water. RNA concentration and purity was measured using Nanodrop.

5.8.6 cDNA synthesis

For PCR experiments the isolated RNA was transcribed into copy DNA (cDNA). In order to only transcribe the messenger RNA (mRNA), coding the information for the protein synthesis, oligo-dT-primer were used, which bind significantly to the poly(A)-tail of the mRNA.

cDNA synthesis was carried out according to the following procedure:

Substances for cDNA synthesis step 1	
RNA	2 µg
oligo-dT-primer (100 µM)	3 µl
DECP water	add up to 21 µl

Samples are denaturized for 5 min at 65°C. Denaturization is stopped by cooling the samples for 2 min on ice. Thereafter, the following substances are added:

Substances for cDNA synthesis step 2	**µl**
dNTP-mixture (2.5 mM)	4
5* RT-buffer	8
reverse transcriptase (200 U/µl)	1
DECP water	add up to 40 µl

Transcription was performed within 60 min at 37°C. Reaction was stopped by heating the samples for 5 min to 65°C.

5.8.7 RT-PCR

Polymerase chain reaction (PCR) amplifies the cDNA. Experiments were performed according to the following procedure:

Substances for RT-PCR	**µl**
cDNA	1
5*PCR-buffer	10
dNTP-mixture (2.5 mM)	4
sense primer	1
antisense primer	1
taq-polymerase (5U/µl)	0.25
ddH_2O	32.75

Within the first step of PCR cDNA is completely denaturized at 95°C (5 min). Thereafter, 35 cycles are performed, each consisting of 3 steps of 30 s: Denaturization at 95°C, annealing (primer depending temperature) and elongation at 72°C. The last step takes 7 min at 72°C for final elongation.

For some samples with a very low RNA content the following procedure was performed: 18 cycles of denaturization, annealing and elongation were completed. Thereafter, a new PCR approach was prepared using 1 µl of the amplified cDNA and carrying out another 45 cycles.

Samples were transferred to a 2 % agarose gel containing ethidium bromide, in order to separate the samples by size. As a marker the 1 kb DNA ladder (0.5 µg/µl) was used.

The following primer sequences were used to perform PCR:

Gene	NCBI accession number	Forward sequence	Reverse Sequence	Melting temperature, °C	Product length, bp
HPRT	NM_000194.2	aagcttgctg gtgaaaagga	tgttctagttc tgtggccatct	58	263
COL I	NM_000088.3	ggaggaatttcc gtgcctggcccc	tcagggtgctc gaggatt gcc	68	250
COL III	NM_000090.3	catctggtca tcctggttcc	tggacgaaatg gagaaaagg	60	267
RUNX	NM_001024630.3	tcctatgacca gtcttacccct	ttccactctcag taagaagagcc	62	189
BSP-2	NM_004967.3	cattttggga atggcctgtg	gcagcagcgg aggagacaat	60	564
OP	NM_001251830.1	ccaggactc cattgactc	atctaagaagtt tcgcagacctg	66	225
BMP-2	NM_001200.2	agacctgtatc gcaggcact	gcagtttccat caccgaatt	60	274
BMP-4	NM_130851.2	gcttccaccac gaagaacat	cgagactggtcc accacaatgtga	60	272
OCN	NM_001199662.1	ggcagcgagg tagtgaagag	ccagttctgc tcctctccag	62	230
AP	NM_000478.4	Ccacgtcttc acatttggtg	acaactacca ggcgcagt ct	60	196

5.8.8 Histological stainings

To fix the cells on the ceramic materials, matrices were washed three times with warm PBS and afterwards incubated 30 min at 4°C in cold ethanol (96 %). Thereafter, matrices were washed again three times with PBS. Soft collagen matrices were embedded in cryosection medium directly after cultivation and frozen at -20°C. Cryosections of 25 µm were made using a Cryostat. In order to fix the cryosections on the glass slide, the slide was once introduced into 96 % ethanol and then dried.

5.8.8.1 DAPI staining

The nuclei of fixed cells can be stained with the fluorescence dye 4',6-Diamidino-2-phenylindol (DAPI). The dye binds on the DNA of the nuclei. For staining of the ceramic samples, the matrices were incubated 15 min in the dark in DAPI-solution (2 µl DAPI-stock solution in 1 ml DAPI buffer). Afterwards, the matrices were washed three times in PBS to eliminate the background. The nuclei could be detected and photographed by the fluorescence microscope at 360 nm excitation and 460 nm emission.

Staining of the nuclei on cryosections was performed with DAPI Roti®-Mount FluorCare. The section was covered with the commercially available DAPI solution and incubated for 15 min in the dark. Sections were washed three times to reduce the background staining. Cryosections were photographed under the fluorescence microscope at 360 nm excitation and 460 nm emission.

5.8.8.2 Calcein-AM staining

The fluorescent dye, calcein acetoxymethylester (Calcein-AM) was used to detect living cells on biomaterials (Fig. 5.10). According to the instructions Calcein-AM was diluted 1:10 with PBS and then 1:10 with culture medium (α-MEM). The matrix containing cells was incubated 30 min in this solution under standard conditions. The green fluorescent staining was detected and photographed using a fluorescence microscope at 485 nm excitation and 535 nm emission.

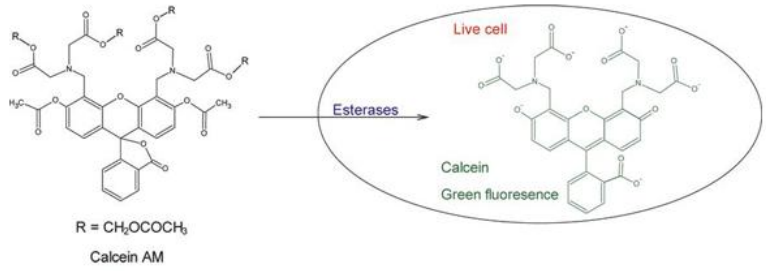

Fig. 5.10: Mechanism of Calcein-AM staining. Viable cells transform with the help of esterases the dye Calcein-AM into the green fluorescent dye Calcein.

5.8.8.3 *AlizarinRed staining*

With the use of AlizarinRed calcium ions within the mineralized ECM can be stained red. AlizarinRed forms with bivalent cations (in this case calcium ions) a chelate complex (Fig. 5.11). For staining, samples were incubated 15 min in AlizarinRed solution (1 % AlizarinRed S w/v in 2 % ethanol). Background staining was eliminated by washing the samples five times with ddH_2O. Mineralized ECM was examined under the microscope and photographed.

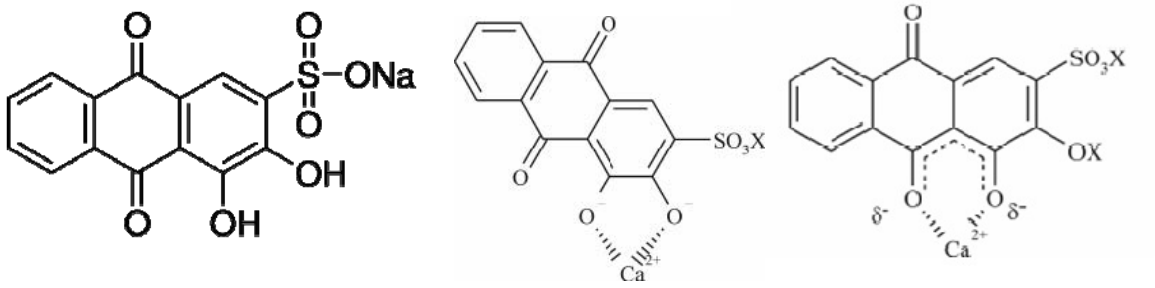

Fig. 5.11: Chemical structure of natriumalizarinsulfonat (left), AlizarinRed S, (adopted from Sigma) and possible structures of AlizarinRed bound to hydroylapatite (middle) and chelate complex (right), X = H, Na [206].

5.8.8.4 *von Kossa staining*

Von Kossa staining is based on a reaction with silver nitrate and used for the detection of calcium accumulations within the ECM. During this reaction calcium ions of calcium phosphate are replaced by silver ions. In a next step these silver ions are reduced to metallic silver, which appears dark brown or black. For staining cell-biomaterial constructs, matrices were washed twice with ddH_2O. Then $AgNO_3$ solution was added and the materials were incubated for 30 minutes in the dark. After incubation, the matrices were washed five times with ddH_2O and subsequently a solution of 5 % sodium carbonate and 0.2 % formaldehyde added. After 1-2 min reaction, formaldehyde solution was removed and the matrices were washed again three times with PBS. Finally the samples were examined under the microscope and photographed.

5.8.8.5 *Calcein staining*

Calcein is a fluorescent dye, which specifically binds to calcium ions. For staining purposes samples were incubated over night in the dark in Calcein solution (5 µg/ml Calcein in ddH_2O). To eliminate background staining, samples were washed three times with ddH_2O. The green staining of calcified tissue was observed and photographed using a florescence microscope at 485 nm excitation and 535 nm emission.

5.8.8.6 Membrane bound alkaline phosphatase

Alkaline phosphatase (AP) is an early indicator for osteogenic differentiation of MSC. Staining of membrane bound AP was performed using the kit SIGMA*FAST*™ BCIP®/NBT. According to the instructions one tablet containing 5-bromo-4-chloro-3-indolylphosphate/nitro blue tetrazolium was dissolved in 10 ml ddH_2O. Samples were incubated with the BCIP/NBT solution for 30 min at 37°C in the incubator. Samples were only washed once with ddH_2O to remove the staining solution. Violet staining was observed and photographed under the microscope.

5.8.8.7 Direct Red staining

Direct Red specifically stains collagen. For staining purposes samples with fixed cells were washed twice with ddH_2O and then incubated in Direct Red solution (0.1 % Direct Red in saturated picric acid) for 15 min. Then, samples were washed again five times with ddH_2O. Finally the samples are examined under the microscope.

6 Lebenslauf

Sonja Kreß

Geburtsdatum/-ort:	01.11.1983 in Hannover
Staatsangehörigkeit:	deutsch

Beruflicher Werdegang

Seit 01.02.2012	Projektmanagerin, Leibniz Universität Hannover, Forschung und EU-Hochschulbüro - Technologietransfer
15.07.2009-23.11.2012	Promotionsstudentin, Leibniz Universität Hannover, Institut für Technische Chemie
01.11.2007 - 05.05.2009	Life Science (M.Sc.), Leibniz Universität Hannover
01.01.2007 - 31.10.2007	Auslandssemester, Universität Linköping, Schweden
01.10.2006 - 31.12.2006	Life Science (M.Sc), Leibniz Universität Hannover
01.04.2004 - 30.09.2006	Life Science (B.Sc), Leibniz Universität Hannover
01.10.2003 - 31.3.2004	Computational Life Science (B.Sc.), Universität zu Lübeck
6.5.2003	Abitur, Gymnasium Neustadt am Rübenberge